LBL-11180
SAC-30
UC-70

SWEDISH-AMERICAN COOPERATIVE PROGRAM ON RADIOACTIVE WASTE STORAGE IN MINED CAVERNS IN CRYSTALLINE ROCK

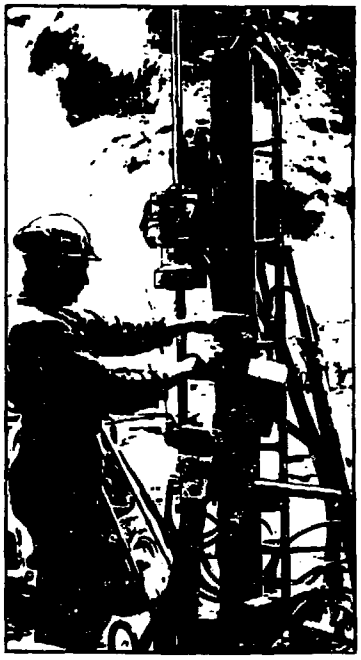

Technical Information Report No. 30

THE EFFECT OF RADON TRANSPORT IN GROUNDWATER UPON GAMMA-RAY BOREHOLE LOGS

P. H. Nelson, R. Rachiele, and A. Smith
Lawrence Berkeley Laboratory
University of California
Berkeley, California 94720

September, 1980

A Joint Project of

Swedish Nuclear Fuel Supply Co.
Fack 10240 Stockholm, Sweden

Operated for the Swedish
Nuclear Power Utility Industry

Lawrence Berkeley Laboratory
Earth Sciences Division
University of California
Berkeley, California 94720, USA

Operated for the U.S. Department of
Energy under Contract W-7405-ENG-48

LBL-11180
SAC-30
UC-70

LBL--11180

DE82 012616

THE EFFECT OF RADON TRANSPORT IN GROUNDWATER UPON GAMMA-RAY BOREHOLE LOGS

P.H. Nelson, R. Rachiele, and A. Smith
Lawrence Berkeley Laboratory
University of California
Berkeley, California 94720

September, 1980

This work was supported by the Assistant Secretary for Nuclear Energy, Office of Waste Isolation of the U.S. Department of Energy under contract W-7405-ENG-48. Funding for this project is administered by the Office of Nuclear Waste Isolation at Battelle Memorial Institute.

PREFACE

This report is one of a series documenting the results of the Swedish-American cooperative research program in which the cooperating scientists explore the geological, geophysical, hydrological, geochemical, and structural effects anticipated from the use of a large crystalline rock mass as a geologic repository for nuclear waste. This program has been sponsored by the Swedish Nuclear Power Utilities through the Swedish Nuclear Fuel Supply Company (SKBF), and the U.S. Department of Energy (DOE) through the Lawrence Berkeley Laboratory.

The principal investigators are L.B. Nilsson and O. Degerman for SKBF, and N.G.W. Cook, P.A. Witherspoon, and J.E. Gale for LBL. Other participants will appear as authors of the individual reports.

Previous technical reports in this series are listed below.

1. Swedish-American Cooperative Program on Radioactive Waste Storage in Mined Caverns by P.A. Witherspoon and O. Degerman. (LBL-7049, SAC-01).

2. Large Scale Permeability Test of the Granite in the Stripa Mine and Thermal Conductivity Test by Lars Lundstrom and Haken Stille. (LBL-7052, SAC-02).

3. The Mechanical Properties of the Stripa Granite by Graham Swan (LBL-7074, SAC-03).

4. Stress Measurements in the Stripa Granite by Hans Carlsson (LBL-7078, SAC-04).

5. Borehole Drilling and Related Activities at the Stripa Mine by P.J. Kurfurst, T. Hugo-Persson, and G. Rudolph (LBL-7080, SAC-05).

6. A Pilot Heater Test in the Stripa Granite by Hans Carlsson (LBL-7086, SAC-06).

7. An Analysis of Measured Values for the State of Stress in the Earth's Crust by Dennis B. Jamison and Neville G.W. Cook (LBL-7071, SAC-07).

8. Mining Methods Used in the Underground Tunnels and Test Rooms at Stripa by B. Andersson and P.A. Halén (LBL-7081, SAC-08).

9. Theoretical Temperature Fields for the Stripa Heater Project by T. Chan, Neville G.W. Cook, and C.F. Tsang (LBL-7082, SAC-09).

10. Mechanical and Thermal Design Considerations for Radioactive Waste Repositories in Hard Rock. Part I: An Appraisal of Hard Rock for Potential Underground Repositories of Radioactive Waste by N.G.W. Cook; Part II: In Situ Heating Experiments in Hard Rock: Their Objectives and Design by N.G.W. Cook and P.A. Witherspoon (LBL-7073, SAC-10).

11. Full-Scale and Time-Scale Heating Experiments at Stripa: Preliminary Results by N.G.W. Cook and M. Hood (LBL-7072; SAC-11).

12. Geochemistry and Isotope Hydrology of Groundwaters in the Stripa Granite: Results and Preliminary Interpretation by P. Fritz, J.F. Barker, and J.E. Gale (LBL-8285, SAC-12).

13. Electrical Heaters for Thermo-Mechanical Tests at the Stripa Mine by R.H. Burleigh, E.P. Binnall, A.O. DuBois, D.O. Norgren, and A.R. Ortiz (LBL-7063, SAC-13).

14. Data Acquisition, Handling, and Display for the Heater Experiments at Stripa by Maurice B. McEvoy (LBL-7062, SAC-14).

15. An Approach to the Fracture Hydrology at Stripa: Preliminary Results by J.E. Gale and P.A. Witherspoon (LBL-7079, SAC-15).

16. Preliminary Report on Geophysical and Mechanical Borehole Measurements at Stripa by P. Nelson, B. Paulsson, R. Rachiele, L. Andersson, T. Schrauf, W. Hustrulid, O. Duran, and K.A. Magnussen (LBL-8280, SAC-16).

17. Observations of a Potential Size-Effect in Experimental Determination of the Hydraulic Properties of Fractures by P.A. Witherspoon, C.H. Amick, J.E. Gale, and K. Iwai (LBL-8571, SAC-17).

18. Rock Mass Characterization for Storage of Nuclear Waste in Granite by P.A. Witherspoon, P. Nelson, T. Doe, R. Thorpe, B. Paulsson, J.E. Gale, and C. Forster (LBL-8570, SAC-18).

19. Fracture Detection in Crystalline Rock Using Ultrasonic Shear Waves by K.H. Waters, S.P. Palmer, and W.F. Farrell (LBL-7051, SAC-19).

20. Characterization of Discontinuities in the Stripa Granite--Time Scale Heater Experiment by R. Thorpe (LBL-7083, SAC-20).

21. Geology and Fracture System at Stripa by A. Olkiewicz, J.E. Gale, R. Thorpe, and B. Paulsson (LBL-8907, SAC-21).

22. Calculated Thermally Induced Displacements and Stresses for Heater Experiments at Stripa by T. Chan and N.G.W. Cook (LBL-7061, SAC-22).

23. Validity of Cubic Law for Fluid Flow in a Deformable Rock Fracture by P.A. Witherspoon, J. Wang, K. Iwai and J.E. Gale (LBL-9557, SAC-23).

24. Determination of In-Situ Thermal Properties of Stripa Granite from Temperature Measurements in the Full-Scale Heater Experiments: Methods and Primary Results by J. Jeffry, T. Chan, N.G.W. Cook and P.A. Witherspoon (LBL-8424, SAC-24).

25. Instrumentation Evaluation, Calibration, and Installation for Heater Tests Simulating Nuclear Waste In Crystalline Rock, Sweden by T. Schrauf, H. Pratt, E. Simonson, W. Hustrulid, P. Nelson, A. DuBois, E. Binnall, and R. Haught (LBL-8313, SAC-25).

26. Part I: Some Results from a Field Investigation of Thermo-Mechanical Loading of a Rock Mass When Heater Canisters are Emplaced in the Rock by M. Hood. Part II: The Application of Field Data from Heater Experiments Conducted at Stripa, Sweden for Repository Design by M. Hood, H. Carlsson, and P.H. Nelson (LBL-9392, SAC-26).

27. Progress with Field Investigations at Stripa by P.A. Witherspoon, N.G.W. Cook, and J.E. Gale (LBL-10559, SAC-27).

28. A Laboratory Assessment of the Use of Borehole Pressure Transients to Measure the Permeability of Fractured Rock Masses by C. Forster and J.E. Gale (LBL-8674, SAC-28).

29. Thermal and Thermomechanical Data for In Situ Heater Experiments at Stripa, Sweden by T. Chan, E. Binnall, P. Nelson, O. Wan, C. Weaver, K. Ang, J. Braley, and M. McEvoy (LBL-11477, SAC-29).

TABLE OF CONTENTS

LIST OF FIGURES

Page

LIST OF TABLES

ABSTRACT

Granitic rock at an experimental waste storage site at Stripa, Sweden is unusually high in natural radioelements (~40 ppm uranium) with higher concentrations occurring locally in thin chloritic zones and fractures. Groundwater seeping through fractures into open boreholes is consequently highly anomalous in its radon content, with activity as high as one microcurie per liter. When total count gamma-ray logs are run in boreholes where groundwater inflow is appreciable, the result is quite unusual: the radon daughter activity in the water adds considerably to the contribution from the rock, and in fact often dominates the log response.

The total gamma activity increases where radon-charged groundwater enters a borehole, and remains at a high level as the water flows along the hole in response to the hydraulic gradient. As a consequence, the gamma log serves as a flow profile, locating zones of water entry (or loss) by an increase (or decrease) in the total gamma activity.

A simple model for flow through a thin crack emanating radon at a rate E shows that the radon concentration of water entering a hole is $E/\lambda h$, where λ is the radon decay rate and h the crack aperture, assuming that the flow rate and crack source area are such that an element of water resides within the source area for several radon half-lives or more. If the water entering the borehole voume V is then mixed with the water already in that volume, then the concentration is $EQ/\lambda^2 hV$. Hence concentration measurements can provide a measurement of the inflow rate Q in cases where these conditions hold. Data from the 127-mm holes in the time-scale drift behave in this fashion.

If mixing within the borehole does not occur, the activity decreases exponentially along the hole away from the entry point, because of the steady decay of radon as it migrates in the water column. This spatial decay rate can be converted to a linear flow rate since the 3.8-day half-life of radon is known. For example, if the volumetric flow rate in a 76-mm hole falls within the range 0.5 to 50 liters per day, and if observations are available from a 10 m length of hole, then the flow rate can be measured quantitatively. Proportionately higher rates can be measured if longer hole lengths are available for observation. If the flow rate is quite high, then the gamma activity away from the entry point is constant because the radon does not have time to decay, and only a minimum flow rate can be established.

Because of its ability to measure flow at very low rates in open boreholes, the radon method or variants of it deserve further investigation. It is also apparent that the natural radioelement distribution at a potential waste storage site must be carefully determined. Even with good baseline data, it is possible that the naturally-occurring radioactive component in groundwater can change in response to changing hydrological conditions.

High levels of radon in subsurface waters can cause high concentrations in air. For health safety purposes, radon levels in air were monitored for a two-year time period. Air samples from the four working drifts almost always registered less than the 0.3 Working Levels required by U.S. mine safety standards. Maintenance of a safe working environment is attributed to the relatively low water infiltration rates, avoidance of ponding, and continual operation of the ventilation system.

1. INTRODUCTION

The motivation for documenting the natural radioelement distribution in and around a potential radioactive waste repository site is easily understood and justified. Without knowledge of the baseline conditions, any changes in the radiation environment during repository operations, whether due to man-made or natural causes, will be difficult or impossible to determine. For this reason, a goodly portion of the geological, geochemical and geophysical effort at the Stripa experimental site in central Sweden has been directed towards establishing the distribution and behavior of the naturally occurring radioelements in the rock and in the groundwater.

Figures 1.1 and 1.2 show the geological setting and the location of underground drifts and long boreholes at Stripa. Detailed maps of the underground test areas are given in Section 4. A large number of shorter boreholes ranging from 10 to 30 m in length were also drilled from the experimental drifts excavated in granite at the 338 m level. The iron ore, which has been extensively mined, is stratiformly bound within the leptite, a meta-volcanic series which forms a folded and faulted synclinal structure with a gently plunging ENE axis (Olkiewicz et al., 1979). Further geological description and cross sections are given by Olkiewicz et al. (1979).

This document reports our results with a total-count gamma-ray probe in boreholes drilled from the surface and from underground experimental drifts at the Stripa site. A companion report by Wollenberg et al. (1981) describes the radioelement distribution within the context of the geological setting. Earlier, Fritz et al. (1979) reported on the geochemical analyses done on water samples recovered from various sampling stations at the site. Besides

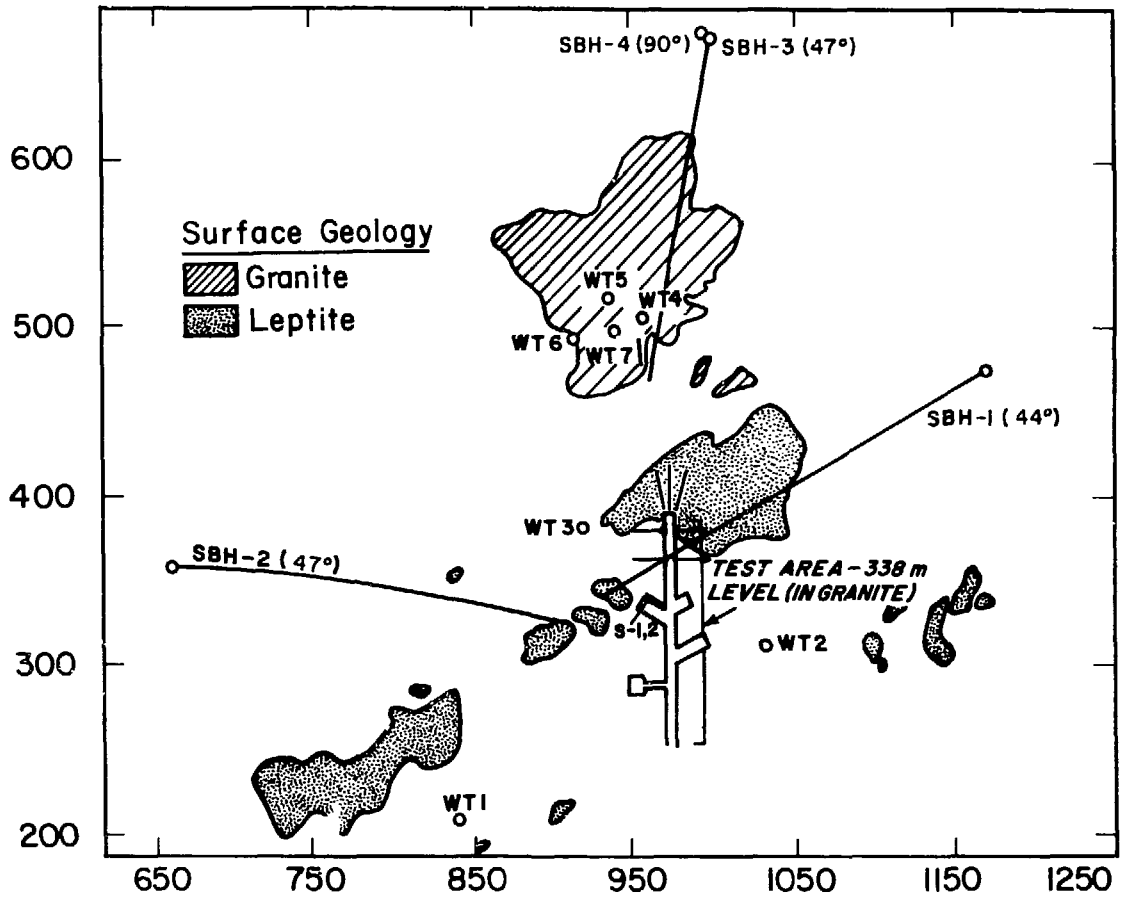

Fig. 1.1 Plan map of the Stripa site showing rock outcrop, inclined surface boreholes and underground experimental drifts. Mine coordinates given in meters.

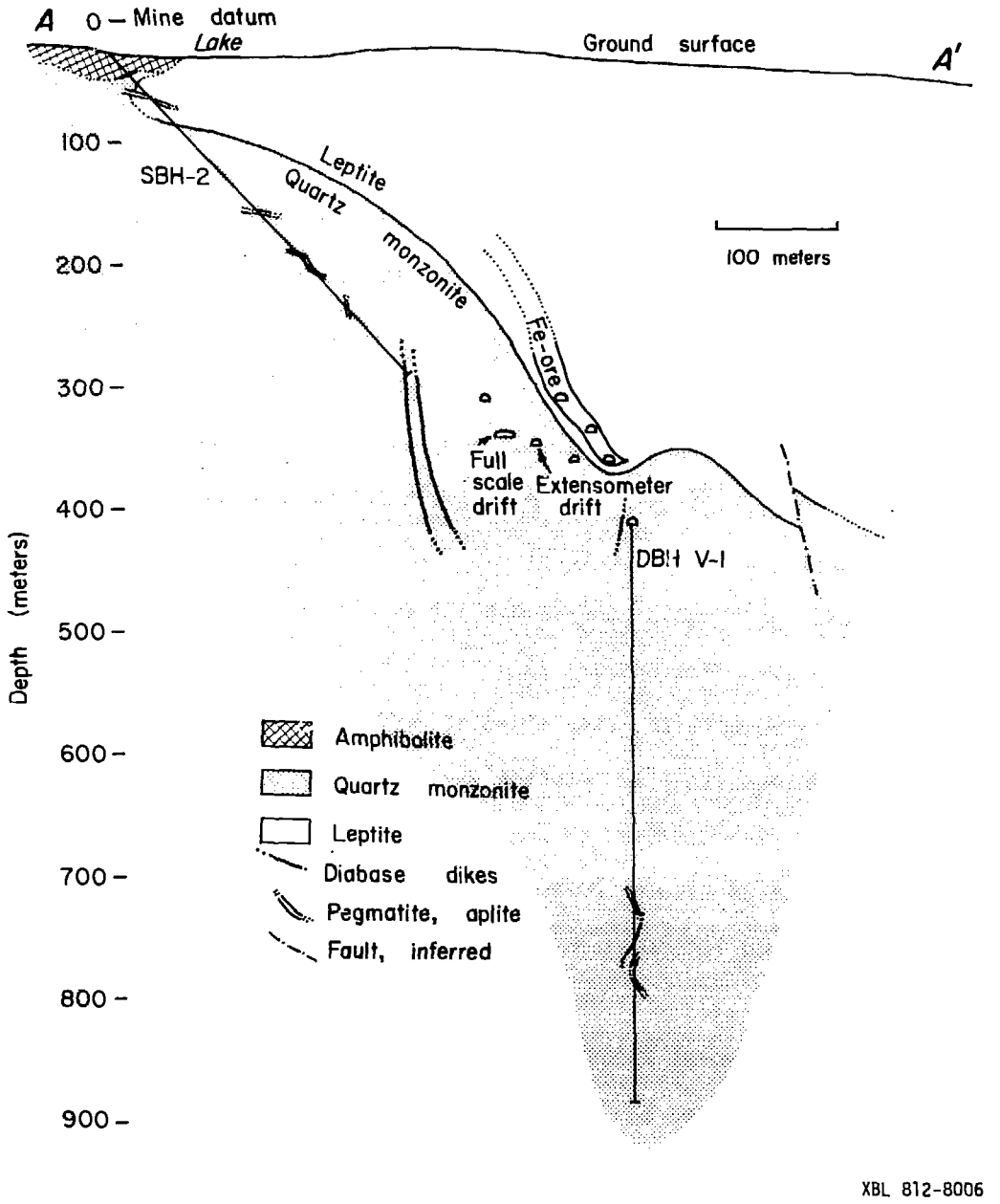

Fig. 1.2 Vertical cross-section bearing N89°E through boreholes SBH-2 and DBH V-1, from Wollenberg et al. (1981). Collar of DBH V-1 is located at x = 244 m, y = 1082 m, z = 410 m.

these programmed research activities, the radon content in the air in the underground working areas has been monitored throughout the experimental period for health safety purposes. The results and recommendations stemming from that data base are therefore included in this report.

As is well known, almost all measurable radioactivity in the earth's crust arises from potassium-40 and the decay series of uranium-238 and thorium-232. In our preliminary geophysical report on the work at Stripa (Nelson et al., 1979), we reported that the uranium and thorium content in the Stripa granite is around 40 and 30 ppm respectively, unusually high for a granitic rock. As a consequence, the decay of uranium and thorium daughter products dominate the total-count gamma-ray response, with the potassium decay contributing only about 10% of the response. We also called attention to an even more unusual aspect of the natural-gamma borehole logs: the response varied with the rate of water inflow into the borehole, a surprising phenomenon that was correctly attributed to the very high concentration of radon-222 dissolved in the groundwater. This result required further investigation, since, at worst, the radon contribution to the logs obscured the desired information on the radioelement distribution in the rock; while, at best, it provided information on the groundwater flow regime. Consequently, the general thrust of this report is the analysis of groundwater movement in open boreholes as detected by the gamma-ray signature of dissolved radon. The gamma-ray borehole logging probe afforded a convenient means of detecting the radon in this particular geohydrological environment.

The properties of radon and its generation, migration, and occurrence in the subsurface have attracted the attention of investigators from many disci-

plines. As a result the pertinent literature is spread throughout diverse journals and reports and would be almost impossible to locate were it not for the pair of review articles by Tanner (1964, 1980), who has painstakingly reviewed the field, providing extensive bibliographies. Since this report will focus mainly on observations of radon transport in boreholes, the reader is referred to Tanner's reviews and citations for background material on such topics as the physical mechanisms of radon emanation.

Although our study was done within the context of siting repositories for radioactive waste storage, our findings draw and impinge upon related work in several applied fields. Several papers concerning the dissolution, mixing, and transport of radon in groundwater were helpful in our studies. Andrews and Wood (1972) considered the emanation of radon in porous media as a function of grain size, coupling this to their observations of radon concentrations at a field site in England. Stoker and Kruger (1975) studied the use of radon as a tracer for geothermal reservoir engineering and developed a model for radial flow in a porous media; we adapted some of their concepts to our model for transport in a thin crack. In addition, D'Amore and Sabroux (1976-77) developed conceptual models for radon concentration in various mixing geometries pertinent to groundwater problems.

The use of gamma-ray spectrometry for uranium exploration has advanced considerably in the last decade, as reported in a state-of-the-art paper by Killeen (1979), which covers the application of spectrometers in airborne, surface, and borehole surveys for discovering, mapping, and quantifying the amount of uranium in place. Killeen also reviews the literature dealing with the practical problems encountered in field surveys and supplies a comprehen-

sive bibliography. Løvborg et al. (1980) conducted a borehole spectrometer survey at a uranium deposit in Greenland, logging 23 boreholes that were subsequently calibrated using core assays from each of the logged holes. Løvborg's work is especially interesting in the context of our study because it documents one of the few cases in the literature where radon present in the borehole fluid demonstrably perturbed the uranium estimate.

Ordinarily the gamma probe or the spectral gamma borehole probe is directly used in determining the distribution of potassium, uranium, and thorium, but occasionally it is useful in locating fossil or active flow systems where uranium, at one time dissolved in the groundwater, has been precipitated onto the surfaces of the permeable unit. A field case in an igneous system is described by West and Laughlin (1976). Spectral gamma logs obtained in a sedimentary sequence (Fertl et al., 1980) display uranium peaks along fractured zones in a chalk, thereby delineating permeable target intervals where the casing was then perforated for the production of oil and gas. These examples demonstrate the use of the spectral borehole probe at repository sites to find fracture flow zones; in fact this application was one of our evaluation goals in using the gamma probe at Stripa. It should also be pointed out that multi-channel spectrometers have been employed at radioactive waste sites to locate radioisotopes migrating away from the site in the groundwater (Eggers, 1976).

The monitoring and control of radon in underground mine atmospheres has become of interest as standards have tightened in an effort to mitigate the health hazard posed by radon and its daughter products. Dungey et al. (1979) describe their experiences in the measurement and control of radon in

the atmospheres of several mines in Cornwall, England. They are particularly cognizant of the role of groundwater in transporting radon from the rock mass into working air, stating that radon is released rapidly from ground-water once the water pressurized in boreholes and fissures is depressurized. Their findings corroborate the report of Jackson et al. (1980), who estimated that only a very small fraction of the radon released from underground uranium mines in the United States is transported by drainage waters, most of it having already been released into the mine ventilation system. Although we made no attempt to assess the interaction of groundwater and airborne radon transport in the Stripa experimental drifts, it is apparent from our experience that the two are closely related.

In this report, Section 2 describes the gamma-ray probe used at Stripa, concentrating upon its response to radon daughters in the borehole. Section 3 describes some simple mathematical models of the consequences of radon present in simple geometries that simulate a fracture and a borehole. These models are then used in Section 4 to explain some of the phenomena observed in the logs; this section also presents almost all the gamma ray logs obtained at Stripa. The report concludes with a section describing the monitoring of radon levels in air in the working areas of the underground experimental areas over a two-year period.

2. GAMMA-RAY MEASUREMENTS

2.1 Basic Considerations

All radioactive phenomena observed in natural earth materials are due to the decay of members of the potassium-40, uranium-238, and thorium-232 decay series. Figure 2.1, showing the results of spectral gamma-ray analyses on Stripa core, demonstrates this fact. The Stripa rock, however is unusual in the amount of uranium and thorium that have been detected in it--approximately 40 ppm uranium and 30 ppm thorium are uniformly present in the N1 core. In most granitic rocks, the concentration of uranium is in the 3 to 15 ppm range and the Th/U ratio ranges from 3 to 5.

A total-count gamma-ray log obtained in the N1 borehole is also shown in Fig. 2.1. The background levels of 40 ppm uranium, 30 ppm thorium and 4% potassium in rock have contributed a 200-cps count rate for the particular probe and geometry used in this study. The total count probe combines the gamma counts contributed by all three decay series, although the energetics of the different species are such that potassium is contributing 10% of the total. Peaks on the total-count gamma ray log generally correlate well with increased uranium and thorium concentration, though the characteristics of the probe tend to broaden the signature of these narrow local concentrations.

A gamma spectrum of a sample of crushed core from Stripa, obtained with a large NaI detector in the low-background counting facility at LBL, is shown in Fig. 2.2. The gamma spectrum emitted by the rock is extremely complex, containing hundreds of spectral lines (Smith and Wollenberg, 1972). This complexity is obscured in Fig. 2.2, however, because most of the individual lines are of such low intensity that only a few dominate the observed spectrum.

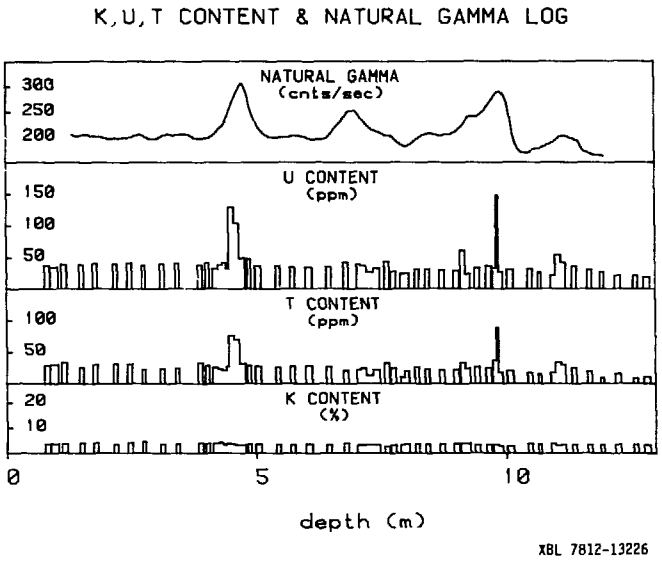

Fig. 2.1 Total-count gamma log from hole N1 and uranium, thorium, and potassium analyses from spectral gamma-ray laboratory method.

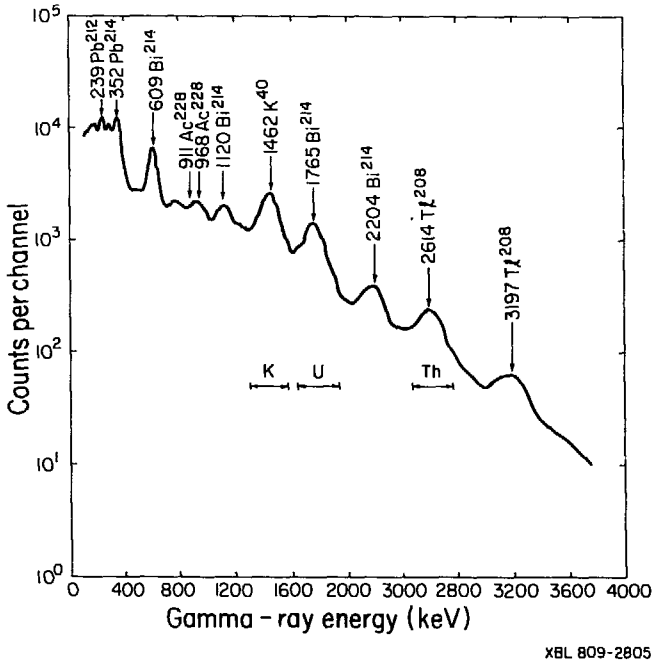

Fig. 2.2 Gamma-ray spectrum on crushed core sample from 3.10 - 3.49 m interval in borehole N1, time-scale drift. Energy (keV) and isotope identified above prominent peaks. Windows for potassium, uranium, and thorium analysis specified by horizontal arrows. Sample contains 44.6 ppm U, 27.0 ppm Th and 4.10% K.

In addition, the characteristics of a NaI scintillation crystal severely limit the obtainable resolution. The spectral assays shown in Fig. 2.1 were obtained from spectra such as that in Fig. 2.2 after appropriate gamma energy intervals were chosen and spectrum stripping techniques were applied. A total-count system with no spectral capability will simply count all events contributing to the spectrum, as long as the energy threshold permits. Hence the total-count borehole measurements are a gross indicator of the summed gamma emissions of all isotopes in the three major decay series.

The uranium-238 decay series is portrayed in Fig. 2.3. The higher members of the series generally have quite long half-lives. Lower members, radon-222 and its daughters, possess comparatively short half-lives. As indicated in the spectrum of Fig. 2.2, the great preponderance of gamma energy emitted by the entire series is due principally to the Bi-214 isotope, with Pb-214 a secondary contributor. Therefore the measured gamma decay of Bi-214 can be quantitatively related to a higher member of the series only if it is in secular equilibrium with that member, that is, only if all of the intervening daughter products have remained in place during the decay processes. As a consequence, the count rate measured by a calibrated borehole probe can be used to assay uranium in place only if all daughter products, including radon, have neither migrated away nor been contaminated by the addition of mobile radioactive species.

Radon is the only gas in the uranium and thorium decay series; consequently it is more mobile than other members of the series and is often responsible for disequilibrium conditions. As indicated in Fig. 2.3, radon-222 results from the decay of radium-226. The mechanism of radon

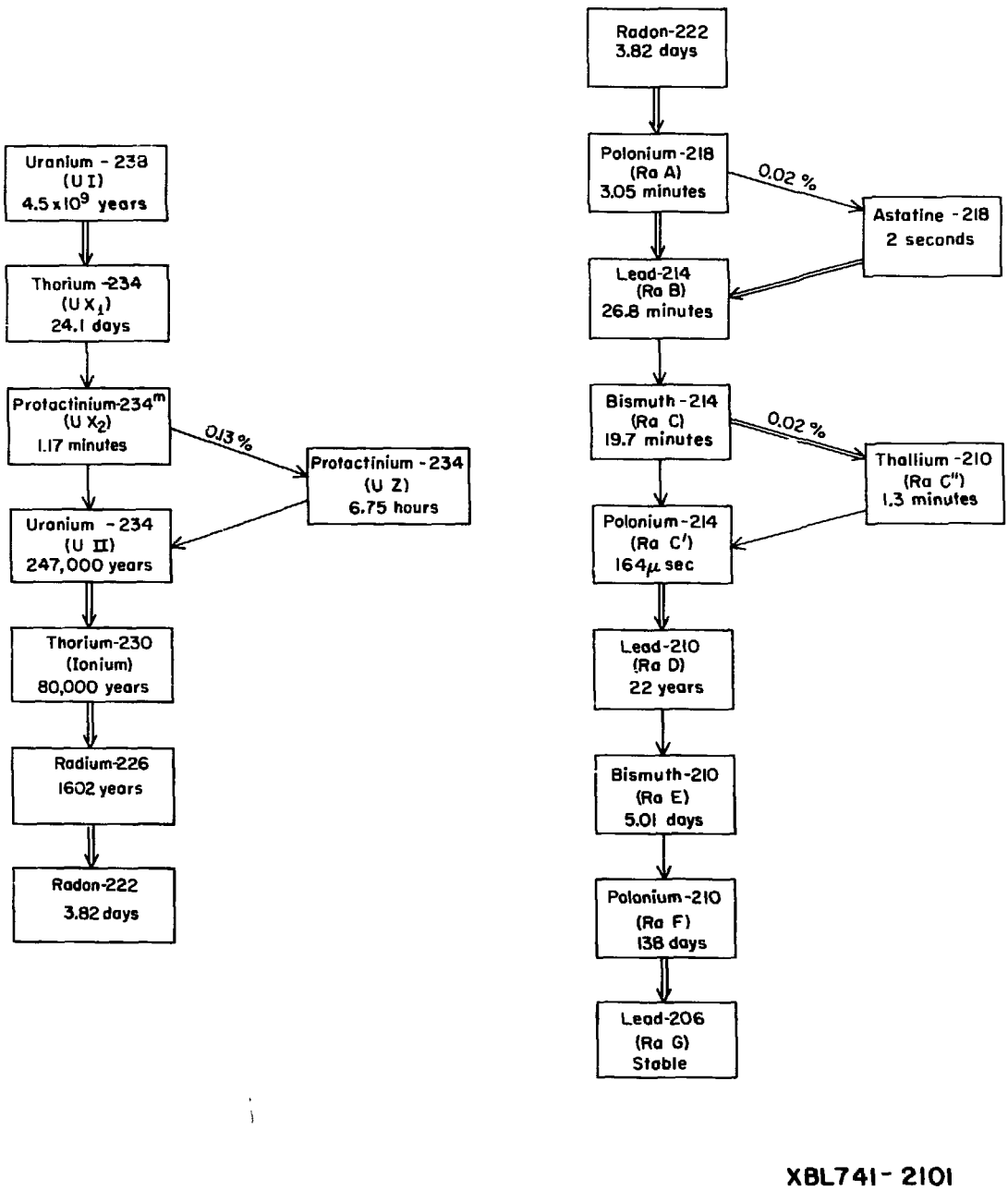

Fig. 2.3 The U-238 series decay chain, adapted from Smith and Wollenberg (1972).

escape and migration are reviewed by Tanner (1964, 1978). The direct detection of radon utilizes the alpha emission characteristic of its decay. However, since the decay times of Bi-214 and Pb-214 are short relative to that of radon, many situations can be envisioned where the radon daughters effectively remain in equilibrium with migrating radon, and hence their gamma activity reflects the amount of radon present. This principle allows us to use the gamma probe as a detector of the presence of radon in a steady-state hydrological situation.

2.2 Instrumentation

The gamma-ray probe was one of a set of borehole geophysical tools used at Stripa (refer to Nelson et al. (1979) for a complete description of the logging system). The total-count gamma probe used for this study was acquired with the Mt. Sopris 3000NB logging system produced by the Mt. Sopris Instrument Co. of Delta, Colorado. Pulses produced by the gamma ray tool were counted and integrated by the Mt. Sopris ratemeter and the output was recorded in the form of counts per second on the chart recorder. Logs were recorded at a depth scale of 50:1 or 1/2 m of borehole per 1 cm of chart paper. Averaging time was 4 sec at a logging speed of 2.5 m/min. Logs were acquired at a scale of 50 counts per second (cps) per cm of chart paper with a backup log at a scale of 25 cps per cm. The dead-time compensation circuitry in the ratemeter was not needed and was not used. Total pulses could also be counted for a specified period of time by a Canberra model 1775 nuclear counter operated in parallel with the ratemeter.

The gamma probe is 32 mm in diameter and 2.07 m in length. Gamma rays are detected by a 12 mm x 38 mm NaI(Tl) scintillation crystal. Gamma rays

interact with the scintillation material to produce flashes of light within the crystal that are then converted to electrical pulses by a photomultiplier tube. Intensity of the flash, and thus the height of the pulse, is proportional to the energy of the incident gamma ray. Sensitivity of the crystal to gamma rays of varying energy is a function of the crystal size. The detector circuit has no adjustable discriminator setting; the low energy cutoff is estimated to be about 50 keV.

Knowing the radioelement concentration allows us to calibrate the probe used at Stripa. The International Atomic Energy Agency (1976) suggests that calibration of a total-count gamma-ray probe be based on a new unit called the unit of radioelement concentration, abbreviated "ur," and defined in terms of the instrument response to one part per million of uranium in equilibrium with its daughter products. An empirical relation between the observed count rate and radioelement concentration (P.H. Dodd, private communication, 1979) that appears applicable to our case is:

$$N(\text{counts per second}) = k\,[1.5\,K(\%) + U(\text{ppm}) + 0.47\,Th(\text{ppm})]. \quad (2.1)$$

Using the data from the upper 4 m in borehole N1, as given in Fig. 2.1 and in Appendix A of Nelson et al.(1979), the average values are K = 4.29 %, U = 42.7 ppm, Th = 31.6 ppm, and N = 205 cps. The resulting sensitivity factor for this particular probe is then k = 3.3 cps/ur.

The gamma probe remained at Stripa for 2.5 years, from January 1978 to mid-1980. During this period, repair work was performed two or three times, which required that the probe housing be opened. No truly adequate provisions were established for referencing the count rate of the probe during its service time, such as a calibration jig and a gamma source would have provided.

However, checks at the top of borehole N1 near the beginning and end of the 2.5 year service period showed that the count rate was within about 5 cps out of 210 cps. Stability was not this good overall, however; a drop in count rate of about 10% was noted during one 3-week operating period. The cause of this instability was not determined.

2.3 Radioactivity in Groundwater

Many gamma-ray borehole logs from Stripa are well above the 200 cps rate for much of their length. Most notable are several logs from the time-scale heater holes. During the time-scale heater experiment, water was regularly removed from the heater holes. Those with high overall gamma count rates were also the holes with the higher water inflow rates. Figure 2.4 demonstrates a good linear correlation between water inflow rate and gamma count rate. Thus the gamma log was recognized as a potential water flow indicator at Stripa.

Radon dissolved in water was the suspected cause of the exceptionally high count rates. To confirm that radon was being transported by water into the boreholes, a sequence of logs was run in borehole M3, a 38 mm diameter hole located at the rear of the time-scale drift. Hole M3 is unusual in that it has an exceptionally high flow rate. The water was removed from M3 and several gamma ray logs were run over a period of a day as water infiltrated into the hole. A gamma log recorded prior to dewatering and the logs run sequentially after the dewatering are shown in Fig. 2.5. Low count rates were observed with the probe in air, high rates in water, and a shelf reflecting the air-water interface can be seen rising upwards progressively in the three logs obtained 0:06, 1:02, and 1:33 hours:minutes after water

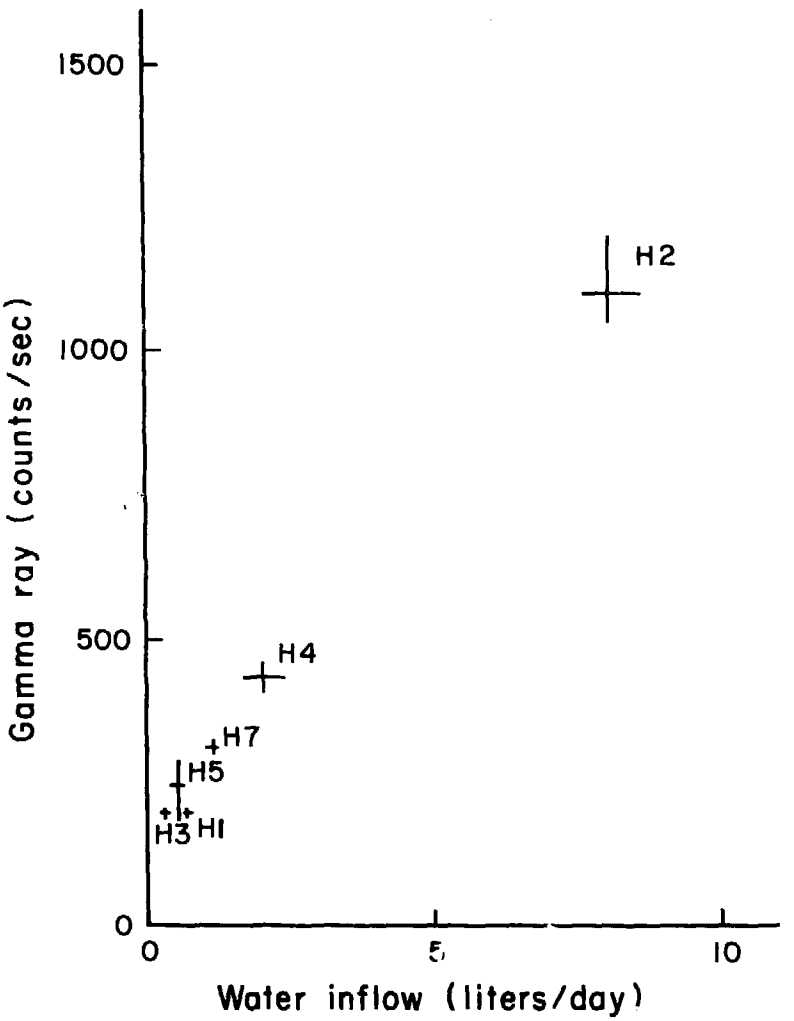

Fig. 2.4 Borehole gamma-ray logs and water inflow rates in time-scale heater holes.

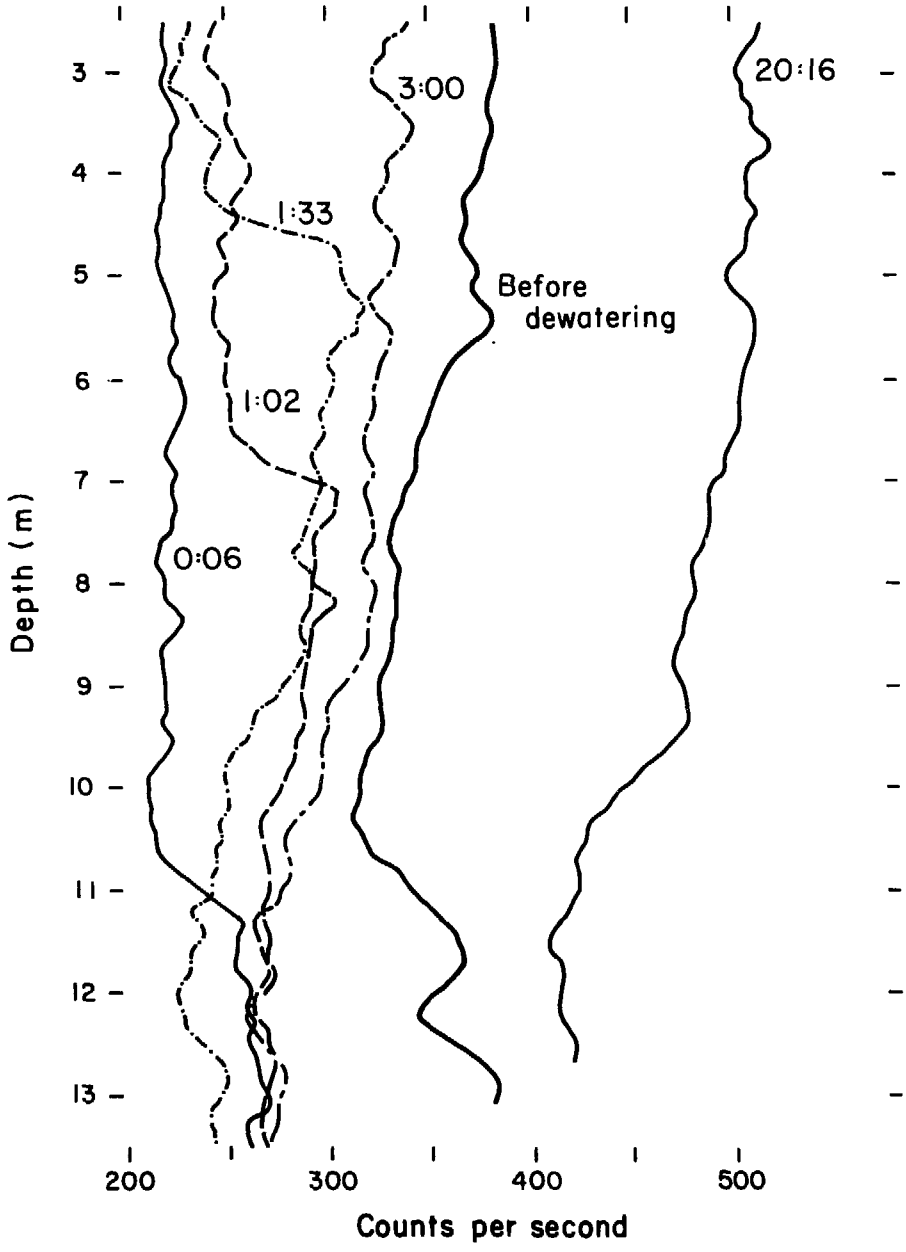

Fig. 2.5 Sequence of gamma-ray logs in hole M3, which was dewatered at 0:00 hours. Final log was run 20:16 hours:minutes later.

removal. The rising shelf confirms that water flowing into the holes was responsible for the high gamma activity seen in the logs.

Of the underground boreholes, M3 has had an exceptionally high inflow since it was first drilled. Water samples for geochemical analysis were taken from M3 in 1977 and 1978 when the inflow was about 216 liters per day (Fritz et al., 1979). The inflow rate can be estimated from the rate of rise of the shelf in Fig. 2.5 to be about 124 liters per day in January 1979. Eleven months later, in December 1979, the outflow from M3 was measured directly as 995 ml in 10 minutes, equivalent to 143 liters per day. This latter measurement was higher than the January rate because the holes in the neighboring ventilation drift were packed off in November 1979 for the macropermeability experiment. The closure of the ventilation drift boreholes noticeably increased the water flow into boreholes and along exposed fractures in the rear of the time-scale drift.

To check that radon was the radioelement being transported by water, a water sample from M3 was collected in a 60-liter vessel of 0.18 m radius and the gamma-ray probe inserted into it through a rubber stopper. The count rate was then monitored for 13 days as shown in Fig. 2.6. The straight line, shifted vertically to match the data, has a slope determined by the decay rate of radon-222.

Fortunately, water from M3 has been analyzed for radon, as reported by Fritz et al. (1979). Table 2.1 shows that the M3 sample yielded radon-222 values of 1.9 and 1.3 microcuries per liter from analyses performed in two laboratories. The concentration level is extremely high, some three to six orders of magnitude greater than radon concentrations normally found

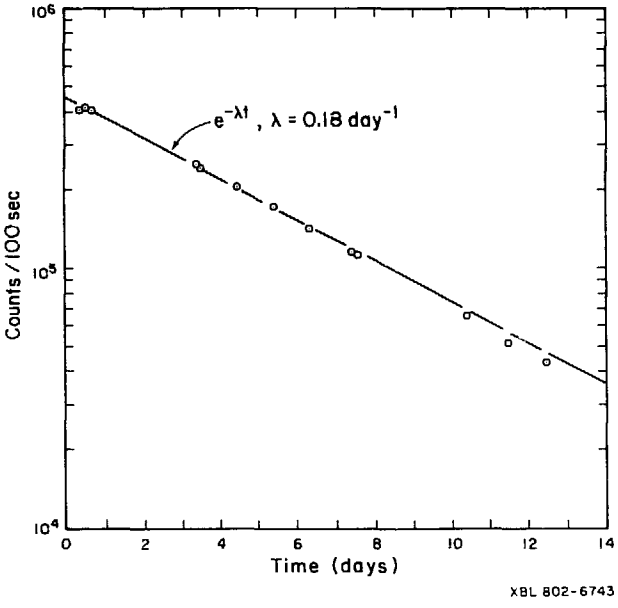

Fig. 2.6 Gamma ray activity of water from M3, measured with probe inserted into 60-liter vessel. Count time is 100 seconds. The straight line gives the decay of radon-222.

Table 2.1 Radon-222 and radium-226 analyses reported by Fritz et al. (1979), Tables 1 and 14. Samples designated AT were analyzed by AB Atomenergi, Sweden; UB, by University of Bath, Great Britain.

Sample number	Location	Sampling Date	Radon-222 (μci/l)	Radium-226 (pCi/l)
16(AT)	M3	9-21 Sept 77	1.9	n.d.
16(UB)	M3	9-21 Sept 77	1.3	34
17(AT)	410-hole 6.3-50m	9-20 Sept 77	0.48	n.d.
29(UB)	410-hole 376.5-471m	Jan-Mar 78	0.56	40

in groundwater. These uniquely high concentrations explain why there are almost no similar observations reported in the literature. The field study by Løvberg et al. (1980) is the only other study known to us where radon in the borehole was reported to perturb the gamma ray measurement.

A second test quite similar to that of Fig. 2.6 was run to examine the early time behavior of the count rate, with the results shown in Fig. 2.7. The activity requires some 3 to 4 hours to reach a maximum before starting to decline, after which the decay rate duplicated that of Fig. 2.6. The build-up time of Fig. 2.7 is controlled by the half-lives of Pb-214 and Bi-214, each being about 20 minutes. The computed curve incorporates the lag introduced by Bi and Pb, providing good assurance that the daughter products have not stayed with the radon parent during the transport process. Presumably they plated out onto the surface of the high-flow, small-diameter hole, or onto the surfaces of the small diameter tubing used to connect hole M3 to the sampling vessel.

The result of Fig. 2.7 would seem to pose a dilemma for the detection of radon in boreholes by gamma techniques, since it indicates that radon is out of equilibrium with its daughter products. But, this is not a problem because of the very low rates of flow. The highest rates observed are on the order of 100 linear meters per day; consequently the one-hour error would result in four meters of mislocation. Most rates are less than this. There is also the question of cations plating onto the probe itself. This was not observed, however, as bi-directional passes of the probe through high count zones did not appear to disturb the patterns.

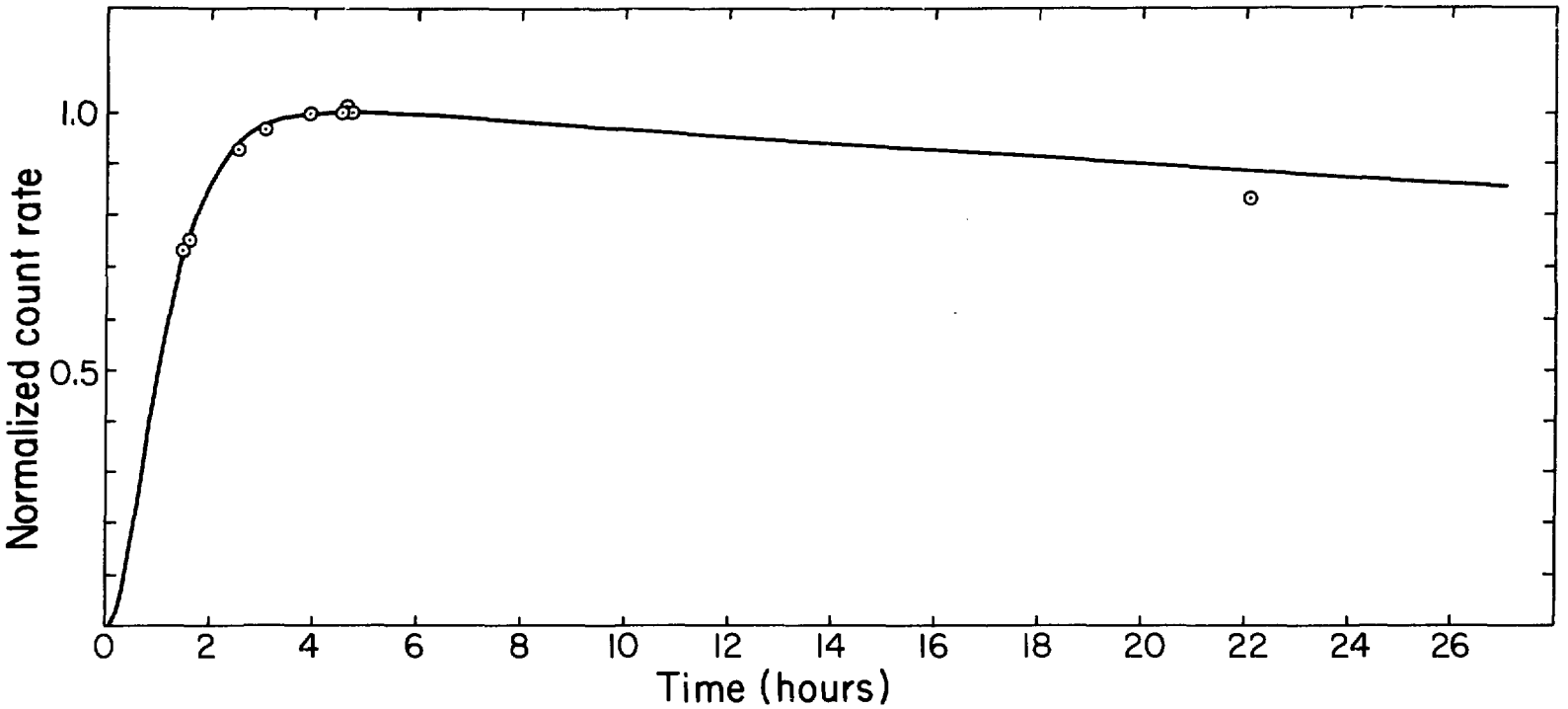

Fig. 2.7 Gamma ray count rate measured in a 127 mm diameter pipe filled with water from borehole M3. The solid computed curve accounts for the buildup and decay of radon daughter products, assuming no daughters were initially present in the sample. The 1.5 hours elapsed time before the acquisition of the first data point is a reasonable estimate of the time required to fill the pipe, including the transit time from the fracture egress to the sample vessel inlet.

A size effect for boreholes containing radon-charged water was quite evident from the logs run at Stripa. High-flow boreholes showed a progressive increase in count rate with hole diameter, which would be expected as the amount of radon present in the probe-wall annulus increases. Both analytical and empirical checks are discussed next to examine the effect of hole size on gamma-ray absorption and generation.

2.4 Computation of Borehole Effects

Case 1 -- general case. Figure 2.8 illustrates the general and specific borehole cases of interest in addressing the problems of borehole attenuation and the impact of a radioactive source within the probe-borewall annulus. In this figure, a source of M_1 photons per cm^3-sec occupies the annulus between a probe of radius c and the borehole of radius a. Outside the borewall is a pervasive source, M_2. We consider the detector to be a spherical detector, localized at the coordinate origin. Conceptually, following Rhodes et al. (1961), the gamma flux at the detector is obtained by integrating over the source volume,

$$I = \int_V M\, G\, \beta\, dV \qquad (2.2)$$

where M (photons/cm^3/sec) is the source strength, $G = 1/4\pi R^2$ accounts for geometric spreading from a point source a distance R from the detector, and β is the dimensionless attenuation factor. The factor β takes the form $\exp(\mu R)$, where μ is the linear attenuation coefficient (cm^{-1}) for gamma rays of a specific energy.

To our knowledge, formulae derived from Eq. (1) for the general case of Fig. 2.8 do not exist in the literature. However, Czubek (1962) and Rhodes

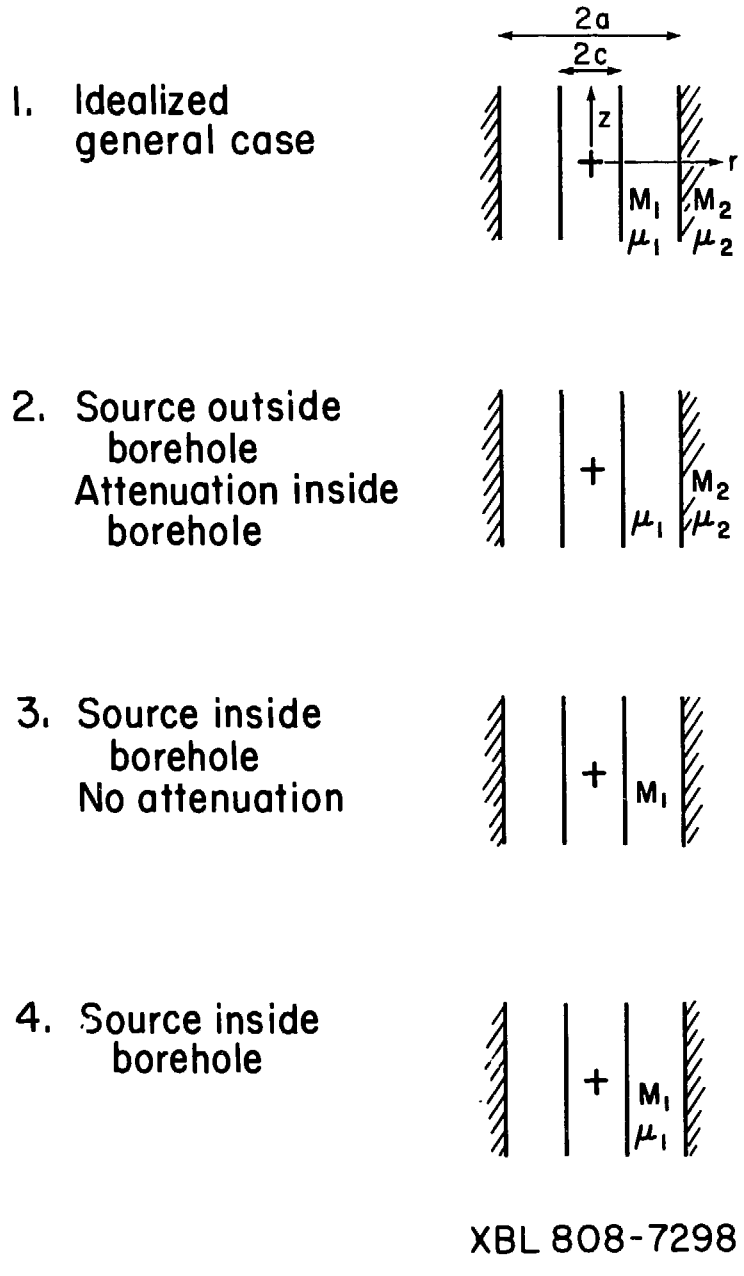

Fig. 2.8 Detector probe in a borehole surrounded by medium of source strength M and attenuation coefficient μ. Probe radius is c, borehole radius is a. The small cross at the coordinate center denotes the location of a spherical point detector.

et al. (1961) present solutions for special cases applicable to our geometry as shown in the following paragraphs.

Case 2 -- external source with attenuation. Czubek (1962) gives results pertinent to case 2 of Fig. 2.8, where we consider the attenuation due to water of gamma rays incident from the rock. (Czubek's flux term J_∞ is equal to M_2/μ_2 in our nomenclature). Using Czubek's results, attenuation curves for the diameter range of interest ($32 < 2a < 127$ mm) are constructed in Fig. 2.9. The formulation by Rhodes et al. provides a check case for the results of Czubek, for the limiting case where the probe radius goes to zero:

$$\frac{\mu_2 I}{M_2} = \int_0^{\pi/2} \cos\phi \exp(-\mu_1 a \sec\phi)\, d\phi \qquad (2.3)$$

The tabulation of this integral by Rhodes et al. confirms the graphical results of Czubek.

The attenuation curves in Fig. 2.9 have a few shortcomings. Because μ varies with photon energy, and because the total count probe measures over a broad energy spectrum, there is an inherent uncertainty in the choice of μ. The range of values shown in Fig. 2.9 illustrate the effect of μ upon the attenuation factor. A second, more serious discrepancy is the apparent discordance between the calculated values and empirical factors available in the literature, which indicate that the real attenuation is less than indicated in Fig. 2.9 for either the centralized or the decentralized cases. Dodd and Eschliman (1972) indicate that the correction for a decentralized probe should be about 0.9 for a 127-mm borehole. Wilson et al. (1979) give a

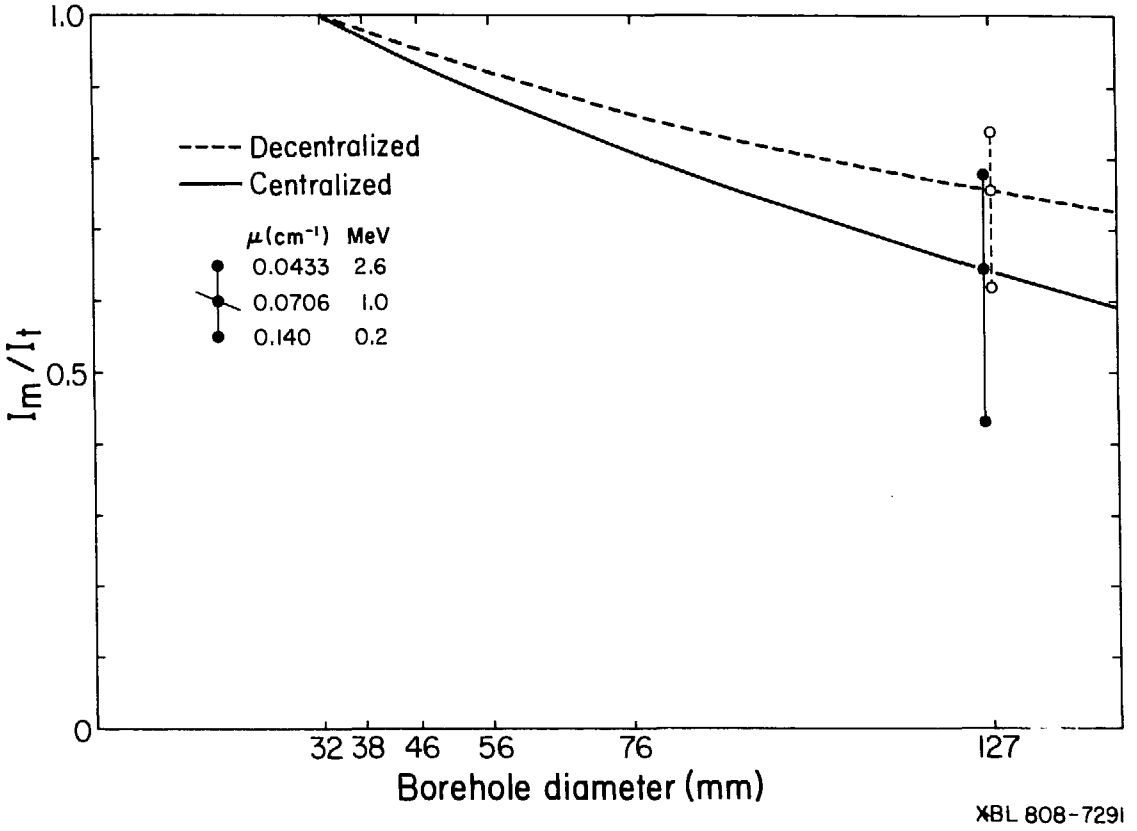

Fig. 2.9 Gamma ray attenuation by water in borehole, Case 2, gamma rays incident from a source external to the borehole, from Czubek (1962). The ratio I_m/I_t indicates the measured/true ratio. The two curves are drawn for an attentuation factor of a 1 MeV photon in water; the upper and lower bounds correspond to the spread of photon energies as shown in the key.

factor of about 0.8 for windowed peaks using a 38-mm crystal. Other empirical data and a subsequent discussion by Wilson et al. indicate that this value will increase for a smaller crystal used in a total-count mode.

A third reason that the curves of Fig. 2.9 appear unsatisfactory for our purposes is that our gamma logs (presented later in this report) show no trends indicating a borehole attenuation effect of more than 10%. Despite the hole-to-hole variability caused by geological and radon variations, a diameter dependence of more than 10% should be evident from inspection of the data, but it is not. For these reasons, no borehole diameter correction for attenuation has been applied to any of the gamma ray logs.

Case 3 -- source inside borehole, without attenuation. We now consider the case applicable to the presence of radon-charged water within the borehole, with no source outside the hole. If attenuation is ignored by setting the factor β of Eq. (1) at one, then the volume integral becomes,

$$I = \frac{M_1}{4\pi} \int_0^{2\pi} \int_c^a \int_{-\infty}^{\infty} \frac{r}{r^2+z^2} \, dz dr d\theta \tag{2.4}$$

the integral over z is

$$\int_{-\infty}^{\infty} \frac{dz}{r^2+z^2} = \frac{1}{r} \tan^{-1} \frac{z}{r} \Bigg|_{-\infty}^{\infty} = \frac{\pi}{r}$$

so that

$$I = \frac{\pi}{2} (a-c) M_1 \, , \tag{2.5}$$

which shows that the intensity increases linearly with borehole size if attenuation can be ignored, as it can be if the diameter is sufficiently

small. Equation (4) is used to construct the uppermost curve ("μ=0,cen") in Fig. 2.10.

Since many of the gamma measurements were made in inclined holes, we need to consider the decentralized case where the probe is positioned against the borehole wall. Figure 2.11 provides the geometry necessary to examine the problem. From the previous integration of Eq. (2.4), it should be clear that the integration over z is not affected by the off-centering of the probe, leaving only the r and θ integrations. With the center of the coordinate system at the probe center, the equation for the outer boundary is:

$$b = -s\cos\theta + \sqrt{a^2 - s^2\sin^2\theta} \quad , \tag{2.6}$$

where

$$s = a-c$$

so that

$$I = \frac{M_1}{4}\int_0^{2\pi}\int_c^b dr\, d\theta$$

$$= \frac{M_1}{2}\int_0^{\pi}\left[-s\cos\theta + a\sqrt{1-(s^2/a^2)\sin^2\theta} - c\right] d\theta$$

$$= M_1\frac{\pi}{2}\left[\frac{2a}{\pi}E\left(s/a, \frac{\pi}{2}\right) - c\right] , \tag{2.7}$$

where the function E is an elliptic integral of the second kind. This latter expression was evaluated to construct the dashed curve (0,decen) in Fig. 2.10.

Case 4 -- source inside borehole, with attenuation. For the geometry of case 4, in Fig. 2.8, the formulae of Rhodes et al. can be reduced to:

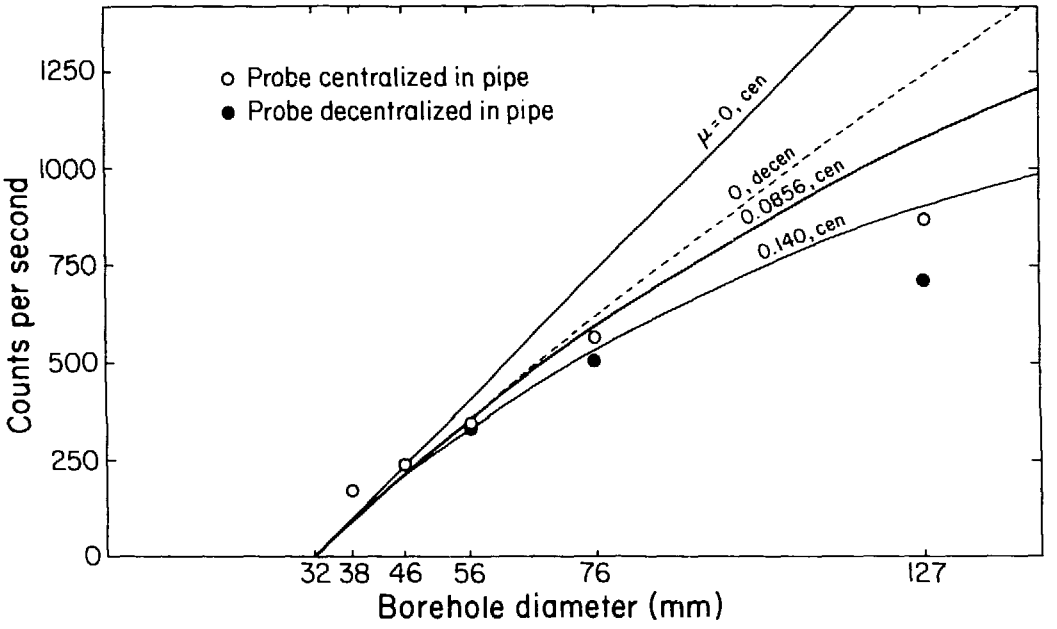

Fig. 2.10 Effect of radon-charged water in boreholes of varying diameter. Upper two curves computed from case 3; lower two from case 4 (see Fig. 2.8). A decentralized model is designated as decen. Data points are the corrected values from Table 2.2.

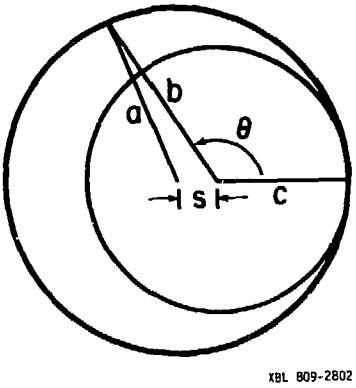

Fig. 2.11 Nomenclature for probe decentralized in borehole.

$$\frac{\mu_1 I}{M_1} = 1 - \int_0^{\pi/2} \cos\phi \exp\left[-\mu(a-c)\sec\phi\right] d\phi \ . \qquad (2.8)$$

This expression was evaluated numerically to construct the lower two curves with non-zero μ values in Fig. 2.10. Note that the effect of attenuation by water in the borehole becomes important in boreholes of diameter greater than 56 mm, until it reduces the observed flux by 1/3 in boreholes of 127 mm diameter. The attenuation by water will not cause the curves to reach an asymptote unless the probe is centered in a borehole considerably larger than 127 mm, however. No curves were developed for the decentralized geometry with the effect of water attenuation.

2.5 Experimental Determination of Borehole Effects

Having determined that radon-charged groundwater in the borehole could dominate the gamma-log response, we assessed the effect of borehole size on the counting rate contributed by the radon daughters. These tests were carried out near the time-scale drift, using a set of iron pipes of appropriate diameter. The pipes were filled with water from borehole M3, and the counting rate read with the gamma ray probe inside each of the pipes, first in a centralized position and then in a decentralized position, with the probe pressed against the wall of the pipe. The measurements were relative only; no attempt was made to measure the amount of radon in the water. The only constraint was to do the measurements in a time that was short compared with the radon half-life so that the radon activity in each pipe would be approximately the same.

The count rates measured with the M3 groundwater in the pipes is given in Table 2.2. It was impractical to distinguish between the centralized and decentralized positions of the 32 mm probe in the 38 mm and 46 mm pipes, and the results seemed to be unaffected by probe position in pipes with a diameter smaller than 56 mm. Hence the 277 and 338 counts per second values in Table 2.2 apply to both the centralized and decentralized positions.

The count rate observed with water-filled pipes also contained a contribution from the background within the drift. The probe suspended in air registered 146 counts per second. The count rate measured in each pipe with no water is given Table 2.3. The decrease from 146 to about 100 cps is attributed to absorption of gamma rays by the wall of the pipe. If the probe-pipe annulus were filled with radon-free water, the water would further attenuate the background contribution. This final correction for water attenuation has minor impact and is difficult to assess, as mentioned previously. Therefore the background contribution was subtracted directly from the second set of measurements (Table 2.2).

The corrected data are plotted in Fig. 2.10. The count rate increases with borehole diameter, linearly at small diameters, and becomes less than linear at larger diameters as the effect of attenuation becomes progressively more important. Superimposed on the data are four curves, computed from cases 3 and 4. The two cases with no attenuation are clearly inadequate, especially at larger diameters. The two curves with attenuation incorporated match the data better as the attenuation factor increases. (The value of 0.0856 cm^{-1} corresponds to a photon energy of 0.6 MeV; 0.14 cm^{-1} corresponds to 0.2 meV). It does appear that a decentralized attenua-

Table 2.2 Count rate measured in water-filled iron pipes, using radon-charged water from borehole M3. The corrected rate accounts for background activity in the drift given in Table 2.3. Measurements were done in the time-scale drift in April 1980. Values are the average of two 100-second counting intervals.

Nominal Diameter (mm)	Measured Count Rate (per second)		Corrected Count Rate (per second)	
	Centralized	Decentralized	Centralized	Decentralized
38	277	---	174	---
46	338	---	241	---
56	437	421	344	328
76	665	602	568	505
127	972	812	872	712

Table 2.3 Count rate measured in air-filled iron pipes of different diameters. The probe suspended in air registered 146 counts per second. Measurements were done in the time-scale drift in April, 1980.

Nominal Diameter (mm)	Measured Inside Diameter (mm)	Wall Thickness (mm)	Count Rate (per second)
38	39.0	3.0	103
46	46.5	4.0	97
56	57.0	4.0	93
76	78.5	3.5	97
127	126.0	3.0	100

tion model would reduce the 0.14 cm^{-1} curve to a level in rough agreement with the decentralized data, judging from the ratios of the case 3 no-attenuation curves.

The limitation of the models appears to be the restriction to monoenergetic photons, without knowledge of a suitable attenuation value. It is quite possible that the attenuation factor will change with borehole diameter, due to skewing of the incident spectrum by the water and probe housing. From the plot it also appears that the 38-mm measured value is too high, possibly from an error in the experimental procedure.

Figure 2.12 furnishes a final observation on diameter dependence. The data are taken from the maximum count rate observed in the highest flow holes of each diameter size, with 200 cps subtracted to remove the gamma flux incident from the rock. Picking high flow rate holes helps ensure that the measured count rate is close to the equilibrium count rate of radon-charged water within the rock mass. As a consequence, the increasing trend of Fig. 2.12 shows that the entering initial concentrations among the several boreholes must be comparable to within a factor of 2. In addition, the plot clearly demonstrates the need for a diametral correction when comparing such data from different size boreholes.

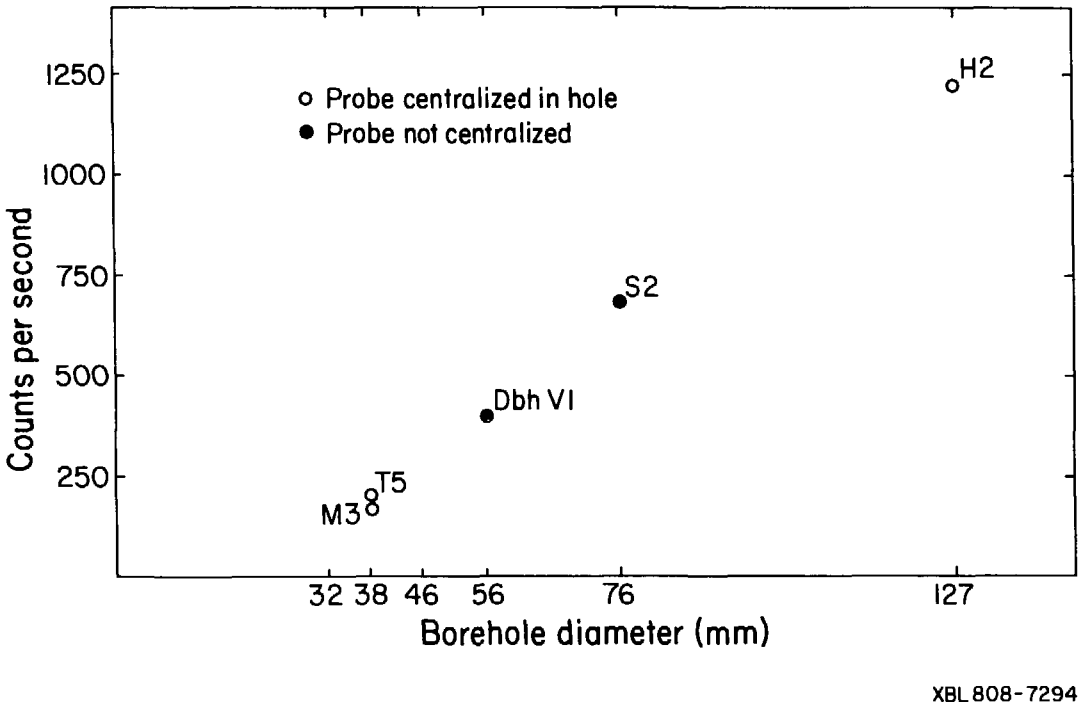

Fig. 2.12 Gamma count rates from different diameter boreholes of relatively high flow rate. Hole DBH V-1 is on the 410 m level, the others are in the time-scale drift. A 200 cps background contribution has been subtracted from the data.

3. MODELS OF RADON TRANSPORT IN FLOWING BOREHOLES

3.1 Introduction

The radon concentration observed in flowing boreholes will be controlled by two factors, the concentration of the radon in water at the time it enters the holes, and the mixing that occurs after entry. The entering concentration will be determined by the emanating power of the rock, the quantity of water moving through the emanating region, and the length of time which a given volume of water spends within the emanating region. As our data were gathered in igneous rocks where the flow is along fractures, we first develop a simple model of flow along a single planar fracture containing a source of radon. Because the flow is the only hydrological quantity measured, the model assumes that only flow is known, and the reservoir and wellbore pressures are not included.

In reality, the distribution of radon within the borehole will depend in a complicated way upon the points of entry, the flow rate, the diffusion of radon in water, and dispersion occurring during flow. It is likely in some situations that convective overturn within the hole will also further mixing. We ignore diffusion and dispersion in developing a few simple models for comparison with the field data. The simplest case considered is the intersection of the borehole by a single fracture, with either uniform, non-dispersive flow or complete mixing within the borehole. Some of the profiles could not be explained in such a simple fashion, and the next complication is to allow continuous water inflow along the length of the hole, retaining the non-dispersive condition. Finally, a discrete model is developed for non-uniform entry, although the resulting non-uniqueness requires that other geological or hydrological information be available to furnish constraints.

3.2 Radial Flow Along a Thin Crack

A simple crack model (Fig. 3.1) can be used to better understand the relation between flow rate and radon concentration. We follow the development of Stoker and Kruger (1975) for porous media, adapted to a thin, flat disk of aperture h which intersects a vertical hole of radius a. Water flows radially inward from all directions through the crack to be collected within the central hole. As it flows inward, it picks up a fraction of the radon atoms produced by radium present on the surfaces of the fracture. The rate of radon production is called the emanating power, expressed as the effective radium (not radon) activity per unit area, or equivalently, as the production of radon per unit time per unit area.

The parameters employed in the crack model are:

h	crack width(cm)
a	borehole radius (cm)
A	cross-sectional area of borehole (cm^2)
b	disc radius (cm)
r	radial distance from borehole axis (cm)
z	axial distance along borehole (cm)
Q	volumetric inflow (cm^3/day)
E	emanating power (number of radon atoms produced per cm^2 per day)
λ	decay constant of radon-222 (0.18/day)
I	radon influx (radon atoms/day)
C	radon concentration (radon atoms/cm^3)
Co	radon concentration of water entering borehole

If an elemental annulus of width dr (Fig. 3.1) produces radon at a rate E, then its contribution to the influx of radon atoms entering the borehole will be:

$$dI = Ee^{-\lambda t}2\pi rdr \tag{3.1}$$

where the time for fluid to move from the annulus to the borehole is:

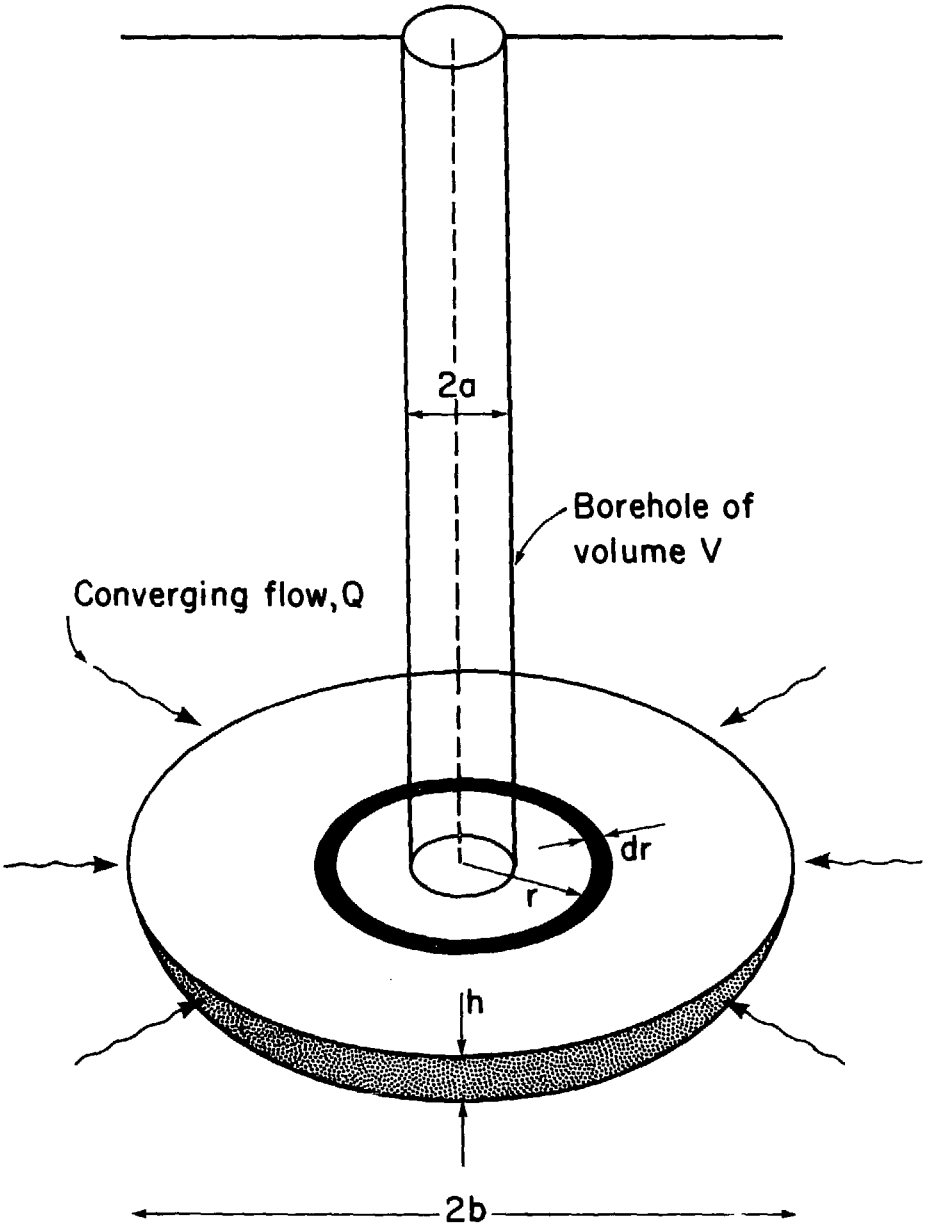

Fig. 3.1 Thin crack model for radon transport. Water flows radially at a rate Q through a thin crack of aperture h into the borehole. The crack contains a circular source area of outer radius b which produces radon atoms at a rate E.

$$t = \frac{1}{-Q} \int_{r}^{a} 2\pi\, hrdr = \frac{\pi h}{Q} \left(r^2 - a^2\right) . \tag{3.2}$$

If radon is produced from a disc source extending outwards from the borehole, then the influx I is obtained by integrating the above expression over its inner radius a to its outer radius b. The result is:

$$I = \frac{QE}{\lambda h} \left[1 - e^{-\lambda\pi h(b^2-a^2)/Q}\right] \tag{3.3}$$

and the concentration C_o in the borehole is simply I/Q,

$$C_o = \left[\frac{E}{\lambda h} \quad 1 - e^{-\lambda\pi h(b^2-a^2)/Q}\right] . \tag{3.4}$$

The flow rate and the source geometry determine the value of the exponent and hence the dependence of the concentration upon flow. If the flow is sufficiently high so that

$$Q \gg \lambda\pi h \left(b^2 - a^2\right) \tag{3.5}$$

then,

$$C_o \approx E\pi(b^2 - a^2)/Q \tag{3.6}$$

and the concentration increases linearly with the source area and decreases inversely with Q. This condition occurs if the source area is small enough so that the fluid crosses it in a fraction of the radon half-life. The 1/Q dependence is quite contrary to our observations at Stripa, hence the high flow condition does not apply to conditions at the Stripa site.

On the other hand, if the flow rate is low enough or the source area large enough that the fluid residence time within the source area is several half-lives or more, so that

$$Q \ll \lambda\pi h \left(b^2-a^2\right) \quad , \tag{3.7}$$

then the exponent can be ignored and

$$C_0 = E/\lambda h \quad . \tag{3.8}$$

Hence, the concentration is independent of flow rate and dependent upon geometry only through the fracture width h. Assuming a flow rate Q of 10 liters per day and a value of h of 0.01 cm, the low flow approximation requires that the outer radius of the disk be at least 13 m. Because there is good field evidence that the radioelement concentration is more or less uniform over a 100 m scale, it is apparent that the low flow approximation applies to the data under consideration here. Therefore, we expect the radon concentration of groundwater entering each borehole to be reasonably constant, subject only to local variations in radon emanation and crack aperture.

3.3 Borehole Concentration for a Single Entry Point, No Mixing

If radon enters at one depth within a borehole and moves upward within the water column without diffusion or dispersion, then a simple exponential decay with distance z from the source should be observed. The travel time from the entry point to the observation point in a hole of area A is simply Az/Q, so the concentration is

$$C(z) = C_0 \, e^{-\lambda Az/Q} \tag{3.9}$$

or

$$\ln [C(z)/C_0] = -\lambda Az/Q \quad . \tag{3.10}$$

Since gamma-ray count is proportional to concentration C(z), Eq. (3.10) suggests that the logarithm of the gamma-ray count rate be plotted against depth. Then a straight-line fit to the decay will give the flow rate Q if the single-entry, no-mixing conditions prevail. For example, if z represents

the distance over which the count rate decreases by half, then Eq. (3.10) shows that Q is $\lambda Az/0.693$.

Figure 3.2 shows Eq. (3.10) plotted for five linear flow velocities, Q/A. The volumetric flow rate Q is also given for a 76-mm-diameter hole. Along a 14-m travel path, different flow rates can be distinguished only within the range 0.1 to 10 m/day. Above 10 m/day there is less than 20% drop over a 10 m length; at higher velocities we can determine only that the flow rate is greater than 10 m/day. At rates below 0.1 m/day dispersion, sensitivity and water displacement by the probe will limit the detection of anomalous concentrations. Figure 3.2 applies to longer or shorter travel paths simply by scaling: over a 140 m path we could evaluate flows ranging between 1 and 100 m/day.

3.4 Complete Mixing

If the inflow Q from a single entry point, or from any distribution of multiple entry points, is somehow mixed throughout a volume V, then the observed concentration will be an average of all contributions, allowing for the amount of decay during the mixing time. This model encompasses the case where the entry point is a fracture at the bottom of an artesian borehole, with complete mixing occurring before an entering elemental volume of water exits at the collar.

For a mixing time of T, the average concentration will be:

$$\overline{C} = \frac{1}{T} \int_0^T C_o e^{-\lambda t} dt \qquad (3.11)$$

or,

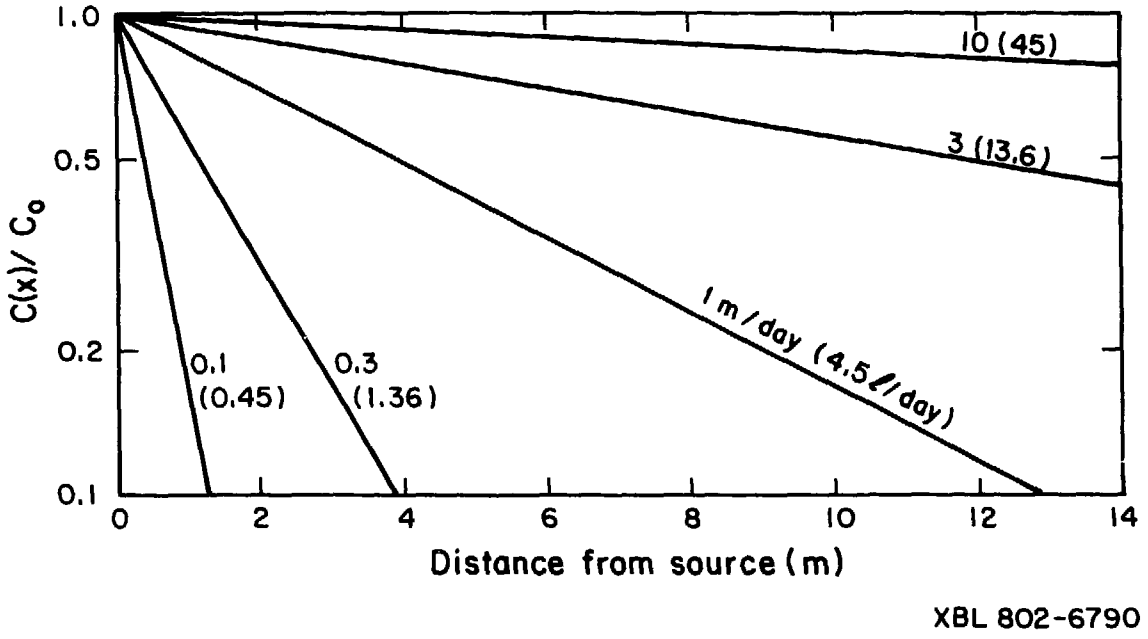

Fig. 3.2 Ratio of the radon concentration in one-dimensional water flow (logarithmic scale), plotted against distance from the source. The radon decay rate is 0.18 per day. Linear flow velocities range from 0.1 to 10 meters/day. Numbers in parentheses give the equivalent volumetric flow in a 76 mm hole.

$$\overline{C} = \frac{C_o}{\lambda T}\left(1-e^{-\lambda T}\right). \tag{3.12}$$

The mixing time can be no less than the time required to fill the volume, which is V/Q, in which case,

$$\overline{C} = C_o \frac{Q}{\lambda V}\left(1 - e^{-\lambda V/Q}\right) . \tag{3.13}$$

This result is shown graphically in Fig. 3.3, and is discussed in conjunction with the model for continuous uniform entry in the next subsection. Values of λV are given in Table 3.1.

3.5 Continuous Uniform Entry

Assume that water enters the borehole uniformly along its entire length, as shown in Fig. 3.4, rather than at a discrete entry point. At the time of entry, each elemental volume of water bears radon at a concentration C_o. Since the infiltration rate is q (l/m-day), the volumetric flow along the axis of the hole is:

$$Q(z) = qz \tag{3.14}$$

and the linear velocity is:

$$v(z) = qz/A \quad . \tag{3.15}$$

The water originating from an elemental length dz' located at z' will occupy a fraction dz'/z of the volume passing an observation point z. The time required to transport the elemental volume from the entry point z' to z is:

$$t' = \int_{z'}^{z} \frac{dx}{v(x)}$$

or:

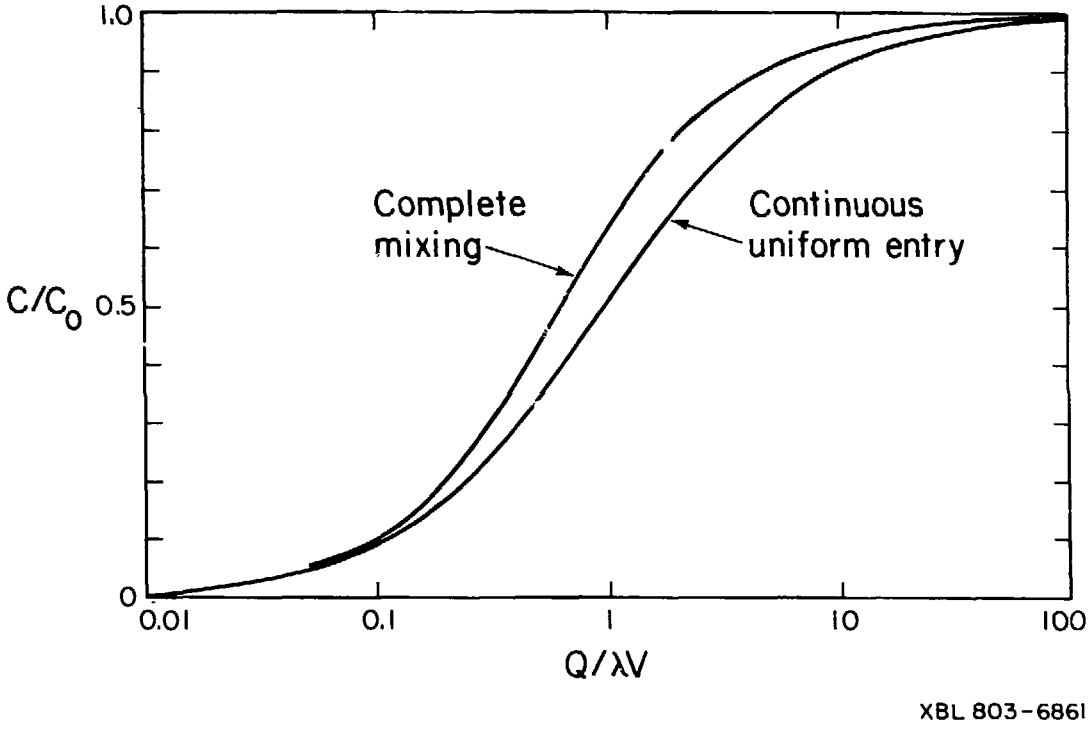

Fig. 3.3 Radon concentration in borehole water for two infiltration models. Values of λV are given in Table 3.1.

Table 3.1 Volume capacity of boreholes, in liters per meter length of hole. The length and diameter of the gamma ray probe are 2.07 m and 33 mm, displacing approximately 1.8 liters. The third column gives the product of λ, the radon decay rate, and V, the volume of a hole 10 m long of specified diameter.

Hole diameter (mm)	Volume per length(l/m)	λV(l/day)
38	1.13	2.0
56	2.46	4.4
76	4.53	8.2
127	12.67	22.8

$$t' = \frac{A}{q} \ln(z/z') \quad . \tag{3.16}$$

The concentration at z due to the contribution from z' is

$$C' = C_o e^{-\lambda t'}$$

$$= C_o (z'/z)^{\lambda A/q} \quad . \tag{3.17}$$

Integrating over all contributions between 0 and z,

$$C(z) = \frac{1}{z} \int_0^z C_o \left(\frac{z'}{z}\right)^{\frac{\lambda A}{q}} dz'$$

$$= C_o \frac{q}{q+\lambda A} \quad . \tag{3.18}$$

Hence the concentration is constant along the borehole length, for any specified q and A (or equivalently, Q and V). The relationship given in Eq. (18) is shown in Fig. 3.5, for two different borehole sizes. The sigmoidal shape is of considerable interest, showing that for high flows the concentration in the hole asymptotes to C_o, at moderate flows it is proportional to the log (q), and at low flow rates it is linear with q, as given by $C_o q/\lambda A$.

In terms of total flow, Eq. (3.18) can be written:

$$C(z) = C_o \frac{Q/\lambda V}{1 + Q/\lambda V} \quad , \tag{3.19}$$

which is compared with Eq. (3.13) for the complete mixing case in Figure 3.3. The two cases are very similar. A borehole log responding to concentration cannot distinguish between the two since both cases produce a constant concentration throughout the hole. At low flows, the concentration ratio for both cases increases linearly with $Q/\lambda V$. At intermediate flows, the depen-

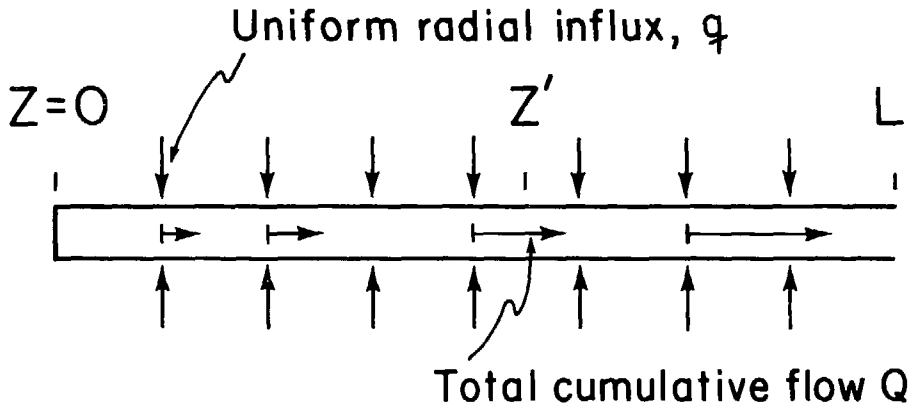

Fig. 3.4 Borehole with a continuous uniform water influx of q liters per linear meter per day. Water entering the borehole has a radon concentration C_o.

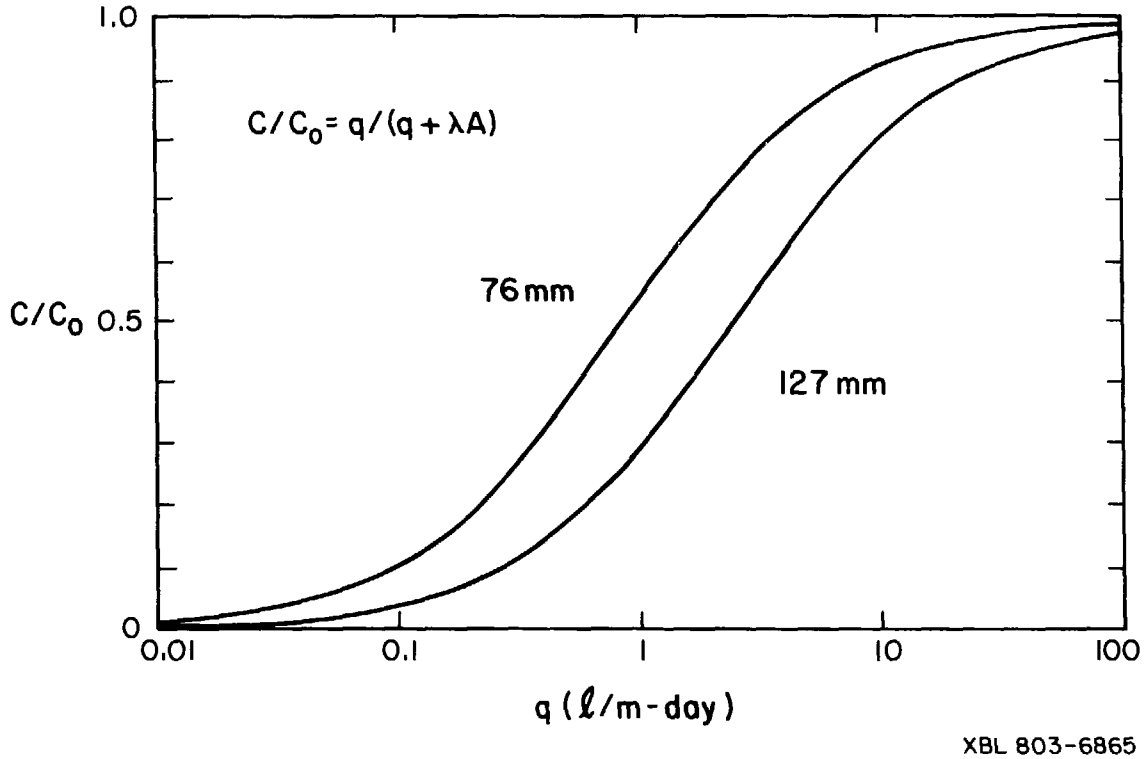

Fig. 3.5 Concentration ratio as a function of continuous fluid entry along the entire length of the hole, for 76 mm and 127 mm diameter holes.

dence is logarithmic, with the mixing model producing concentrations higher than the continuous entry model. At very high flows the entry concentration will be observed.

3.6 Continuous Non-Uniform Entry

We now extend the model of Fig. 3.4 to include non-uniform inflow. The borehole length is divided into N discrete equal segments of length Δz, each contributing a flow of q_i liters per meter. The time required to move a volume of water from segment i to segment i + 1 is

$$\Delta t_i = A\Delta z/Q_i \quad , \tag{3.20}$$

where

$$Q_i = \sum q_j \Delta z \quad . \tag{3.21}$$

The concentration in the first segment is:

$$C_1 = C_o \frac{q_1 \Delta z}{q_1 \Delta z} \tag{3.22}$$

and in subsequent segments the concentration is computed sequentially:

$$C_2 = \frac{C_o q_2 \Delta z + C_1 Q_1 e^{-\lambda A \Delta z/Q_1}}{Q_2} \quad ,$$

$$C_3 = \frac{C_o q_3 \Delta z + C_2 Q_2 e^{-\lambda A \Delta z/Q_2}}{Q_3} \quad , \tag{3.23}$$

$$C_i = \frac{C_o q_i \Delta z + C_{i-1} Q_{i-1} e^{-\lambda A \Delta z/Q_{i-1}}}{Q_i} \quad .$$

The result expressed in the set of Eqs. (3.23) represents a numerical approximation, the accuracy of which improves as Δz becomes smaller. A particular case of non-uniform entry can be modeled by assigning one or more of the segments Δz to each inflow interval.

The discrete model can be checked by examining the case where the inflow is constant along the length of the borehole. Then Eq. (3.23) becomes,

$$C_i = \frac{C_o q\Delta z + C_{i-1}(i-1)q\Delta z e^{-\lambda A/(i-1)q}}{iq\Delta z} \quad . \tag{3.24}$$

After rearranging,

$$C_o = i\, C_i - (i-1)C_{i-1} e^{-\frac{\lambda A}{(i-1)q}} \quad . \tag{3.25}$$

At the Nth interval, $i = N$, and $N\Delta z = L$, so:

$$C_o = \frac{L}{\Delta z} C_i - \left(\frac{L}{\Delta z} - 1\right) C_{i-1} e^{-\frac{\lambda A}{q} \cdot \frac{\Delta z}{(L-\Delta z)}} \quad . \tag{3.26}$$

Now let $r = \Delta z/L$:

$$rC_o = C_i - (1-r) C_{i-1} e^{-\frac{\lambda A}{q} \cdot \frac{r}{1-r}} \quad . \tag{3.27}$$

As the segment length becomes small, C_i becomes approximately equal to C_{i-1}:

$$C_i = C_o \frac{r}{1 - (1-r)e^{-\frac{\lambda A}{q}\frac{r}{1-r}}} \quad . \tag{3.28}$$

The limit as $r \to 0$ is obtained by applying L'Hospital's rule,

$$C_i = C_o \frac{q}{q + \lambda A} \quad , \tag{3.29}$$

which is identical with Eq. (3.18) obtained for the continuous and uniform model.

Two cases based on Eq. (3.23) are presented in Fig. 3.6, where the initial concentration is given in counts per second to simulate a gamma ray log. Two different q_i distributions along the 12 m hole length give the same concentration (count rate) profile, illustrating the problem of non-uniqueness that arises for multiple entry situations. Other combinations of initial concentration and inflow distribution could be contrived to produce approximately the same profile.

3.7 Discussion

We have developed four simple models to describe the radon concentration within the hole, using different assumptions for mixing and for the entry point locations. The resulting expressions for the four borehole models are given in Eqs. (3.9), (3.13), (3.19), and (3.23), where the borehole concentration can be expressed as a function of the entering concentration C_0. The concentration ratio is generally dependent only upon the volumetric flow rate Q and the borehole volume V. For the single entry point with no mixing, the flow rate can be inferred from a log that is proportional to the concentration. For the other three cases, C_0 cannot be determined from the log, and Q must be separately determined before C_0 can be estimated, or, conversely, C_0 must be independently established if Q is to be estimated. We have also pointed out that the case of complete mixing cannot be distinguished from the case of continuous uniform fluid entry into the hole. Independent hydrological evidence is needed to distinguish them.

The thin crack expression for C_0 of Eq. (3.4) can be merged with any of the four borehole models to provide an expression for the borehole concentration in terms of the flow and source parameters. As an example, the thin

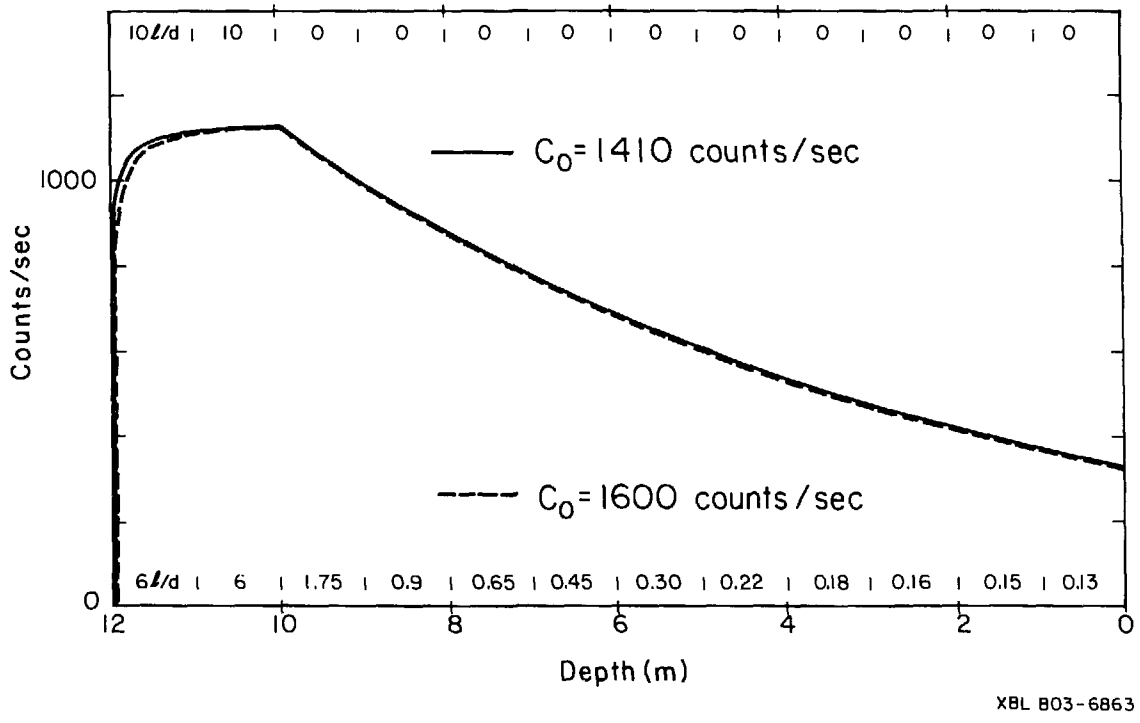

Fig. 3.6 Two hypothetical gamma logs for two different water inflow distributions along a borehole. The graph illustrates the problems of a non-unique solution if the radon concentration of water flowing into the borehole is unknown.

crack result of Eq. (4) is combined with the mixing model of Eq. (3.13) to give

$$\overline{C} = \frac{EQ}{\lambda^2 hV}\left[1 - e^{-\lambda V/Q}\right]\left[1 - e^{-\lambda\pi h(b^2-a^2)/Q}\right] \qquad (3.30)$$

We have already stated that Q/λ will be small compared with the source volume in the crack, making the term in the second pair of brackets in Eq. (3.30) approximately equal to one. For the larger borehole, Q/λ will also be small compared with the mixing volume (see Table 3.1 for values of λV), and hence the first term in brackets will also be approximately one, so that:

$$\overline{C} \simeq \frac{EQ}{\lambda^2 hV} \quad . \qquad (3.31)$$

This result seems appropriate for the Stripa results of Fig. 2.4, since the flow values are reasonable and the concentration increases linearly with the flow rate. It must be emphasized however, that this dependence upon Q is really a result of the fluid residence time within the borehole rather than a consequence of the flow rate within the radon source area.

For various limits of the groundwater inflow rate, Eq. (3.30) yields quite different expressions for the radon concentration in a borehole. Table 3.2 summarizes the four conditions where the flow is either very high or very low with respect to the product of the radon decay time and the radon source and borehole volumes. As the table shows, only if the fluid spends considerable time in both the source area and within the borehole does borehole concentration increase linearly with flow rate. Otherwise, if the fluid spends only a fraction of the radon half-life in either of these volumes, the concentration either remains constant or depends inversely upon Q. In the right-hand column, where $Q>\lambda V$, the flow is so high that the

borehole does not affect the concentration, which maintains its entry point levels.

Table 3.2 Expressions for average radon concentration in borehole of volume V, after inflow from a thin, flat source of volume $\pi h(b^2 - a^2)$, and with mixing within the borehole. (See Subsection 3.2 for nomenclature.)

Flow rate vs. source volume	Flow rate vs. mixing volume	
	$Q < \lambda V$	$Q > \lambda V$
$Q < \lambda\pi h(b^2-a^2)$	$EQ/\lambda^2 hV$	$E/\lambda h$
$Q > \lambda\pi h(b^2-a^2)$	$E\pi(b^2-a^2)/\lambda V$	$E\pi(b^2-a^2)/Q$

4. GAMMA-RAY BOREHOLE LOGS

A large number of total count gamma-ray logs were collected in the underground and surface boreholes at Stripa during 1978 and 1979 (Table 4.1), a limited selection of which were presented and discussed in Nelson et al. (1979). In this section we present almost all of the gamma-ray logs acquired at Stripa and discuss them in terms of the associated data which provide information on the groundwater flow. Figure 4.1 shows the location of the underground drifts and boreholes in which many of the logs were acquired. Surface boreholes are shown in Fig. 1.1.

At the time the logging was done, the importance of the radioelement content of the water was not suspected; in fact, the unusually high count rates were quite puzzling at the time. As a consequence no special care was taken regarding the source of water in the boreholes, except that all boreholes were filled with water before being logged if they were not already full. The source of the water for topping off the boreholes was the mine water supply, which comes from a 700-m^3 holding reservoir at the 260 m level. A container full of this mine supply water was checked with the gamma probe and registered no indication of radon content. Hence at the time of logging, the water in any hole could be a combination of water which had flowed through the rock and into the borehole under existing pressure gradients, plus an additional amount of radon-free water poured in from the mine water supply to bring the level up to the top of the borehole. However, most of the holes were full from infiltration and did not require artificial filling.

Table 4.1 List of boreholes at Stripa logged for total gamma-ray counts, by date and location.

Full-Scale Drift	
1 Feb 78	C1, E11, M6, M8, M9, T13, T14, T15, U1, U2, U3
3 Feb 78	E6, E7, E8, E9, E10, H9, M7, T16
7 Feb 78	E7, E8, E9, E10, T16
10 Mar 78	E12, E13, E14, T19, T20, T22, U11, U12
Time-Scale Drift	
27 Jan 78	E1, E2, E3, H1, H3
30 Jan 78	E4, E5, H1, H2, H4, H5, H6, H7, H8, M1, M2, M4, M5, N1, N2, T2, T3, T4, T7, T8, T12
31 Jan 78	H2, T1, T2, T5, T6, T9, T10, T11
16 Feb 78	H3, N2, T3
7 Dec 78	M2, M4
17 Jan 79	M3
Extensometer Drift	
12 Jul 78	N3, N4
Ventilation Drift	
17 May 78	HG3, HG4, R4
26 May 78	R3, R5
15 Jun 78	S2
30 May 79	S2
21 Nov 79	S1
22 Nov 79	S2
410 m Level	
5 Jun 79	DBH V-1
Surface	
17 Feb 78	SBH-1
Dec 78	SBH-1 (SGU)

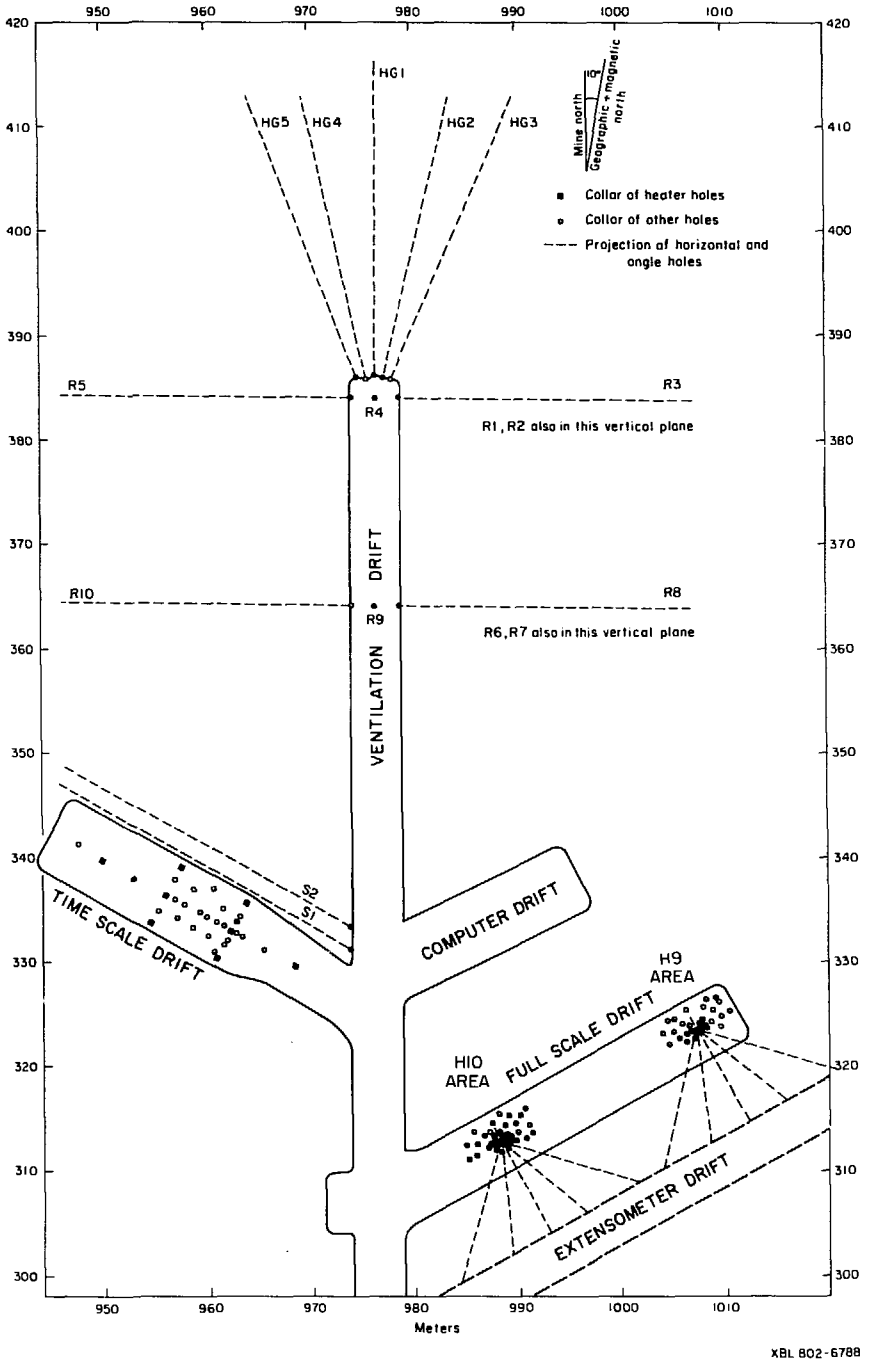

Fig. 4.1 Plan map of the LBL experimental drifts at the 343 m elevation at Stripa.

4.1 Full-Scale Drift

The gamma-ray logs from the full-scale drift (Fig. 4.2) are presented in Fig. 4.3, which shows the holes located along the central axis of the drift, and in Fig. 4.4, which contains holes from the H9 test area. These two figures contain all the logs obtained in the full-scale drift. Most, but not all, of the holes in the H9 area were logged, but only the holes along the centerline of the drift were logged in the H10 area.

The horizontal and vertical spatial scales are the same in Fig. 4.3, thereby portraying the logs superposed on a true cross-sectional view of the rock mass, except for the break in the cross-section between holes E8 and E13. All the gamma ray baselines in this figure are given as 200 cps, with the exception of heater hole H9 where the count was much reduced due to the increased attentuation in the water-filled, large-diameter (406 mm) hole. One prominent feature can be seen in Fig. 4.3. An anomalous decrease in the count rate with a half-width of less than 0.5 m indicates a planar feature dipping downwards from right to left in holes E6 through U2. This feature is caused by a pegmatite dike, which in most granitic rock would produce a count rate increase due to the higher potassium content of pegmatites. Here, however, the count rate in the pegmatite decreases because its uranium and thorium content is lower than that of the Stripa granite.

Figure 4.4 is not a cross section like Fig. 4.3; instead, the remaining holes from the H9 area are grouped according to their diameter, which decreases from left to right. Where the pegmatite intersects boreholes M9, C1, and T15, a small count decrease can again be seen. A positive 500 cps anomaly peak occurs near the bottom of hole M7. Because of our experience

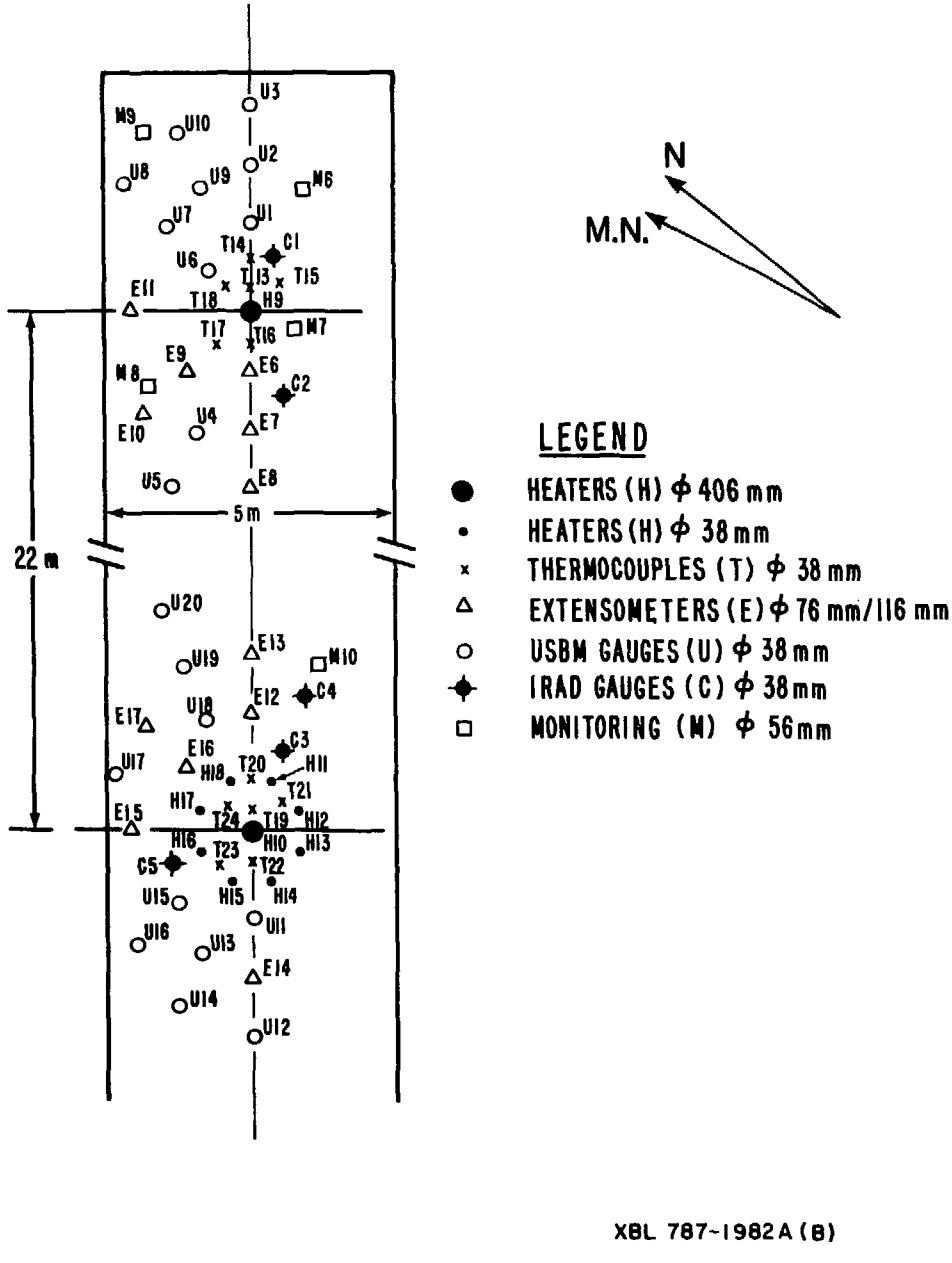

Fig. 4.2 Borehole layout in the full-scale drift.

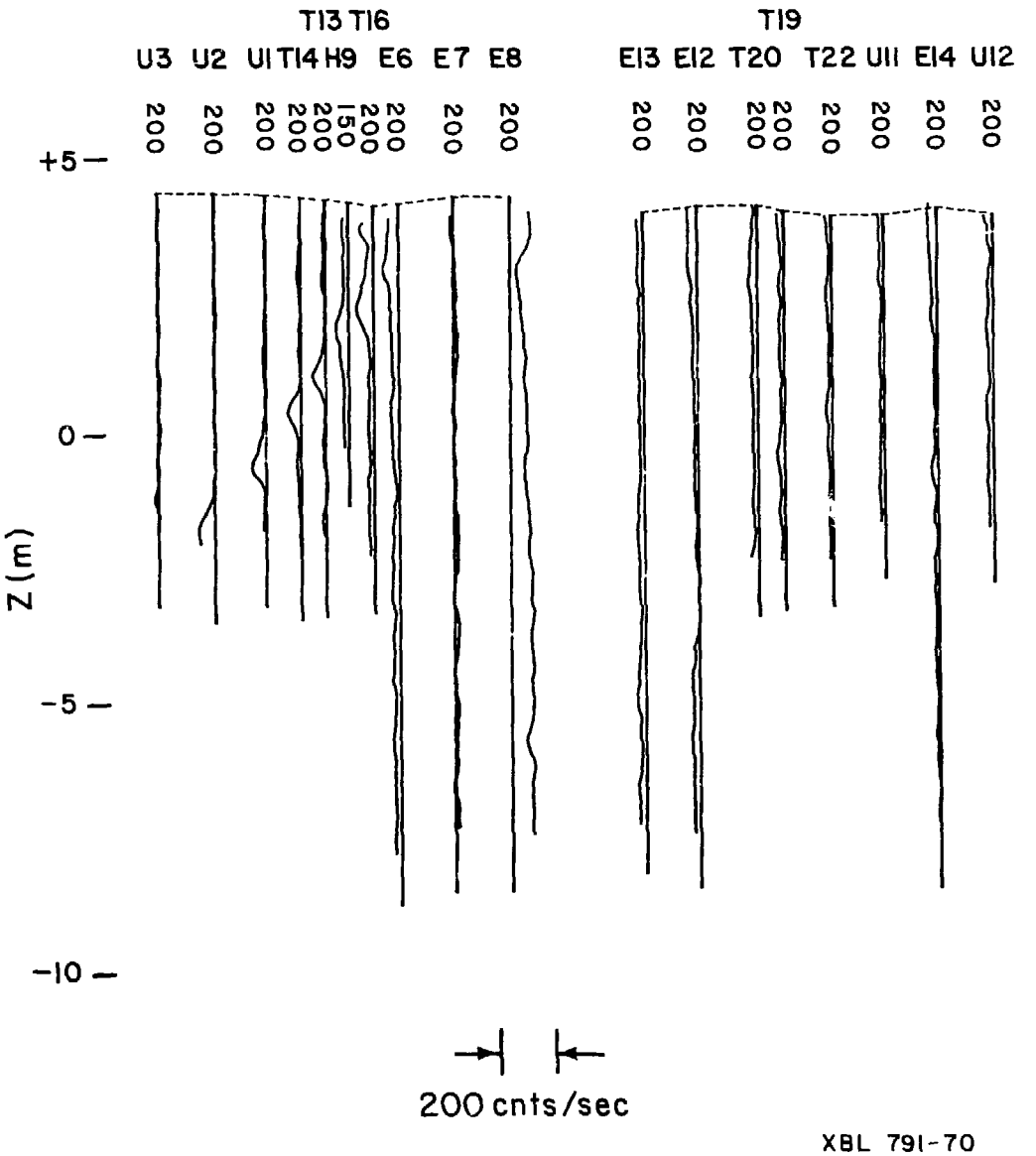

Fig. 4.3 Gamma-ray logs along axis of the full-scale drift. Vertical and horizontal spatial scales are identical except at discontinuity between E8 and E13. Baseline counting rate (counts per sec) is given above each hole.

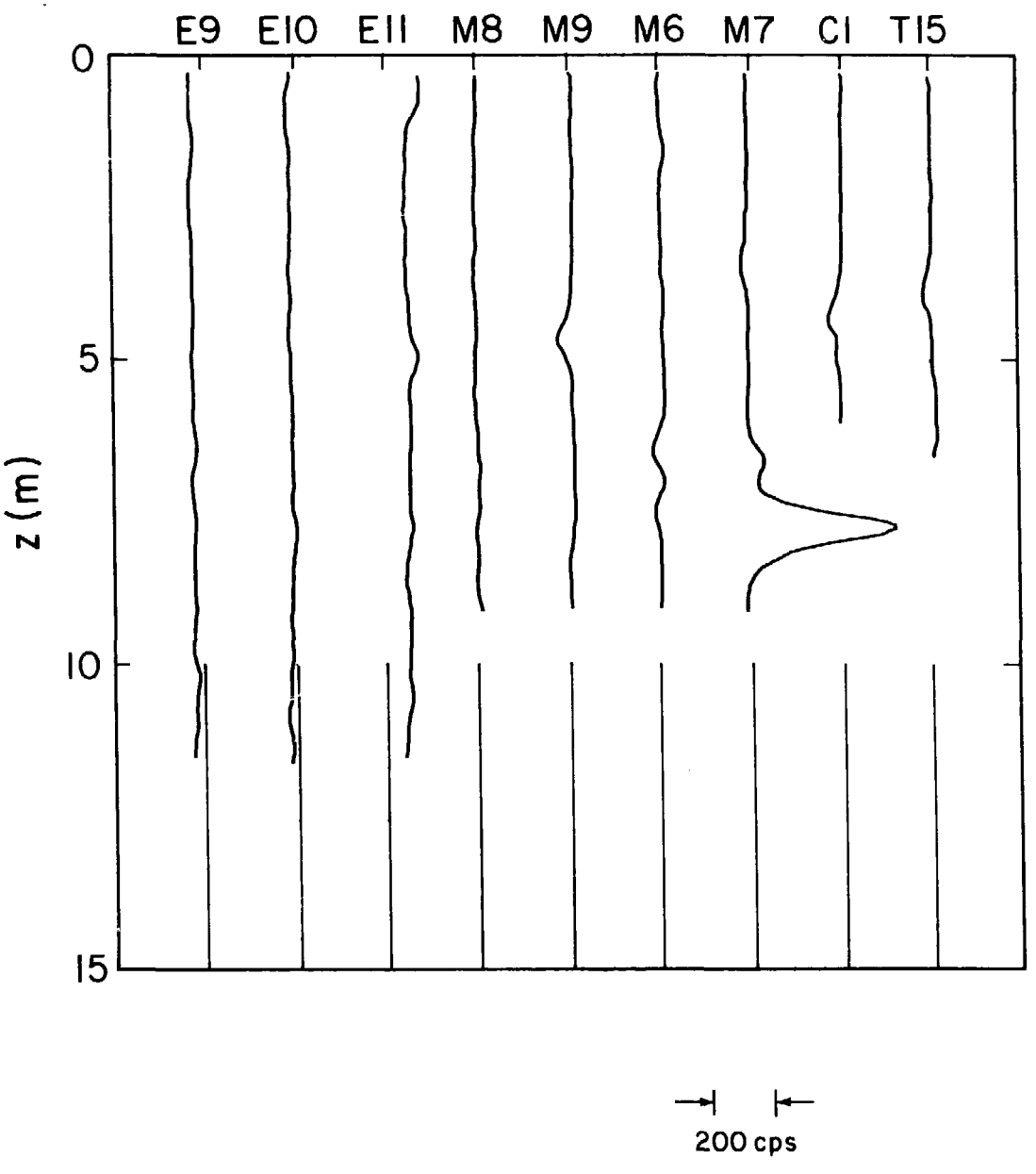

Fig. 4.4 Gamma-ray logs from the H9 area in the full-scale drift. Since this is not a profile, there is no horizontal spatial scale.

with similar positive peaks in hole N1 in the time-scale room, we attribute the peak to the occurrence of a local concentration of uranium and thorium, probably associated with a mafic (chloritic) zone within the granite.

Only two holes in Figs. 4.3 and 4.4 display anomalously high count rates that can be attributed to the inflow of water. Both E8 and E11 are roughly 50% higher in count rate for almost their entire lengths. Based on the previous discussion and on the data reviewed in the following subsections, we suspect that E8 and E11 have significantly higher inflows of water than any other holes logged for gamma rays in the full-scale drift. Unfortunately, no water inflow data are available for comparison. As described by Schrauf et al. (1979), the holes were grouted when the extensometers were installed prior to the initiation of the heater experiments in the summer of 1978.

4.2 Time-Scale Drift

Figure 4.5 shows the collar locations of all the boreholes located in the time-scale drift. The appropriate logs are presented in five cross sections, three parallel with the long axis of the drift and two transverse to it, in Figs. 4.6 through 4.10. Figure 4.6 shows logs along the drift centerline and Figs. 4.7 and 4.8 show logs from sections parallel with the centerline section. Because of the overlap on intersecting orthogonal sections, the two transverse sections shown in Figs. 4.9 and 4.10 each contain three logs also displayed in the longitudinal sections. Borehole M3, discussed in the Section 2, is the only time-scale borehole log not shown in Figs. 4.6 through 4.10. In all five figures the horizontal and vertical scales are equal so that the gamma-ray logs are projected upon a scaled

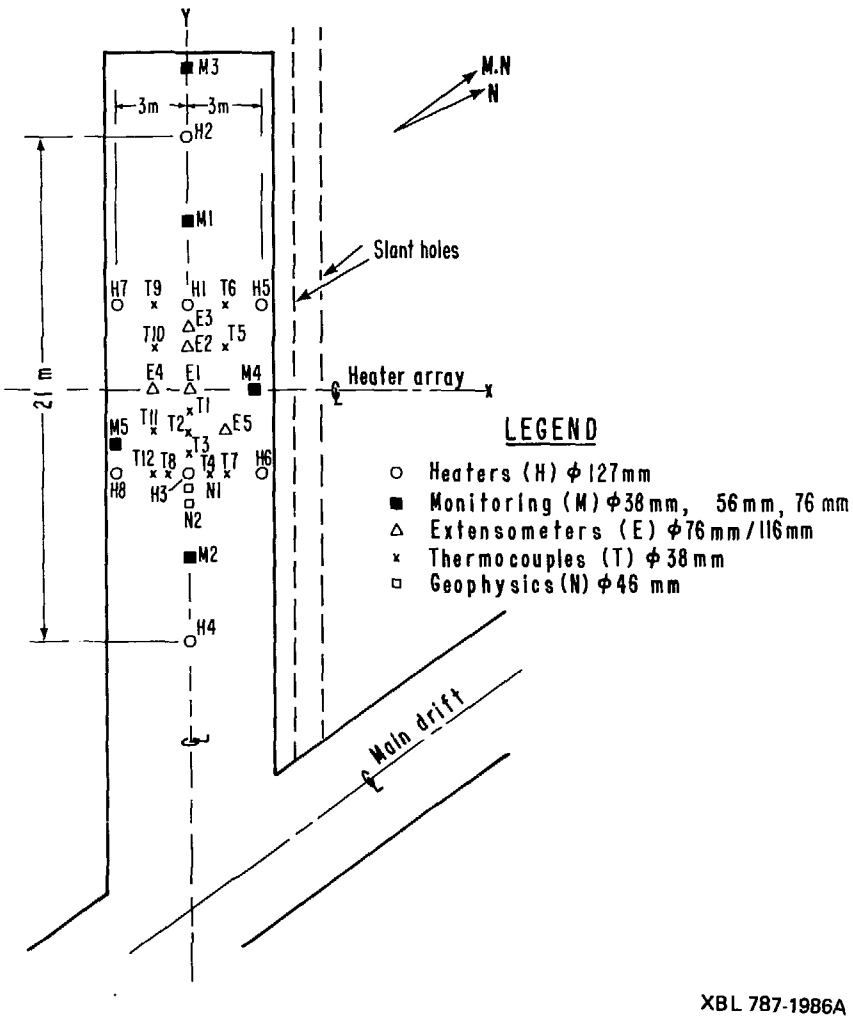

Fig. 4.5 Borehole layout in the time-scale drift.

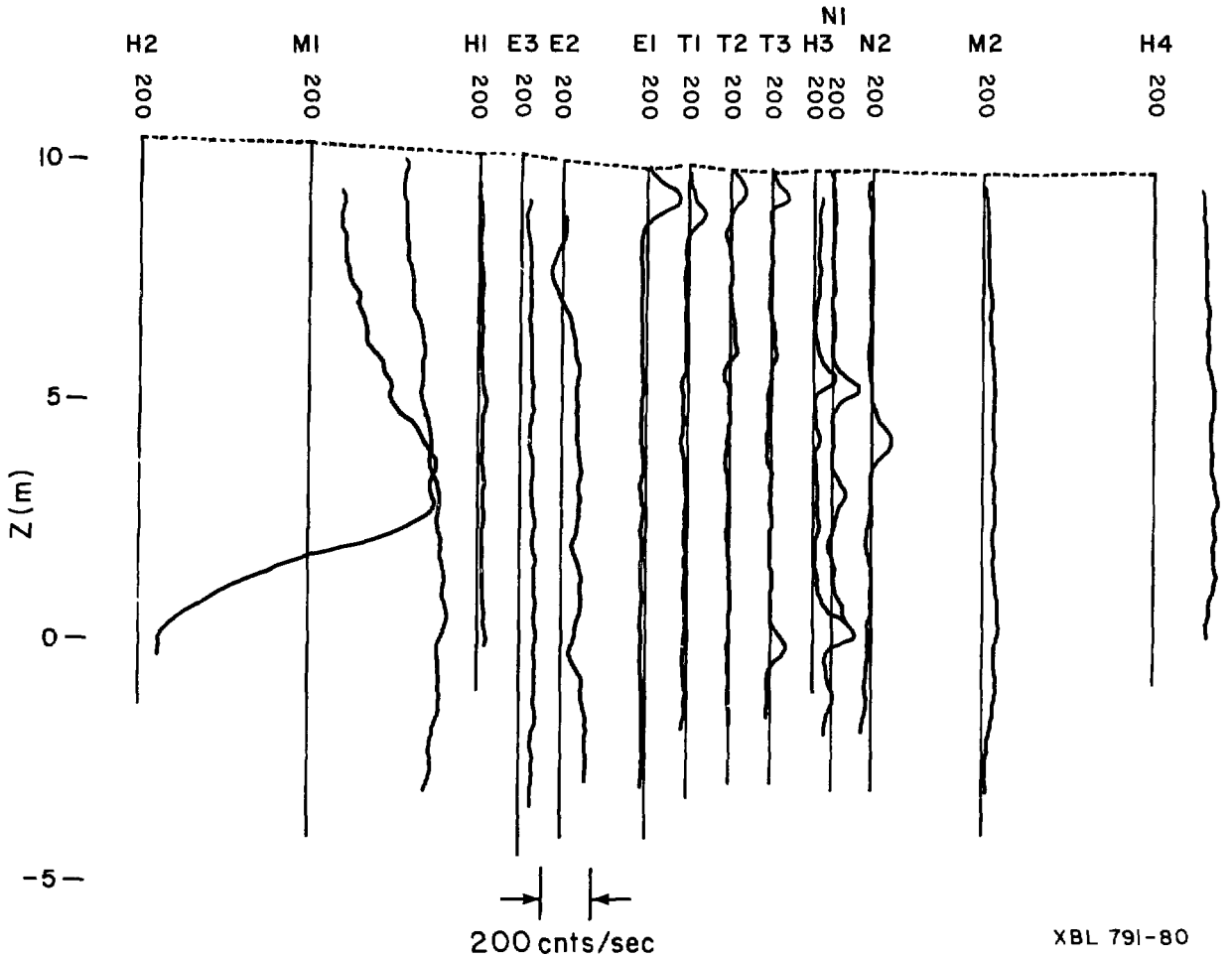

Fig. 4.6 Gamma-ray logs along the axis of the time-scale drift. Count rate increases to the right.

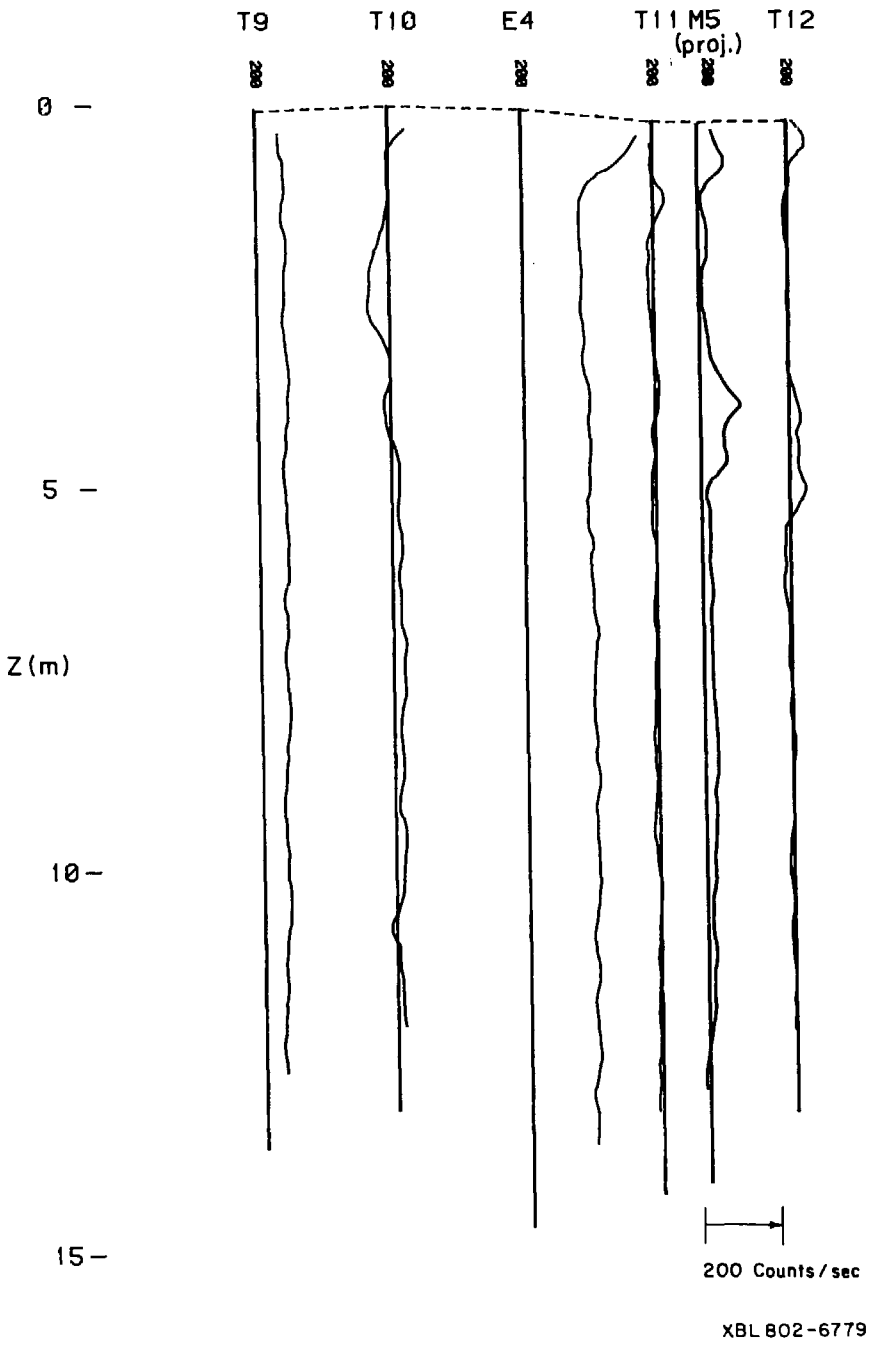

Fig. 4.7 Gamma logs along T9-T12 cross-section in time-scale drift.

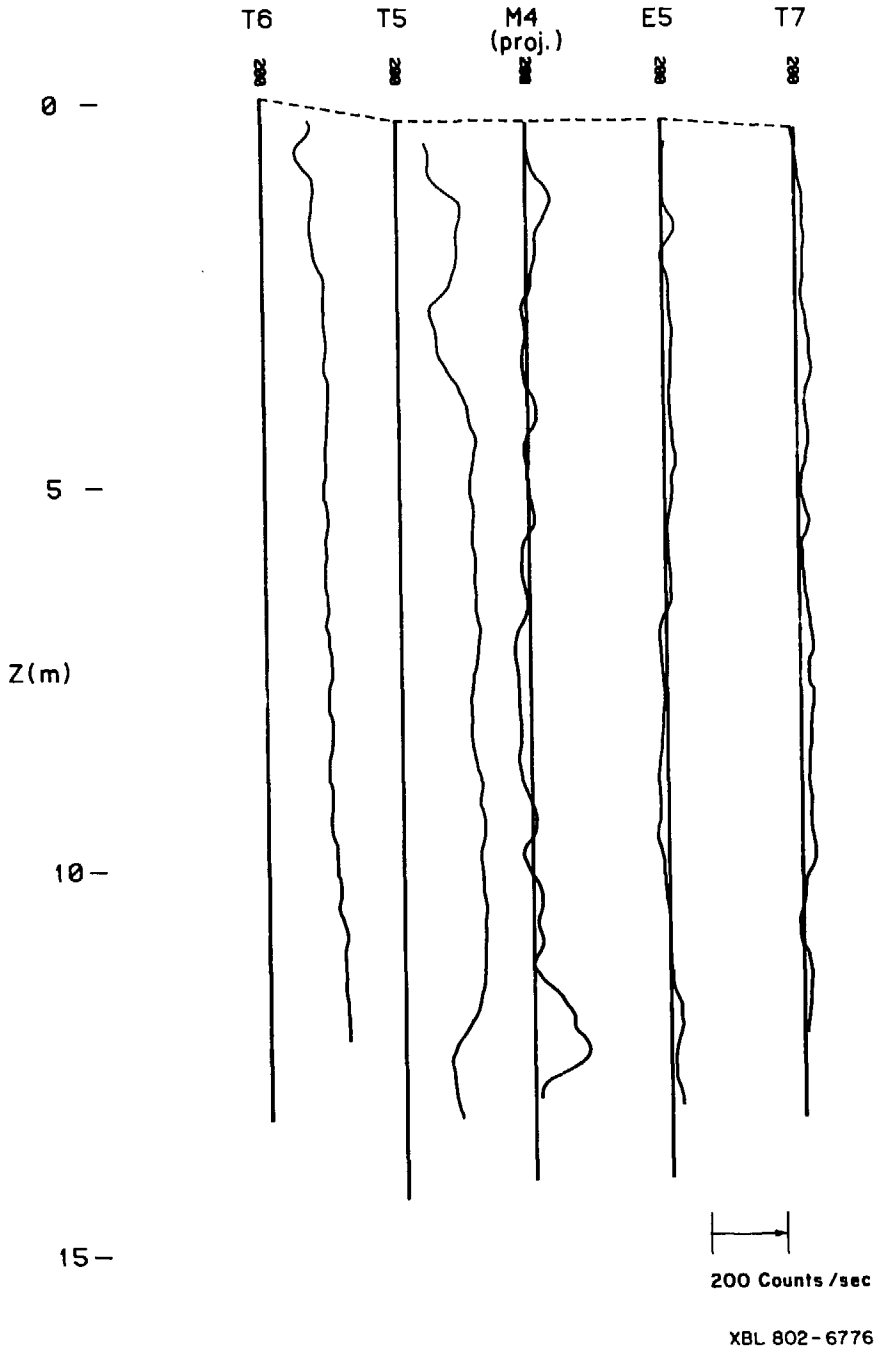

Fig. 4.8 Gamma logs along T6-T7 cross-section in time-scale drift.

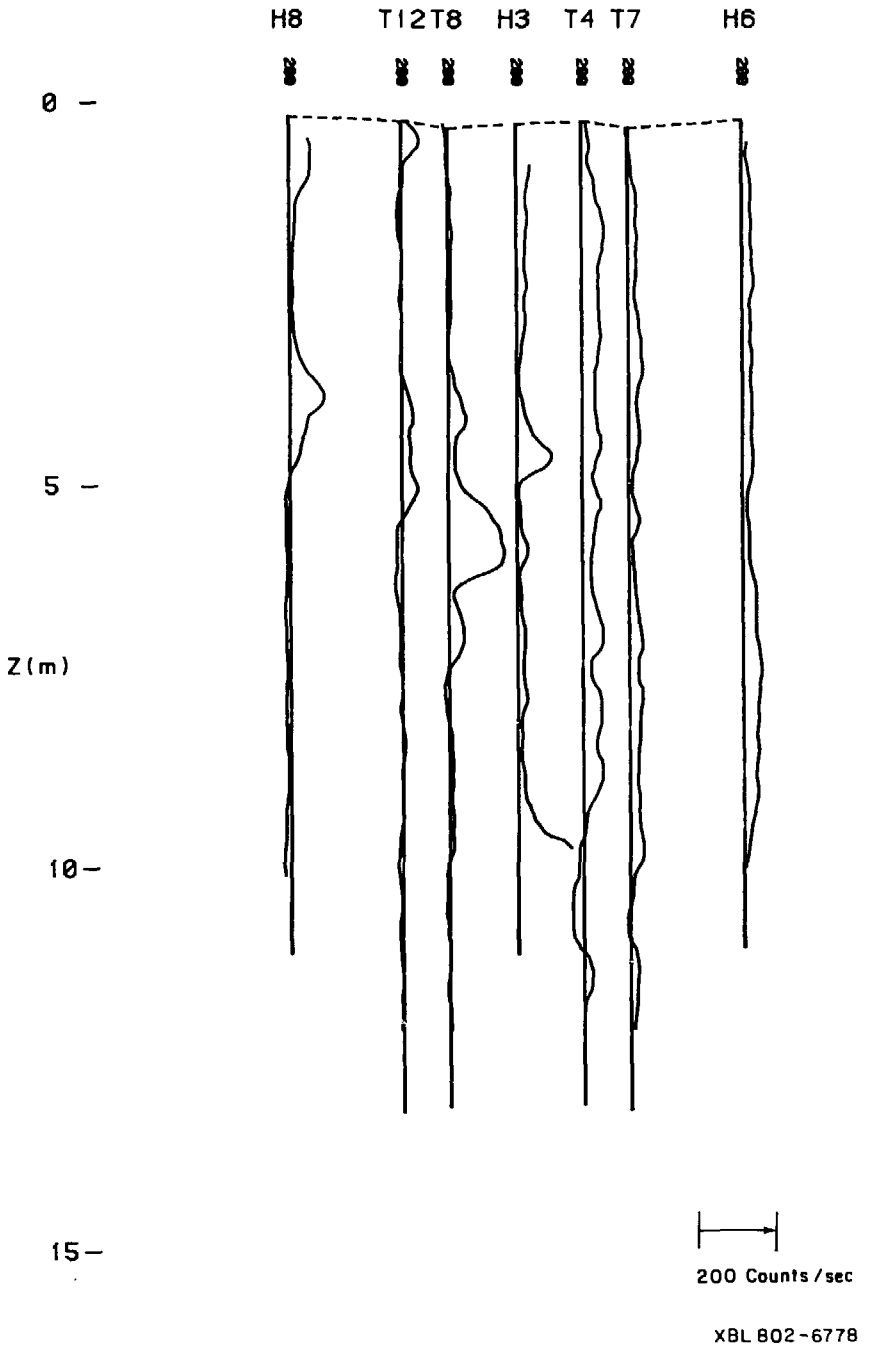

Fig. 4.9 Gamma logs along H8-H6 cross-section, time-scale drift.

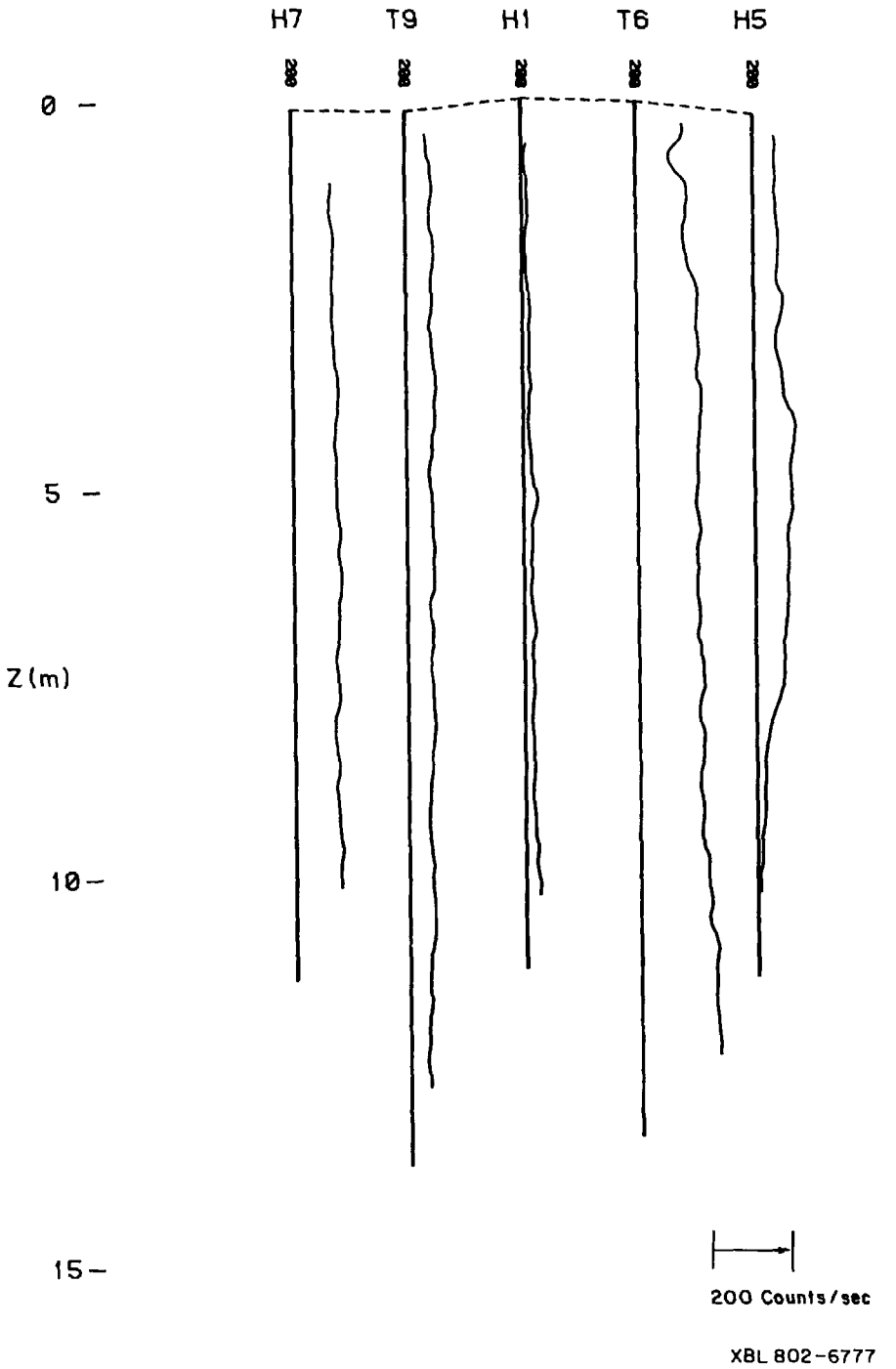

Fig. 4.10 Gamma logs along H7-H5 cross-section, time-scale drift.

vertical section of the rock mass.

The three types of features observed in the full-scale logs are also apparent in the time-scale logs. A pegmatite dike intersects borehole E2 at two different depths (Thorpe, 1979), but the corresponding decrease in count rate, although visible, is not as obvious as it was at the pegmatite in the H9 area.

Positive increases in the count rate are much more common, however, and are due both to local concentrations of uranium and thorium in the rock and to increases in the concentration of radon in the water. Anomalous increases of the first type are discrete features, usually of less than one meter vertical extent in any one hole and usually also visible in one or two neighboring holes. Examples can be seen at three elevations in Fig. 4.6: near the surface in holes E1, T1, T2, and T3; at five meters above the heater centerline in holes H3, N1 and N2; and at zero elevation in holes T3, H3, and N1. These high-count zones can also be seen in other holes on some of the adjoining cross-sections. For example, the feature at the five-meter elevation can also been seen in Fig. 4.9 in holes H8, T12, and T8 as well as H3. The combined view shows that the anomalous feature is dipping downwards from H8 to N2. Similarly, the extension of the feature near the floor of the drift can be viewed in holes M4 and E5 in Fig. 4.8. The logs suggest that these mafic zones, which contain high uranium and thorium concentrations, are flat features with long dimensions of several meters, and short dimensions, here vertical, of less than one meter. Core observations show that these zones are generally highly fractured, the fractures healed with chlorite and other minerals. The thicknesses of the chloritic fractured zones were

everywhere less than 0.2 m. Nelson et al. (1979) discuss the effect of these mafic zones on other types of logs that were run in the underground holes.

Positive increases in the count rate due to radon in the water can be observed in all but two heater holes and in several of the smaller diameter holes. Heater holes H3 and H8 in Fig. 4.9 have count rates close to the 200 cps background rate, while all the rest have count rates greater than 200 cps. Average count rates from these logs have been shown in Fig. 2.4 and discussed in the section on gamma ray measurements. A number of the smaller diameter holes also have high count rates that can only be explained by radon in the water. These are E3, E2, and M2 (Fig. 4.6), T9 and E4 (Fig. 4.7), T6 and T5 (Fig. 4.8), and T4 (Fig. 4.9). Only heater holes H1 - H8, however, furnished data that could be used for comparison with the gamma-ray logs because they were equipped with dewatering apparatus (Burleigh et al. 1978) that was operated during the heater experiments. The smaller diameter T and E holes in the time-scale room were grouted when the instrumentation was emplaced (Schrauf et al. 1979), and no water inflow information was collected.

The anomalous boreholes are summarized in Table 4.2, where the count rate in excess of 200 cps is tabulated. By spotting the data onto the plan map of Fig. 4.5, it is easy to see that most of the unusually high counts occur in holes at the rear of the drift, as has also been demonstrated by the sectional presentations.

Most of the high-count gamma-ray logs in Figs. 4.6 through 4.10 do not vary much with depth, indicating either complete mixing or multiple entry, as discussed in the section on models. However, hole H2 is an exception, as the count rate decays from bottom to top of the hole. As suggested by Eq. (10),

Table 4.2 Boreholes in the time-scale drift with a counting rate above the 200 cps background. Counts from the gamma logs are averaged over the entire hole length or over intervals of several meters where the count rate was high and uniform. A 200 counts per second rate was subtracted from the data to remove the average rock contribution.

38 mm		76 mm		127mm	
M3	180	M1	550	H1	20
T4	40	M2	50	H2	1000
T5	200	E2	82	H4	240
T6	175	E3	50	H5	100 (max)
T7	20	E4	170	H6	25
T9	60			H7	110

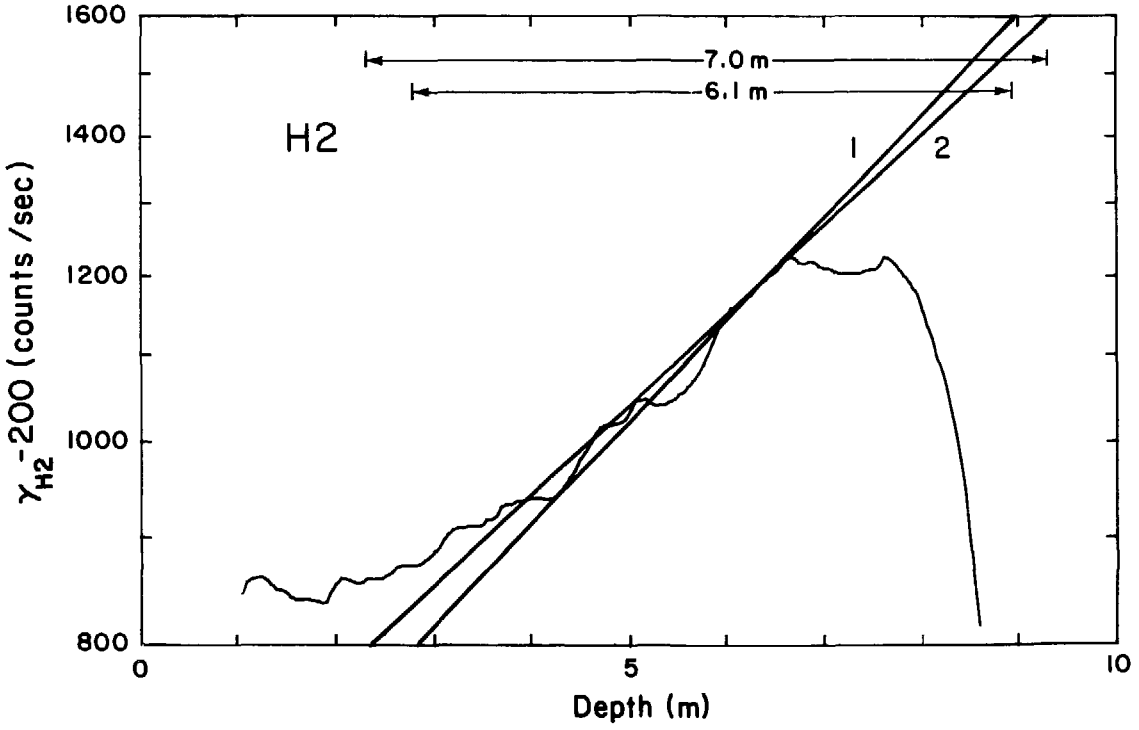

Fig. 4.11 Logarithmic plot of the H2 gamma log; 200 cps were subtracted from the gamma log to remove the background effect of the rock. Curves 1 and 2 are plausible fits over the depth range 4.0 to 6.5 m. Curve 1 indicates that the water moves 6.1 m while losing half its activity, which is equivalent to a flow rate of 20.1 liters per day. Curve 2 indicates a flow of 23.1 liters per day.

the H2 log is replotted in Fig. 4.11, with the count rate on a logarithmic scale. The portion of the log from 4.5 m to 6.0 m shows a reasonable straight-line decay, and curves 1 and 2 represent two fits through that interval of the log. Curve 1 indicates that the water moves 6.1 m while losing half its activity, equivalent to a velocity of 6.1 m in 3.84 days, or 1.59 m per day. This converts to a volumetric flow rate of 20.1 liters per day (see Table 3.1). Similarly, curve 2 indicates a linear velocity of 1.82 m per day, or 23.1 liters per day. These estimates are 2.5 times greater than the flow in H2 that was measured during the summer of 1978, plotted in Fig. 2.4. The discrepancy could be due to the crudeness of the gamma-ray estimate, or it could be due to a real change in the average flow. The average flow into H2 could have changed either due to a change in hydraulic gradient or as a result of the commencement of the time-scale experiment. Obviously, it is desirable to do a controlled experiment to check the effectiveness of the gamma-ray estimate of flow rate.

Figure 4.1 shows two holes, S1 and S2, collared in the main drift and positioned parallel with the time-scale drift. Both dip at a 30-degree angle with the horizontal, so that borehole S1 passes within 1.5 m of the heater in H5, which is centered at 10 m below the floor of the time-scale drift. Hydrological and fracture data from S1 and S2 have been reported by Gale and Witherspoon (1979), a portion of which is shown in Figs. 4.12 and 4.13. These figures also show gamma logs acquired during 1978 and 1979.

Both the S1 and S2 logs show prominent increases in the count rate in the lower halves of the holes. Hole S1 shows a peak between 35 m and 39 m, a decrease, and another peak over the 20 to 29 m depth interval. Hole S2 has

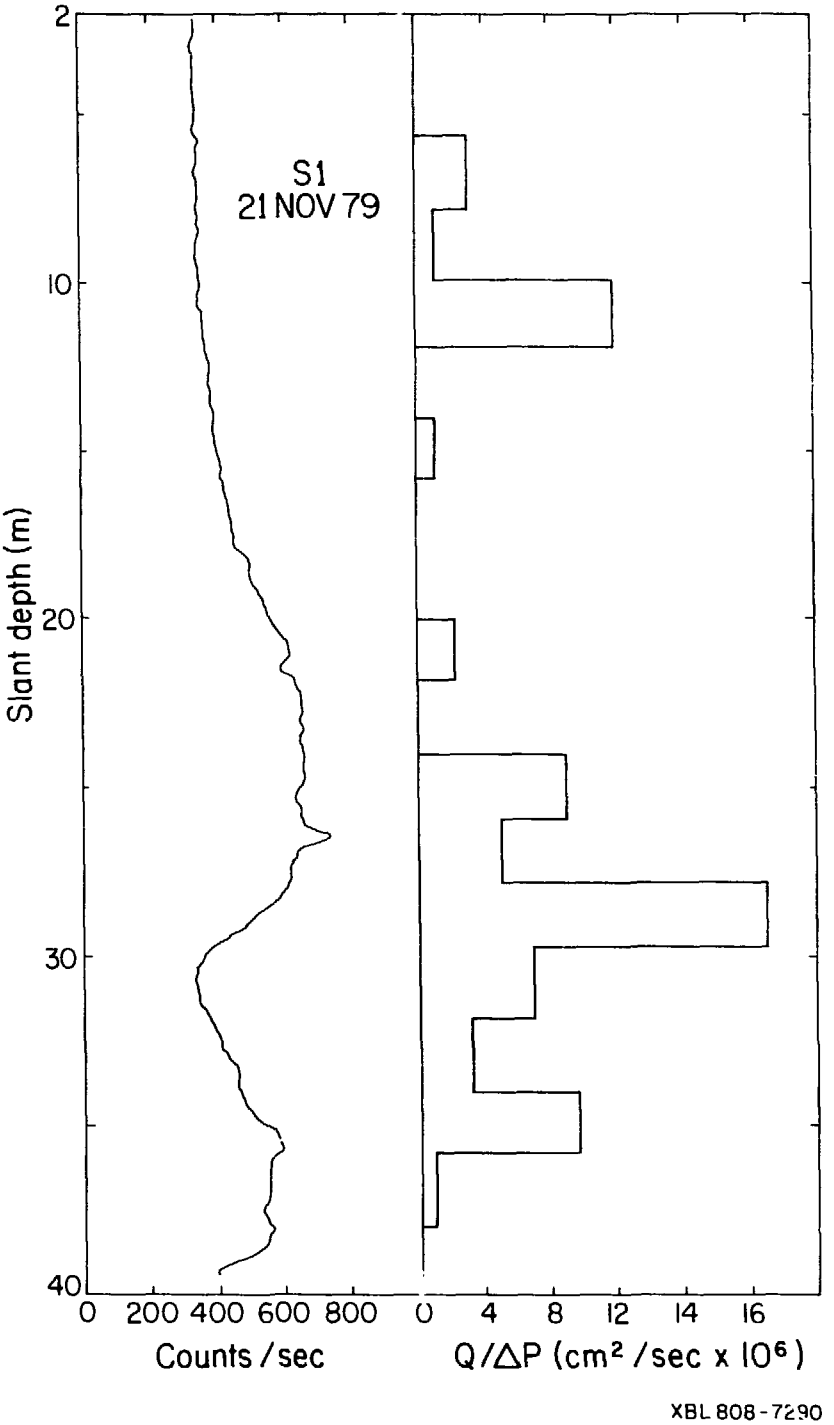

Fig. 4.12 Gamma log and injection test data from borehole S1. The ratio $Q/\Delta P$, taken from Fig. 10 of Gale and Witherspoon (1979), is proportional to the permeability.

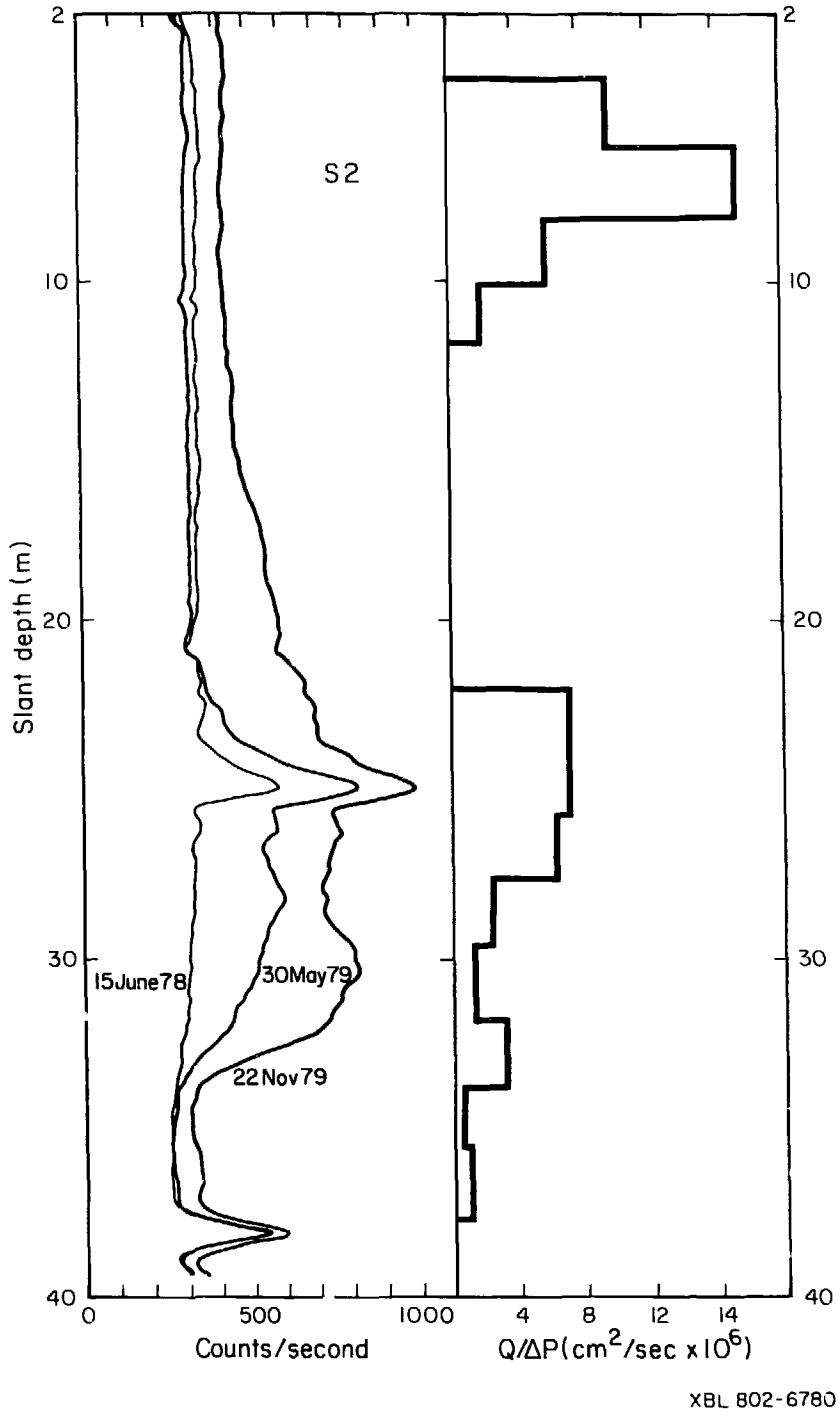

Fig. 4.13 Gamma log and injection test data, taken from Fig. 11 of Gale and Witherspoon (1979), from borehole S2.

two sharp peaks on all three gamma logs located at 25 and 38 m depth. These peaks are attributed to contributions from uranium in rock, because of their narrow half-width, and because of their additive contribution to the three logs. The broader increase over the interval 24-32 m is attributed to radon in water. The Q/P rate ratios given in Figs. 4.12 and 4.13 are directly proportional to the rock permeability. The radon increases depicted in the figures occur within the permeable zones, and decay above them. The upper permeable zones do not appear to be contributing radon, however. In accord with the previous discussions, we believe that radon-charged groundwater is entering the boreholes at the lower permeable zones, moving up the holes, and exiting near the collars.

Hole S2 was logged three times during 1978 and 1979. The first log, obtained on June 15, 1978, was made exactly 15 days after the turn-on of the time-scale heaters at the 1.125 kW power level. The second log was taken on 30 May, 1979 just six days before the turn off-of the heaters. The third log, on November 21, 1979, was taken almost six months after the cessation of heater operation, but unfortunately its flow cannot be related to heater operation because a major change occurred in the local hydrologic flow regime in early November as a result of packing off a copiously flowing interval in borehole R1. A logarithmic plot of the count rate in S2 is shown in Fig. 4.14, establishing flow-rate estimates of 3.0 and 11.5 liters per day over the indicated intervals for the latter two logs.

Hole S1 was logged once, on November 21, 1979. The log shown in Fig. 4.12 exhibits two peaks, indicating a zone of influx at 35-39 m and at 26-28m. The straight-line fit on semi-logarithmic paper (not shown) establi-

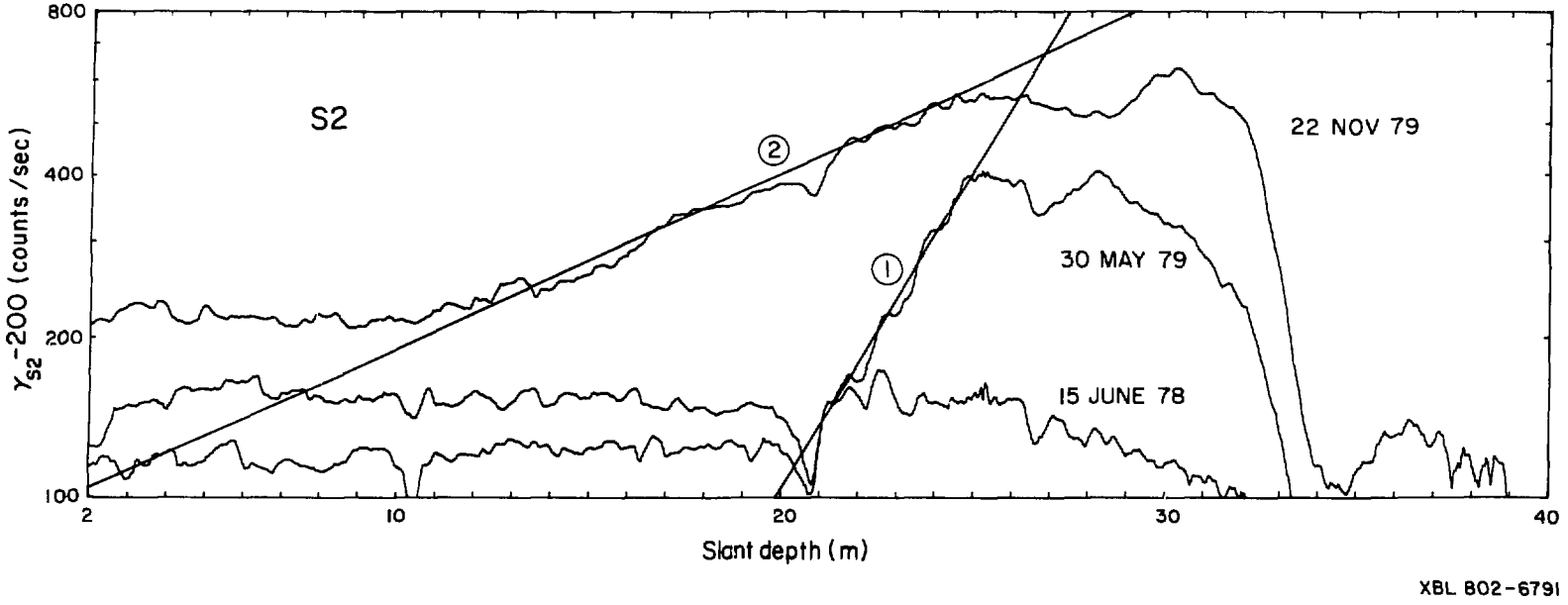

Fig. 4.14 Logarithmic plot of S2 gamma logs for three different dates. The 200 cps background due to the rock and the anomaly at 25 m have been subtracted out. The slopes of lines 1 and 2 indicate flows of 3.0 and 11.5 liters per day, respectively.

shes that the lower zone contributes 3.7 liters per day to the flow up the borehole. The flow rate above the upper zone is estimated to range between 7.2 and 11.6 liters per day; the uncertainty is due to ambiguity in picking the slope, but the higher estimate is preferred. Accepting the 11.6 value as the total flow and subtracting the lower zone contribution, we find the upper zone is contributing 7.9 liters per day.

The outflow at the collars of S1 and S2 was measured with the bucket-and-stop-watch method in February 1980, and found to be 12.7 and 13.4 liters per day, a very encouraging check with the November 1979 estimates of 11.6 and 11.5, respectively, from the gamma log. (No known hydrological changes occurred between late November and February.) However, the earlier two logs in S2 cannot be tied with confidence to any of the time-dependent heating or flow occurrences, because records were inadequate.

4.3 Ventilation Drift

Five holes in the ventilation drift were logged with the gamma probe, and the results are compared with two independent sets of hydrological data in Fig. 4.15. All the holes have gamma count rates above the 200 cps base rate, and all display one or more transitional increases in rate, progressing from the bottom to the top of the hole. The bar graphs represent the results of hydrological tests in packed-off intervals conducted by J.E. Gale and his associates of the University of Waterloo. This inflow is the product of the permeability and the drain pressure for each interval, and reflects the flows to be expected in an open hole. Intervals with flows less than one milliliter per minute are not shown. Hydrological testing was not done within 2 to 4 m of the drift face.

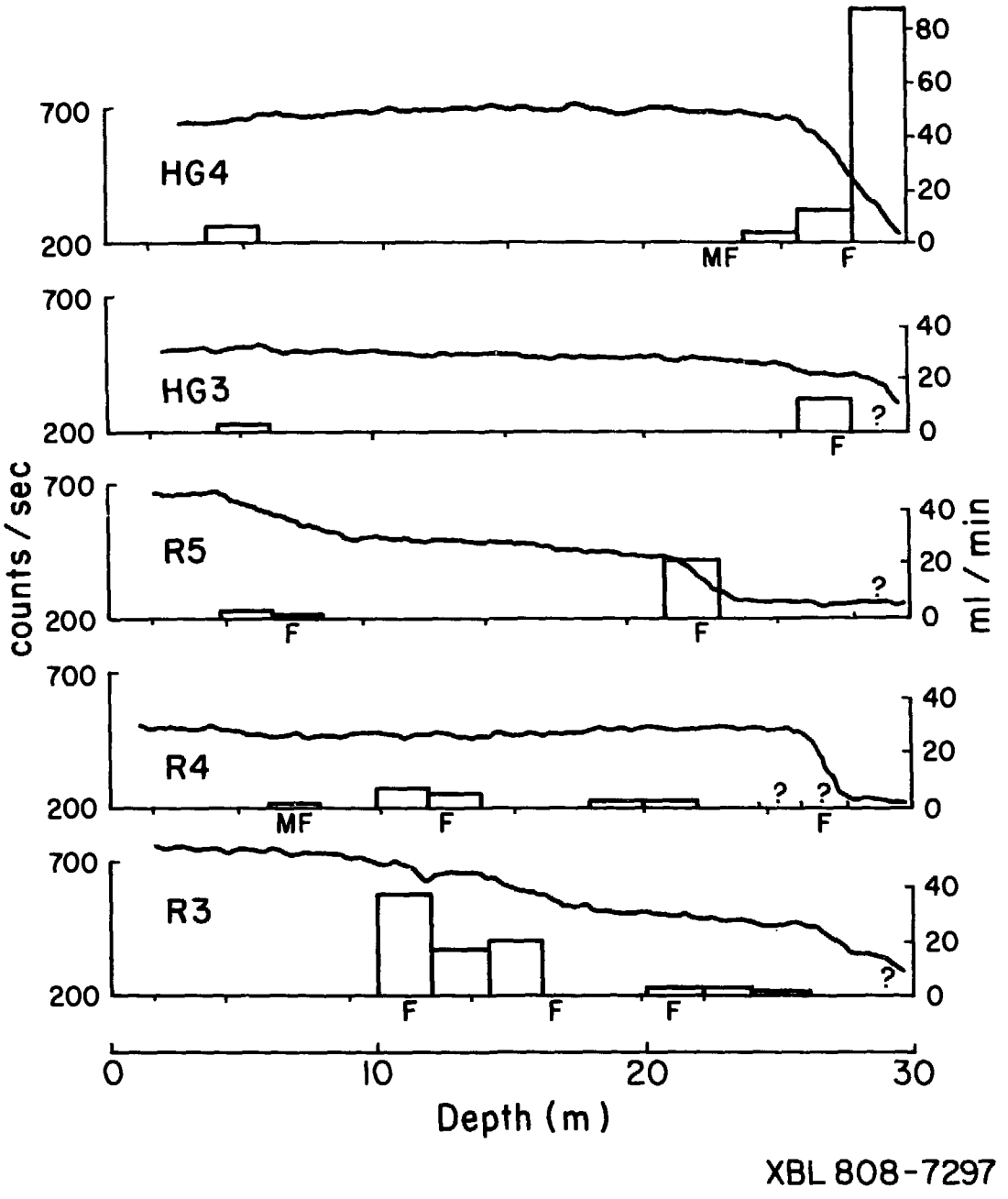

Fig. 4.15 Gamma logs and hydrologic measurements at rear of ventilation drift. Inflow into packed-off intervals at atmospheric pressure is given by the bar graph. Question marks indicate missing data. The letters F and MF designate fast and moderately fast pressure build-up within packed-off intervals.

Below the 200 cps base line are tick marks and the letters F and MF. These data were provided to us by J. Long of LBL, based upon measurements made by R. Galbraith during the installation of the packers for the macro-permeability experiment. After a given zone was packed off, the water pressure within the zone builds up to a steady-state value, with the rate of build-up controlled by the rock permeability of the zone. The letter F indicates that the build-up was fast, reflecting a zone of relatively high permeability, while the letters "MF" indicate a moderately fast build-up. Unmarked intervals, where the pressure build-up was slow, are inferred to be relatively impermeable.

The correlation between the gamma increases and the hydrological information in Fig. 4.15 is very encouraging. All the gamma increases occur at zones where either the flow data or the pressure buildup data, or both, indicate that the zones are more permeable than the rest of the hole. At this stage, however, the correlation is only qualitative.

4.4 Borehole DBH V-1

One deep hole designated DBH V-1 was drilled early in the course of the experimental work at Stripa for hydrological studies conducted by members of the Swedish Geological Survey. The hole is 56 mm diameter and was drilled vertically for more than 400 meters from its collar in the 410 m level of the mine (see Fig. 1.2). Its approximate collar location is x = 294, y = 1082, z = 410 in mine coordinates, located to the southeast and below the level of the plan map in Fig. 4.1. The hole is artesian. Water was flowing from the collar when the hole was logged in June 1979.

In Fig. 4.16 the gamma log is plotted with the permeability data collected by the Swedish Geological Survey (Olkiewicz et al., 1978). The lower limit of measureable permeability was determined by the in-situ pressure and the flow measurement capability. The permeabilities range over three orders of magnitude, with a bottom 160 m zone of measurable, erratic values, a middle interval from 100 to 300 m where the permeability was generally so low as to be unmeasurable with the system used, and an upper 100 m zone of measurable values.

Note that the log of Fig. 4.16 is greatly compressed compared with those plotted in the earlier figures, so that individual features appear to have a very narrow width. Most of these individual spikes are probably caused by uraniferous zones in rock, such as those shown in Fig. 2.1.

The data points posted on Fig. 4.16 are taken from Table 4.3. The potassium, uranium and thorium analyses done with gamma spectrometry on core samples are converted to a count rate for the gamma probe using the calibration expression derived earlier. It is these calculated points that are plotted in Fig. 4.16, representing the gamma component originating within the rock mass. The calculated values justify the subtraction of 200 cps background from the log prior to estimating the flow rate.

The outstanding features in Fig. 4.16 are the high gamma-count rate, which is well in excess of background for the entire hole length, and the qualitative correlation between the gamma ray and permeability data. The high rate is due to radon entering the lower portion of the hole and migrating upward in the flowing water column. From 300 m downward, both the gamma log and permeability measurements vary considerably. Because of the

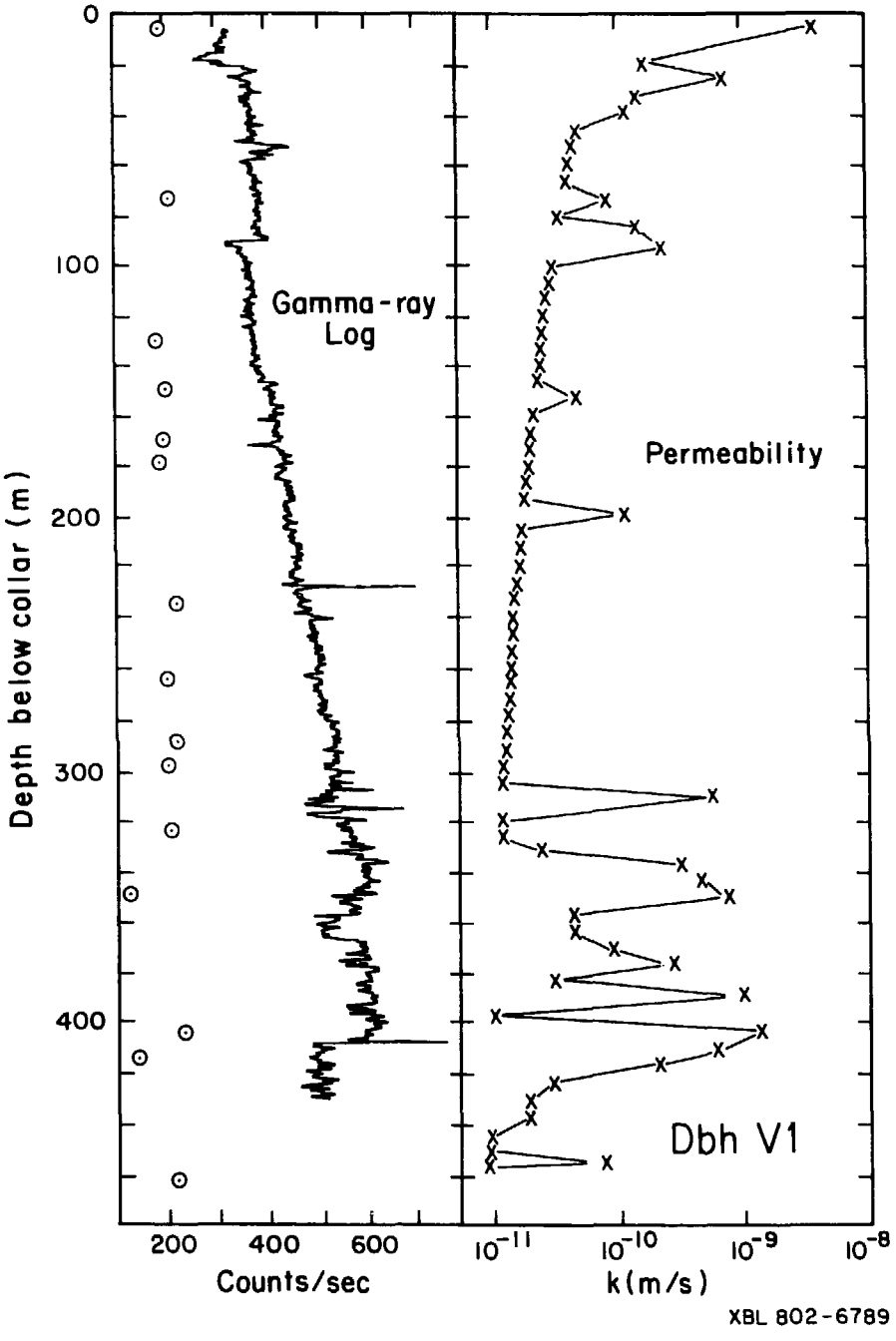

Fig. 4.16 Gamma log and permeability measurements in the 410 m level borehole, DBH V-1. Data points calculated from core analyses. Permeability data taken from Olkiewicz et al. (1978).

Table 4.3 Potasium, uranium, and thorium analyses on 20-cm crushed core samples from holes DBH V-1 (410 m level) and SBH-1. The calculated count rate is based on the empirical expression for the total count probe. Measured count rate is taken from gamma-ray logs.

					Count Rate (counts/sec)		
	Depth(m)	K(%)	U(ppm)	Th(ppm)	Calculated	Measured	Difference
Dbh V-1	4.73	3.75	39.5	31.1	197	325	127
	73.41	3.83	43.8	33.1	215	385	170
	125.30	3.49	38.9	26.4	187	380	193
	149.51	3.38	42.6	30.6	205	400	195
	168.59	3.10	41.5	30.6	200	410	210
	178.10	3.77	39.6	29.1	194	435	241
	234.70	3.89	46.1	35.8	227	475	248
	264.99	3.79	41.2	32.2	205	475	270
	289.79	3.92	46.6	34.1	226	510	284
	299.44	4.17	41.2	30.9	205	530	325
	325.25	3.78	43.4	32.4	212	550	338
	349.62	4.57	12.8	39.6	126	530	404
	404.77	3.90	47.4	38.3	235	585	350
	414.52	4.74	20.9	33.5	144	470	326
	464.62	4.10	45.5	35.4	225	---	---
SBH-1	148.65	2.42	4.14	11.3	43	178	135
	232.85	4.26	39.9	28.7	197	325	128
	255.20	3.89	38.8	30.3	194	315	121
	320.36	3.87	35.7	29.4	183	368±33	185
	371.75	4.02	41.3	30.6	204	190	-14

fluctuations, the geologic noise evidenced by the calculated single points at 350 and 408 m, and the lack of a gamma log below 430 m, it is not possible to state exactly where water is entering DBH V-1, although it is apparent that most of it enters below 300 m, and that a substantial fraction comes from below 400 m. The low permeability interval from 100 to 300 m produces no gains or losses in radon, with the resulting steady decline in count rate as water moves up the hole. In the upper 100 m the decline continues at a reduced slope above the step-like increase at 90 m. The permeable zone at 90 m is contributing radon-charged water and increasing the upward flow rate.

Using the "half-life decay length" method on the gamma log over the low-permeability section at 100 m to 300 m depth, we obtain a flow rate of 114 liters/ day in the 56-mm-diameter hole. Above the influx at 90 m, the method yields a flow rate of 192 liters/day, showing that the 90-m zone contributes about 80 liters/day or 40% of the total. This zone seems to be contributing more to the total flow than would be expected from its permeability-thickness product compared with that below 300 m depth. The consistency of the radon-derived flows cannot be checked until a full analysis is performed on the permeability and hydraulic head measurements. However, the overall flow rate seems quite reasonable, as other estimates of the artesian flow range between 120 and 240 liters per day (J.E. Gale, private communication).

4.5 Borehole SBH-1

The surface borehole SBH-1 (see Fig. 1.1 for location) was logged by the LBL and Swedish Geological Survey (SGU) logging systems on different dates, as shown in Fig. 4.17. The LBL log has more averaging than the SGU log, as

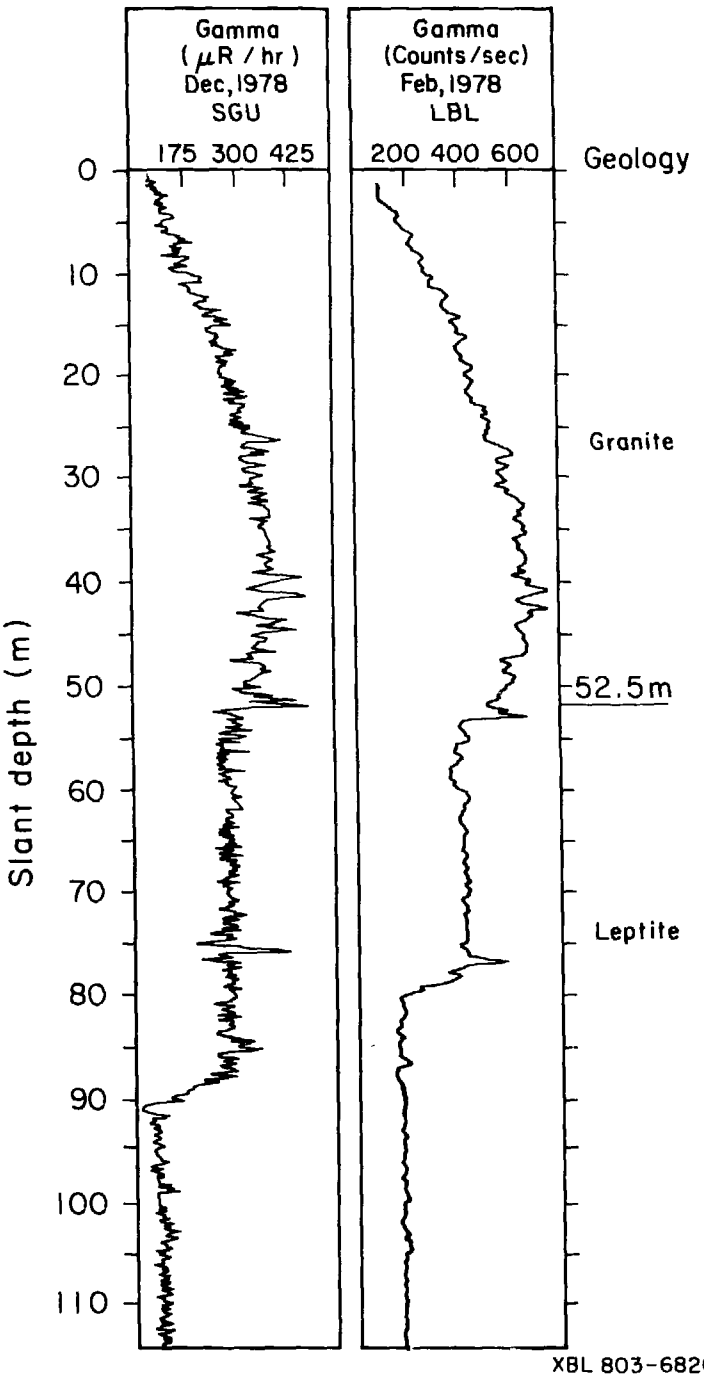

Fig. 4.17 Gamma-ray logs in SBH-1 taken with the LBL system in early 1978 and with the SGU system in late 1978. Water level, as indicated by other logs, fell from 80 m to about 90 m between the first and second logging runs.

shown by the finer structure on the SGU log. Except for this detail, the two logs overlaid perfectly below 100 m. Above 100 m, the logs are also quite similar except for the discrepancy between 78 m and 90 m, where the SGU log registers a higher rate than the LBL log. The decrease at 78 m in the LBL log and the decrease at 90 m in the SGU log each corresponds to the depth of the standing water level in the borehole at the time of the logging, as determined from the response of other logs.

We interpret the log behavior above the water level to be caused by the introduction of radon into the wellbore by groundwater infiltrating into the open hole and trickling down the lower side. The higher count rate observed above the water level is attributed to the fact that radon is more soluble on a volumetric basis in air than in water. In other words, water entering the hole gradually releases its radon to the air as it trickles down the hole. The steady release during trickle flow could be coupled with diffusional loss of radon upwards and out the open collar to cause the count rate gradient observed above the water column. Once the radon-charged water reaches the top of the water column, the count rate drops because the water has already released some of its radon.

The radon-charged water trickling down the open bore does not mask the spikes caused by uraniferous zones, nor does it mask the count decrease observed at the granite-leptite contact near 52.5 m. The count rate in leptite above the water level is constant because the leptite does not contribute radon-charged water. This does not exclude the possibility that water is entering through fractures in the leptite, however, because above the water column the count rate would not be affected.

The complete log of SBH-1 is shown in Fig. 4.18. The individual data points are based on spectral analyses, calculated according to the Eq. (2.1) for calibration of the probe. Two of the features are ascribed to geological effects. The step-like increase of about 140 cps at 208 m at the granite-leptite contact checks quite nicely with the data of Table 4.3, which shows a computed count difference of 150 cps between granite and leptite (compare samples 148.65 m with 232.85 m, etc.). A second feature, a reduced count rate at 280 m, is associated with a 2.5 m intercept of "greenstone," which may be a leptite xenolith.

Most important in SBH1, however, is the excess of actual counts above the expected rate indicated by the five data points. In the leptite, the gamma log should be indicating 40 to 50 cps; instead, it registers almost 200 cps. In the granite, 200 cps is expected, based upon the logging in underground holes as well as the computed response; instead, the count rate is in excess of 300 cps. These excess rates are attributed to radon transported downward in the water column and eventually exiting the borehole at depths where fracture zones occur. The most prominent of these fracture zones occurs at about 320 m, below which depth the count rate declines to the expected value of 200 cps. The gradual decline below 325 m indicates some further loss of water below 320 m, as discussed below.

This interpretation of fluid movement is consistent with other data available on SBH-1. The fractures observed in core and the geophysical logs (see Figs. 2.3 and 2.4 in Nelson et al.) reveal the presence of an 8 m interval of fractured rock centered at 320 m. A shift in the static temperature gradient at that depth also convincingly indicates that outflow

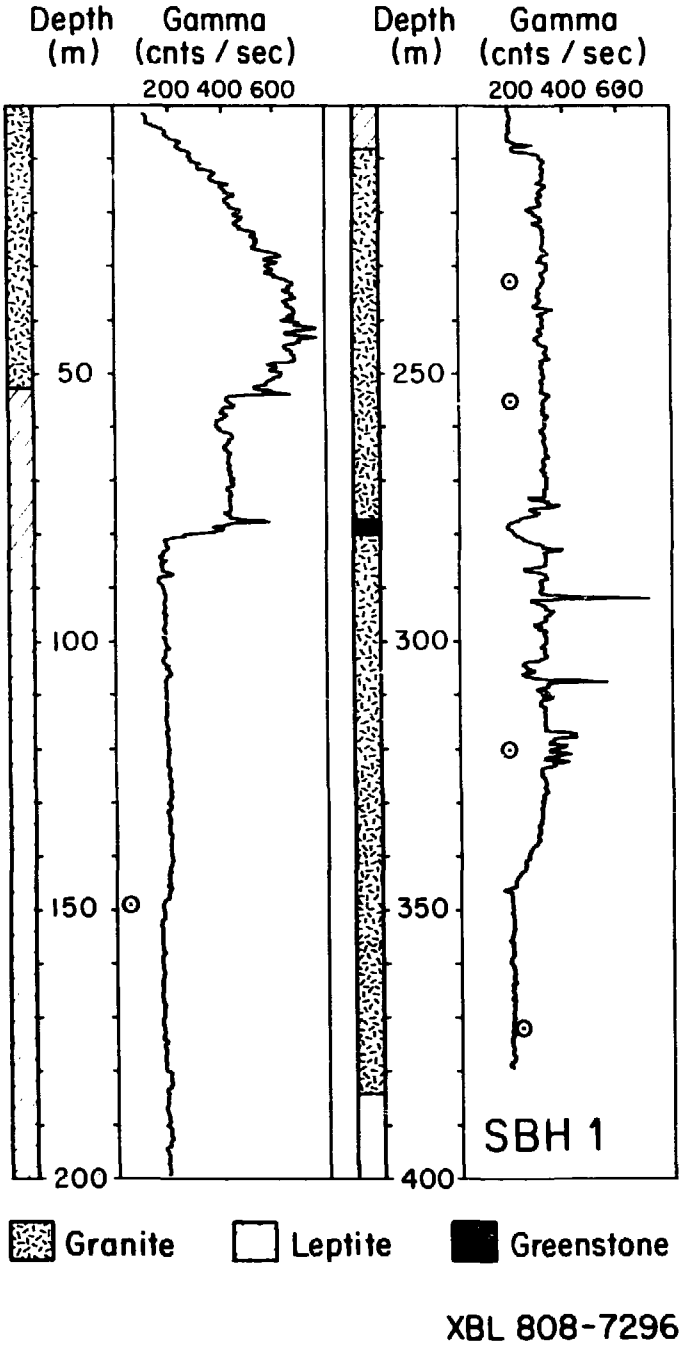

Fig. 4.18 Complete gamma log of hole SBH-1, logged in February 1978. The five data points are computed from laboratory spectral gamma analyses of core samples.

occurs. And finally, water pressure measurements (see Fig. 7 of Gale and Witherspoon, 1979) show that in-situ pressure is less than hydrostatic below a depth of 150 m.

The downward flow rate must be quite high above 325 m in SBH-1 because no gradient in the gamma log is discernible, as it is in DBH V-1 (Fig. 4.16), for example. As a consequence, only a minimum flow rate can be established using the concept presented in Fig. 3.2. Multiplying the length parameters in that figure by a factor of 20 provides an assessment of the SBH-1 case where we observe no gradient over the 240 m column of flowing water. A conservative estimate of the minimum flow rate down to 325 m in SBH-1 is then 1000 liters per day.

Below 325 m the flow rate reduces to about 50 liters per day with most of it existing at another fracture zone at 337 m, as shown in the detailed gamma log of Fig. 4.19. Hydrological and geophysical data also indicated in Fig. 4.19 confirm the location of the fracture zone. Below 337 m the flow reduces to 3 liters per day. The measurement sensitivity does not permit detection of the exodus of this small amount of flow.

In sum, the downward flow rate in SBH-1 under static open hole conditions is in excess of 1000 liters per day. Over 90% of this flow exits the hole at a fracture zone at 320 m. Less than 10% of the flow exits at a second fracture at 337 m.

4.6 Borehole SBH-2

The log from SBH-2 (see Figs. 1.1 and 1.2 for location), shown in Fig. 4.20, was obtained in August 1980. Water level at time of logging is un-

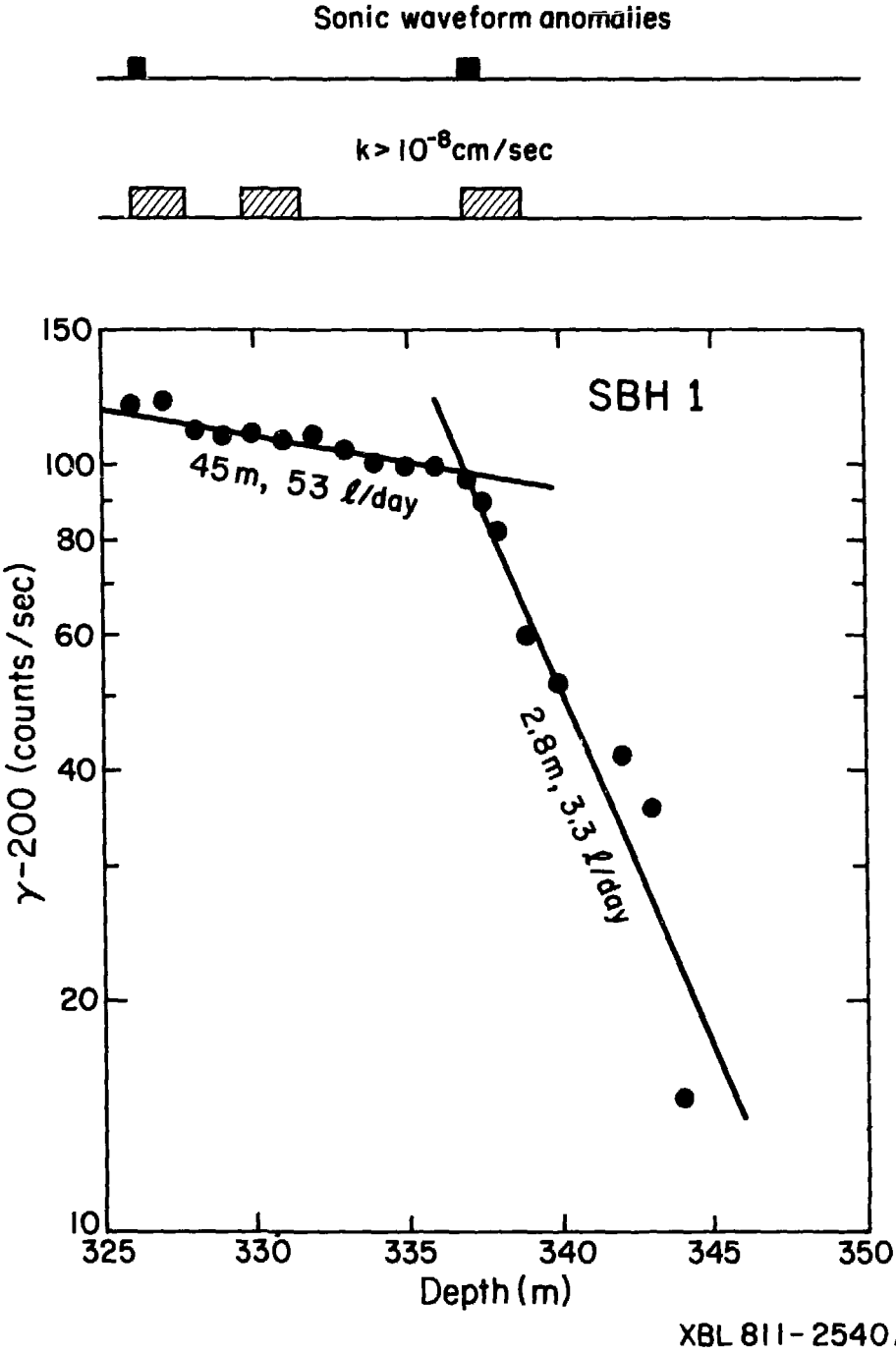

Fig. 4.19 Detail of gamma log in SBH-1 over the interval 325-350 m, with 200 cps background subtracted. Half-life distances and volumetric flow estimates are posted next to straight-line segments. Sonic waveform anomalies (Nelson et al., 1979) and straddle packer injection tests (Witherspoon et al., 1980) show possible flow zones.

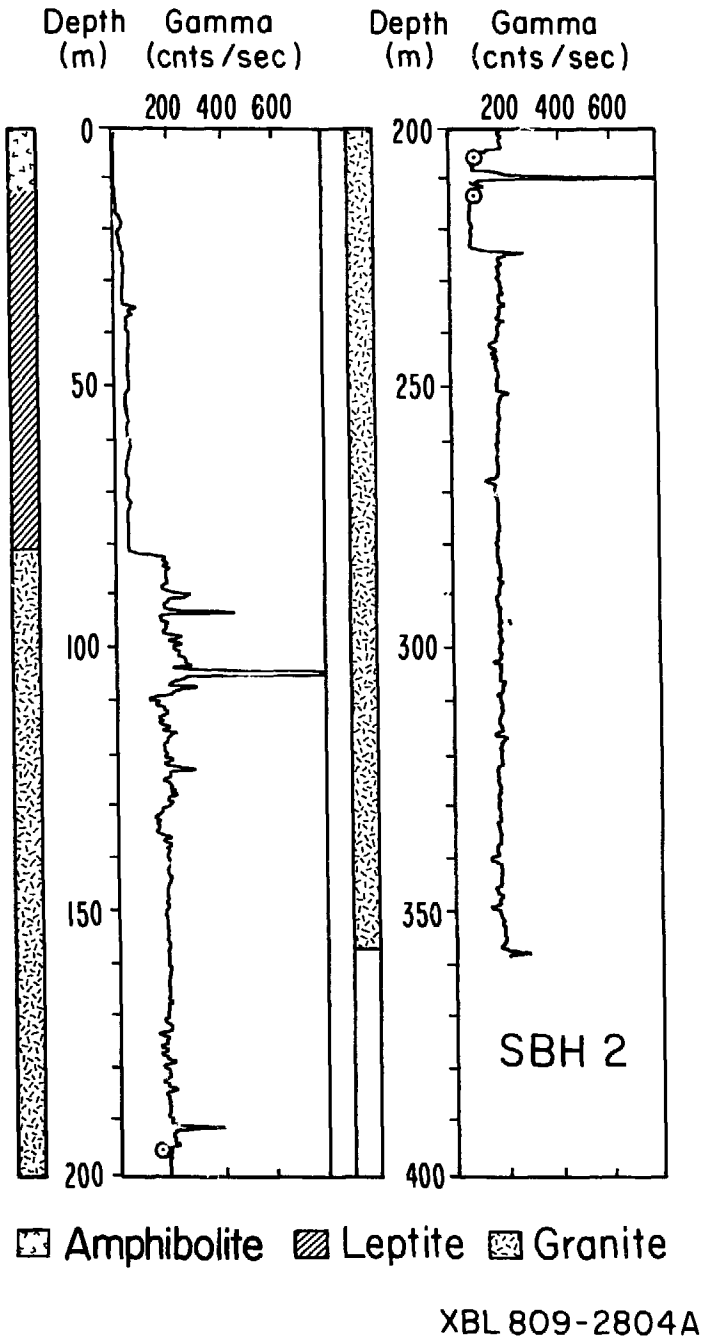

Fig. 4.20 Complete gamma log of hole SBH-2, logged on August 21, 1980.

known, but generally is at 20 m slant depth, with fluctuations from 0 to 35 m (C. Wilson, private communication). No other geophysical logs were run in SBH-2.

There is no evidence that radon is present in this borehole, as the count rate exceeds 200 cps only in a few short intervals. There are three possible reasons for this absence. First, SBH-2 is collared at the edge of the tailings pond. If a high-flow conduit existed between the pond and the borehole that contributed most of the water inflow into SBH-2, the radon concentration would be quite low because the tailing pond water would be "old" with regard to radon. This possibility seems unlikely but cannot be ruled out. Second, hydrological conditions in SBH-2 could be such that there is no flow in the hole under open hole conditions. However, pressure measurements in SBH-2 indicate that this is not the case (C. Wilson, private communication); the heads are such that there should be downward flow in SBH-2.

The third and most likely possiblity is that groundwater is entering the borehole in the upper intervals, but is not picking up radon from the rock. As reported by Olkiewicz et al. (1979), the upper intercept in SBH-2 is neither leptite nor granite, but "appears to be amphibolite or diorite near the surface, grading into leptite in the upper 30 m." As shown in Fig. 4.20, the count rate in the amphibolite is even lower than in the leptite, a fact confirmed by a surface measurement on amphibolite with a portable gamma spectrometer which gave 0.7% K, 0.8 ppm U, and (not detectable) Th (Wollenberg et al. 1981). The leptite, which also has considerably less uranium content than the granite, extends from 30 to 81 m, as shown in Fig. 4.20. As

a consequence, water entering the borehole through fractures anywhere in the upper 81 m slant depth would not be anomalous in radon concentration.

Some of the individual features in Fig. 4.20 warrant comment. The two spikes at 105 and 210 m are the largest responses observed in the Stripa gamma logs and must represent very high localized concentrations of uranium. A much smaller peak at 34 to 36 m within the leptite is caused by two granite intercepts observed in core. The gamma record from 90 to 130 m has a spiky appearance with above-average count rate. This interval overlaps the interval 88-118 m, which on the basis of hydrological tests appears to be the most permeable zone in the SBH-2 granite (C. Wilson, private communication), along with a narrow (2 m) permeable zone at 222-224 m. The low count interval from 204 to 224 m occurs in granite in which no unusual characteristics are visible. Laboratory spectral gamma measurements confirm that the low count rate is caused by a marked reduction in uranium content. Two samples from 206.7 and 213.1 m have an equivalent uranium content of 7.2 and 8.7 ppm, respectively (see Appendix A). The computed total counts for the gamma probe are shown as three data points in Fig. 4.20; values are 168, 93, and 94 cps at 196.4, 206.7, and 213.1 m, respectively. This single intercept of granite with 7 to 8 ppm uranium shows that not all of the Stripa granite is uniformly high in uranium content.

4.7 Borehole SBH-3

The character of the SBH-3 log (see Fig. 1.1 for hole location) shown in Fig. 4.21 is strikingly similar to that of SBH-1, especially so once the geological differences are recognized and accounted for. Radon-charged water enters the borehole through fractures in the granite, trickles down the

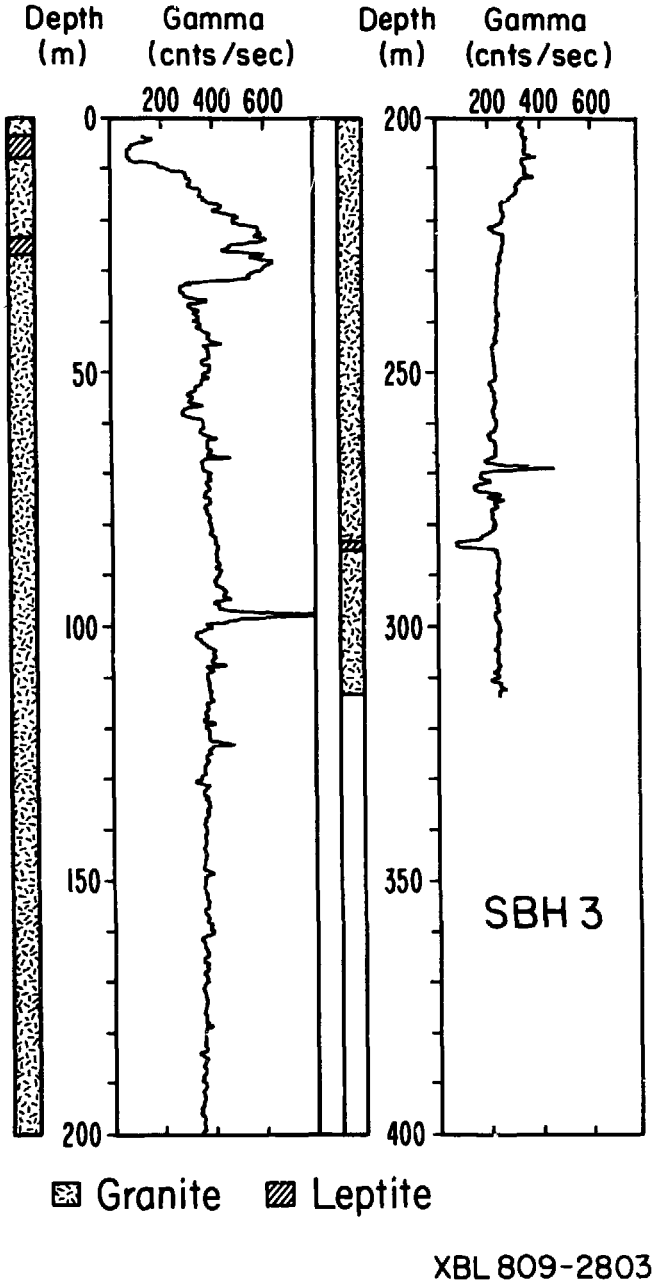

Fig. 4.21 Complete gamma log of hole SBH-3, logged on August 27, 1980. Water level at time of logging was not measured, but is inferred to be at 32 m from this log.

sides, and causes the high, progressively increasing count rate over the interval 0 to 32 m. The count rate drops within the two leptite intercepts because the background level is lower. At the top of the water column, here located at 32 m, the count rate drops sharply. There may be further radon influx within the water-filled hole between 32 and 100 m, as the gamma log appears to increase slightly.

Other features in Fig. 4.21 correlate with observations of core. The decrease at 284 m is caused by a leptite intercept. The positive-going spike at 268 m lies within a two-meter interval where a number of fractures filled with calcite and fluorite were noted. The positive-going spike at 97 m lies just above a one-meter interval described as highly fractured, weathered granite. Other geophysical correlations are not posible because no logs other than gamma ray were run in SBH-3.

There appear to be two fluid loss zones in SBH-3. Between 100 and 200 m the count rate decreases from 390 to 345 cps. Applying the "half-life decay length" method over this interval yields a linear flow rate of 68 m/day, or a volumetric rate of 307 liters/day. The zone of water outflow from the hole appears to be in the 210 to 220 m depth. Between 220 m and 260 m the count rate drops again, from 345 cps to about 215 cps. The estimate obtained over this interval is 3.7 m/day or about 17 liters/day. Due to the slow rate and the consequent long decay tail on the record, it is difficult to pick the loss interval, but it appears likely to be at the fracture zone at 268 m. Hence two loss zones are interpreted in SBH-3: one at 210 - 220 m taking about 290 liters/day and another, probably at 268 m, taking about 17 liters/day.

5. IMPLICATIONS FOR RADON EMANATION AND URANIUM DISTRIBUTION

5.1 Emanating Power and the Thin Crack Model

The thin crack model and the measurements of radon activity in the M3 water allow us to make some estimates, admittedly crude, of the emanating power of a "typical" fracture in the Stripa granite. Equation (3.31), for the case where the inflow rate Q is small with respect to both the crack and borehole mixing volumes, allows us to compute the emanating power:

$$E_A = \lambda^2 hVC/Q \quad . \tag{5.1}$$

A crack width of 0.01 cm is assumed. The volume V is based on the borehole volume of 127 liters for a 127 mm hole (see Table 3.1), and the inflow Q is taken as 10 liters per day. The measured activity in the M3 water was about 1 μCi per liter (Fritz et al., 1979), which converts to 18 x 10^6 atoms per cm^3 using:

$$N = \frac{1}{\lambda}\frac{dN}{dt} = \frac{1}{0.18} \times 3197 \times 10^{12} \times 10^{-6} \times 10^{-3} \quad .$$

The factor 3197 x 10^{12} converts the activity in Ci to the number of disintegrations per day.

The numerical values are:

$\lambda = 0.18$ (day^{-1})

$h = 0.01$ (cm)

$V = 1.3 \times 10^5$ (cm^3)

$Q = 1 \times 10^4$ (cm^3/day)

$C = 18.0 \times 10^6$ (radon atoms/cm^3)

yielding an emanating power from Eq. (5.1) of:

$E_A = 7.3 \times 10^4$ (radon atoms/cm^2 - day).

Obviously this estimate is not much better than order-of-magnitude, as the

value for the average fracture estimate is only a rough guess, and the model itself is rather simplistic. Nevertheless, the above value for E_A gives a rough indication of the number of radon atoms escaping daily from a square cm of rock into the water filling a crack.

At this point it is necessary to relate the surface emanating power, E_A, a parameter derived from the thin crack model, to the volumetric emanating power, E_V, which gives the radon produced per volume (or weight of rock. Emanation values E_V measured on Stripa core samples are tabulated in Appendix A. Excluding the hand specimens listed there and the samples with uranium content less than 25 ppm we have 18 samples for which the average value of E_V is 1.57 pCi/gm, equivalent to:

$$E_V = 1.57 \times 10^{-12}(\text{Ci/gm}) \times 2.63\ (\text{gm/cm}^3) \times 3197 \times 10^{12}(\text{dis./day/Ci})$$

$$E_V = 13 \times 10^3 \text{ radon atoms per day per cm}^3 \text{ rock}$$

whereas our surface area emanation was estimated to be

$$E_A = 73 \times 10^3 \text{ radon atoms per day per cm}^2 \text{ of fracture surface.}$$

The ratio $E_A/E_V \sim 5.5\ \text{cm}^3/\text{cm}^2$ forms a measure of the rock volume contributing radon to unit area of fracture surface. The ratio of 5.5 suggests that a square centimeter of fracture surface has an effective volume extending about 2 cm from either side of the fracture. Radon must diffuse through the pore space to reach the fracture surface. Interestingly, I. Neretniks (personal communication, 1980) indicates that a diffusion distance of a few centimeters is reasonable, based upon $\sqrt{Dt}$, for the radon half-life t and for known estimates of the diffusion coefficient D.

This comparison between laboratory data and the thin crack model coupled with field data is quite satisfactory in demonstrating that the emanation numbers thus obtained are physically reasonable.

5.2 Geological Considerations

The development in the preceding paragraphs indicates that the high radon concentration in Stripa groundwater is satisfactorily explained by a combination of high uranium content and thin fracture aperture. This result also implies that other igneous rocks with similar fracture characteristics will produce radon concentrations differing from that at Stripa in proportion to the fraction of the uranium present. If so, then many sites must exist where the radon concentration is 10% or more of the Stripa concentrations, yet there is little documentation to support this.

Only a fraction of the radon produced within a cubic cm of rock escapes from the matrix. The data in Appendix A show that 0.10 is quite a reasonable value for the fractional emanation coefficient, which conforms well to the estimates of escape to production ratio obtained by Barretto et al. (1972). With reference to this data base, the Stripa samples do not appear to be unusual in fractional emanation.

Another possibility is that radon emanation is extraordinarily high along permeable fractures and that these surfaces were not represented in the core samples reported in Appendix A. Mobilization and deposition of any member of the U-238 series higher than radon could produce such an effect. Two likely candidates are uranium and radium. Wollenberg et al. (1981) used the fission track-radiographic method to locate and determine the abundance of uranium in uncovered thin sections. They find that uranium is localized

in the Stripa granite (quartz monzonite) in three distinct mineralogical associations. In brief, they find that uranium is found concentrated in:

1) tiny euhedral opaque grains found usually in chlorite, but also in muscovite-chlorite-sericite filled fractures, and even within quartz or feldspar grains.
2) anhedral opaque grains associated with both a quartz-epidote-sericite-filled fracture and with fine carbonate-sericite stringers. The absolute abundance of uranium in this second category is greater than in the first.
3) dispersed along chlorite-filled fractures without associated discrete grains.

The number of thin sections examined was small, so no statistical inferences were possible. At the present time, the petrographical evidence indicates that uranium is preferentially disposed along flow paths, but the evidence is far from conclusive.

However, Wollenberg et al. (1981) present another line of evidence indicating that uranium is located in sites that can be leached by groundwater rather than in inaccessible sites in accessory minerals. Although the outcrops at Stripa are comparatively fresh as a consequence of glaciation, the uranium content in surface outcrop is depleted (mean of 27 ppm) relative to subsurface samples (values in the range 40 to 45 ppm). The data provide good evidence that uranium sites within the rock favor its leaching by acidic near-surface groundwater.

6. RADON MEASUREMENTS IN AIR

6.1 Introduction

As mentioned in Section 1, the role of groundwater in transporting radon from the rock mass into the air in underground drifts has been recognized by previous studies. Our monitoring of radon daughter activity in the air of experimental work areas stemmed from health safety concerns rather than a study of radon transport. Hence the results of this action are not closely tied to the models and data presented in previous sections, but are given here for the sake of completeness and to emphasize the assumed relationship between water-borne and air-borne transport of radon in underground workings.

Measurements were taken in the Stripa workings at approximate weekly intervals, beginning in late April 1978 and continuing until late May 1980. Four stations were included in almost every survey: the computer room (CR), the full-scale drift (FS), the time-scale drift (TS), and the ventilation drift (VD). From mid-July 1978 onwards, an instrument peformance check routine has been followed that permits re-normalization of results obtained from this sampling monitoring program, based on the response observed from check sources and from field intercomparisons with Swedish measurement teams. Such re-normalization has been done by Carl Lionberger (private communication, 1980), and all results presented here are taken directly from Lionberger's analysis.

6.2 Measurement of Airborne Alpha Activity

Estimation of the health hazard associated with inhalation of atmospheric Rn-222 and its daughters is based mainly on considerations of the

alpha decay of these radionuclides while they are within the pulmonary system. Three alpha-decay nuclides are of primary concern here: Rn-222, Po-218, and Po-214. The latter two may be present in varying proportions with respect to Rn-222: secular disequilibrium is frequently encountered in mine environments. Thus, measurement of Rn-222 concentration alone would not always provide sufficient information for health protection purposes.

A more adequate measurement is the determination of airborne alpha-decay activity, leading to the specialized concept of the Working Level (WL), widely used in the uranium mining industry. The WL and its derived unit of integrated exposure, the Working Level Month (WLM), are defined and discussed in Appendix B. This appendix contains material extracted from the chapter in Instrumentation for Environmental Monitoring--Radiation (LBL-1, Vol. 3) that deals with Rn-222, including part of its bibliography.

Briefly, the method involves drawing air at a known flow rate through a filter for a measured time; subsequently, the alpha-activity trapped on this filter is measured. Given the sampling rate, the collection time, the delay before counting, the counting time, and the counter background, results of this procedure are converted to units of WL, as reported here.

6.3 Results

Working Level (WL) values for each individual station are listed on Table 6.1 for the period July 1978 through May 1980. In general, values at all four stations change concordantly, suggesting that the average of values from all stations measured on a particular day is a useful quantity, particularly for very low values. A value reported as 0.01 WL is based on approximately 10 counts, measured against a counter background that produces

Table 6.1. Radon levels, in units of Working Level, measured in air samples from four underground drifts: CR, computer room; FS, full-scale drift; TS, time-scale drift; VD, ventilation drift.

Year	Month/Day	CR	FS	TS	VD	Avg.
1978	7/14	.02	.08	.06	.05	.05
	7/28	.08	.22	.13	.05	.12
	8/11	.02	.11	.11	.10	.08
	8/21	.11	.32	.22	.15	.20
	9/ 4	.19	.03	.35	.28	.21
	9/ 8	.06	.12	.14	.12	.11
	9/15	.13	.15	.06	.16	.12
	9/22	.09	.17	.16	---	.14
	9/28	.07	.15	.17	---	.13
	10/ 5	.01	.07	.03	.08	.05
	10/12	.14	.26	.27	---	.22
	10/20	.01	.09	.19	---	.10
	10/26	.05	.06	.09	.08	.07
	11/ 2	.14	.26	.27	---	.22
	11/ 9	.14	.20	.21	---	.18
	11/16	.01	.03	.08	.08	.05
	11/23	.04	.06	.10	.06	.06
	11/30	<.01	<.01	.01	<.01	.01
	12/ 7	<.01	.01	.02	.01	.01
	12/22	.12	.30	.24	.18	.21
1979	1/12	.06	.04	.14	.11	.09
	1/18	.02	.10	.16	.11	.10
	1/26	.02	.09	.03	.06	.05
	2/ 2	.11	.19	.20	.16	.16

Table 6.1, cont'd.

Year	Month/Day	CR	FS	TS	VD	Avg.
1979	2/ 9	.06	.10	.11	.05	.08
	4/20	---	.01	---	.02	.02
	4/23	.01	---	.05	.01	.02
	5/10	.08	(.01, .30)	.01	.02	.08
	5/15	(.44, .24)	.22	(.61, .26)	.28	.34
	6/28	.01	---	.15	.22	.13
	7/27	.09	.22	.17	.22	.18
	8/ 2	.43	---	(.17, .17)	---	.26
	8/ 7	.13	---	---	---	.13*
	8/ 8	---	.17	.22	.27	.20*
	8/13	---	.02	.23	.23	.16
	8/14	.08	(.21, .19, .11)	.26	.27	.19
	8/21	---	.23	(.16, .09)	.03	.13
	9/ 4	---	---	---	---	---
	9/ 5	---	---	---	---	---
	9/11	.04	(.02, .27)	.08	.08	.10
	9/21	---	.01	.08	.04	.04
	10/ 1	---	.02	.03	.01	.02
	10/ 8	.02	.06	.05	.03	.04
	10/30	---	<.01	.03	.05	.03
	11/ 6	.03	.06	.08	.05	.06
	11/15	---	.02	.02	.19	.08
	11/27	.01	.02	.04	.03	.02
	12/ 6	---	.07	.08	.07	.07
	12/14	.02	.03	.04	.04	.03

Table 6.1, cont'd.

Year	Month/Day	CR	FS	TS	VD	Avg.
1980	1/7	---	.10	.09	.16	.12
	1/17	---	.01	.01	.01	.01
	1/22	---	.01	<.01	.01	.01
	2/ 4	---	.21	.27	.32	.27
	2/ 7	---	(.16, .21)	---	.19	.19
	2/14	---	.34	.34	.25	.31
	2/21	---	.30	.40	.28	.33
	2/22	---	---	.15	---	.15
	2/28	---	.12	.19	.15	.15
	3/13	---	.20	.19	.16	.18
	3/20	---	.16	.23	.23	.21
	4/ 2	---	.15	.26	.15	.19
	4/17	---	.12	.09	.09	.10
	4/25	---	.06	.03	.11	.07
	5/ 7	---	.13	.11	.09	.11
	5/22	---	.09	.08	.08	.08

1 to 5 counts in the typical five-minute count time.

The last column on Table 6.1 lists the average WL value obtained on each survey day. The range of this average is 0.01 to 0.34 WL. (For purposes of averaging, values reported as < 0.01 WL are assigned the value 0.01 WL.) The averages are also plotted on Fig. 6.1. The averaged WL values are presented in different format on Fig. 6.2, where they are grouped according to the number of cases that lie within increments of 0.05 WL. Of the 62 cases, 12 lie below the value 0.05 WL, while only 3 lie above the value 0.30 WL.

The wide range of WL values observed (greater than a 10-fold change in successive measurements) make it difficult to infer time-average values without a clearer understanding of the physical mechanisms that accompanied them. However, some of the observed variations known to have occurred during the two-year measurement period can be enumerated:

1) Groundwater inflow into the drifts through boreholes and seeps. Water influx has been found to be an important source of radon in mines (Dungey et al., 1979). Most of the inflow into the time-scale and ventilation drifts came from a few boreholes, but, to avoid ponding, their flow was diverted out to a point in the main drift opposite the entry of the full-scale drift. These diversions and the extent of ponding within individual drifts changed somewhat during the two-year period.

2) Seasonal and short-term weather variations caused dramatic fluctuations in the humidity and temperature of the inlet ventilation air from surface. Consequently, the evaporation rate of water from drift surfaces

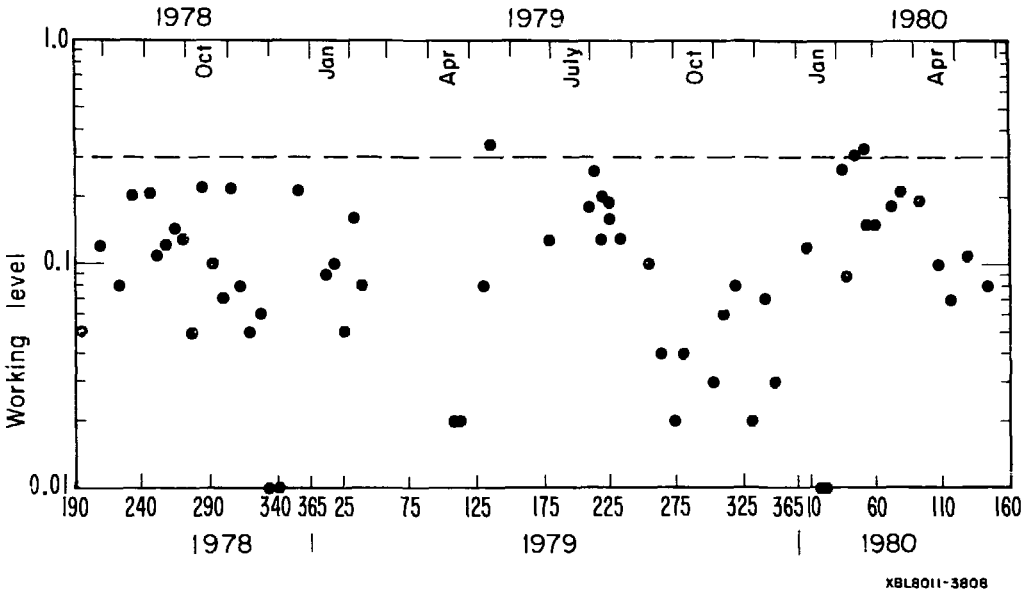

Fig. 6.1 Average values of working level, taken from Table 6.1.

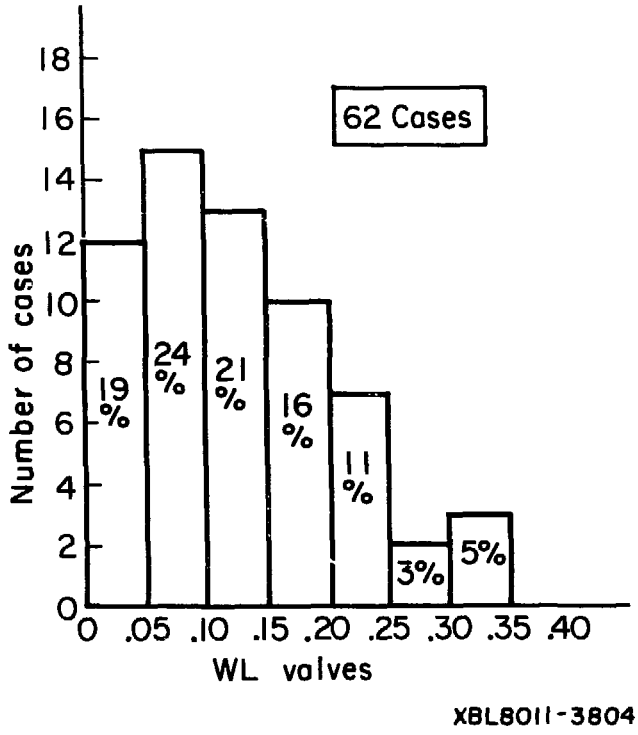

Fig. 6.2 Histogram of all WL measurements for the two-year monitoring period.

changed noticeably from time to time.

3) A variety of circumstances caused changes in the mass flow rate of ventilation air. In October 1978 the ventilation flow rates were approximately: main tunnel to experimental areas: 3.5 m/s; ventilation drift: 1.5 m/s; time-scale drift: 0.3 m/s; full-scale drift: 1.5 m/s. The installation and operation of the ventilation (macropermeability) experiment changed this air-flow distribution, as did numerous undocumented short-term changes in the local ventilation system within the experimental drifts. Other alterations affecting air-flow were also made in the unused mine areas adjacent to the experimental area.

4) Radon levels in the computer room were substantially below values in the other working areas because of filtration by the air conditioning unit provided for the computer system.

In summary, it was early recognized that there was a potential radiological health hazard due to natural occurrences of radon in the underground experimental areas, even before the high concentrations of radon in groundwater were known. Periodic sampling in the four work areas showed that the levels were generally below 0.3 WL during the two-year operational period and hence within the requirements of the U.S. mine safety regulations (see Appendix B). No systematic efforts were made to correlate radon levels with changes in the ventilation system or with groundwater influx rates.

7. SUMMARY

1) At Stripa the groundwater contains sufficient amounts of radon to be observed on the total-count gamma-ray log, over and above the gamma contribution from the rock itself. The radon level is high at Stripa because:

a) the uranium content in the Stripa granite is high, between 35 and 40 ppm.

b) the uranium seems to be localized along fractures.

c) groundwater flow is along fractures in low porosity rock so that dilution is minimal, and the flow rates are high enough to bring in sufficient radon to be detected.

2) Step-like increases (decreases) in radon levels reflect zones of fluid entry (loss). Examples are the fluid loss zones at 320 m slant depth in SBH-1 (Fig. 4.18) and at 210 m in SBH-3 (Fig. 4.21). Examples of fluid entry can be seen clearly on the five HG and R holes in Fig. 4.15. These examples establish that the radon-charged water provides a flow profile of the hole, showing which zones produce or take water under the hydrostatic conditions prevailing under open hole conditions.

3) If mixing occurs within the borehole, then the average concentration of radon may depend upon the volumetric flow rate as Q^{-1}, Q^{0}, or Q^{+1}, depending upon the ratio of Q/λ to the source and mixing volumes (see Table 3.2). We mainly see evidence for mixing in the largest (127 mm) diameter holes in the time scale drift (refer to Fig. 2.4), where the inflow rate Q is always low enough that the concentration varies linearly with Q. In this case, concentration is controlled by the residence time in the hole that is less than the radon half-life. Fluid entry from a single fracture followed by mixing

cannot be distinguished from uniform fluid entry along the borehole length (refer to Fig. 3.3 and the corresponding discussion).

4) If mixing does not occur, and if the flow rate falls within a range of values determined by the radon half-life and the observation length within a hole, then the flow rate can be estimated from the exponential decay of radon activity along the hole (refer to Fig. 3.2). Applying the method to borehole H2 (Fig. 4.11) yields an inflow estimate of 20 liters per day (l/d). Flow estimates in boreholes S1 and S2 were both about 11 liters per day, within 2 l/d of the flow measured with the bucket-and-stopwatch method. Upward flow in DBH V-1 is about 192 l/d. The downward flow in SBH-1 is so high that the activity level remains constant down to the loss zones; the rate must exceed 1000 l/d. The downward flow in SBH-3 is considerably lower, about 300 l/d. No independent checks on the SBH-1 and SBH-3 estimates are available.

5) Naturally occurring radon may also be useful as a tracer at other sites in igneous rock. If the radon levels are too low to be detected with a total-count gamma tool, then we might consider:

a) a spectral gamma probe, to be used where the bismuth-214 counts associated with radon in water are higher than those from rock, but are masked by potassium-40 counts from rock;

b) water sampling, followed by spectral gamma or chemical analysis;

c) some method of alpha counting in the borehole.

6) The natural radioelement distribution at a waste storage site must be carefully determined during the site characterization phase, to determine levels of the natural radioisotopes in rock and groundwater. Although not

many cases have been documented, high radon levels in groundwater may not be all that unusual in igneous rock sites: a recent groundwater study in Maine by Hess et al. (1980) shows that radon levels in groundwater are higher in granitic than in metamorphic rock, ususally above the nanocurie per liter level, with some samples as high as 0.2 μCi per liter. Hence careful baseline studies are necessary, and even then one must remain aware that the natural radioactive component of groundwater may change due to changes in the hydrological regime.

ACKNOWLEDGMENTS

We wish to thank H. Wollenberg for his continued support and insightful suggestions during the course of this work, and S. Flexser for discussions of geological questions. L. Andersson and B. Paulsson assisted with the acquisition of many of the gamma-ray logs, and R. Galbraith did most of the calibration tests. K.A. Magnusson of the Swedish Geological Survey contributed a gamma ray log of hole SBH-1. C. Lionberger, J. O'Riva, G. Ramqvist and M. Saarloos were all involved with the airborne radon measurements and equipment.

REFERENCES

Andrews, J.N. and D.F. Wood, 1972. "Mechanism of Radionuclide Rock Matrices and Entry into Groundwaters." Trans. Inst. Mining Metallurgy (London).

Barretto, P.M.C., R.B. Clark, and J.A.S. Adams, 1972. "Physical Characteristics of Radon-222 Emanation from Rocks, Soils and Minerals: its Relation to Temperature and Alpha Dose," in The Natural Radiation Environment II, J.A.S. Adams, W.M. Lowder and T.F. Gessell, eds., Vol. 2. U.S. Department of Commerce, CONF-720805-P2, 1972.

Burleigh, R.H., E.P. Binnall, A.O. DuBois, D.U. Norgren, and A.R. Ortiz, 1978. Electrical Heaters for Thermo-mechanical Tests at the Stripa Mine. Lawrence Berkeley Laboratory report LBL-7063, SAC-13. Berkeley, California.

Czubek, J.A., 1962. "Quantitative Interpretation of Gamma-Ray Logs," Proc. Nuclear Geophys. Conf., Krakow, Poland, September.

D'Amore, F., and J.C. Sabroux, 1976-77. "Signification de la Presence de Radon-222 dans les Fluids Geothermiques." Bull. Volcanol., Vol 40-2, pp. 2-10.

Dodd, P.H. and D.H. Eschliman, 1972. "Borehole Logging Techniques for Uranium and Exploration and Evaluation," in Uranium Prospecting Handbook, S.H.U. Bowie et al., eds., Inst. Min. Metall., London, p. 244-276.

Dungey, C.J., J. Hore, M.D. Waller, 1979. "An Investigation into Control of Radon and its Daughter Products in Some Cornish Mine Atmospheres." Tran. Inst. of Mining and Metallurgy, April. pp. A35-43.

Eggers, D.E., 1976. "The Application of Borehole Geophysics to the Selection and Monitoring of Nuclear Waste Disposal Sites," in Site Characterization, Proc. of 17th U.S. Symposium on Rock Mechanics, pp. 4B3-1 to 4B3-7.

Fertl, W.H., W.L. Stapp, D.B. Vaello, W.C. Vercellino, 1980. "Spectral Gamma-Ray Logging in the Texas Austin Chalk Trend." J. Petroleum Technology, pp. 481-488.

Fritz, P., J.F. Barker, and J.E. Gale, 1979. Geochemistry and Isotope Hydrology of Groundwaters in the Stripa Granite: Results and Preliminary Interpretation. Lawrence Berkeley Laboratory report LBL-8285; SAC-12, Berkeley, California.

Gale, J.E. and P.A. Witherspoon, 1979. An Approach to the Fracture Hydrology at Stripa: Preliminary Results. Lawrence Berkeley Laboratory report LBL-7079, SAC-15. Berkeley, California.

Hess, C.T., R.E. Casparius, S.A. Norton, and W.F. Brutsaert, 1980. "Investigation of Natural Levels of Radon-222 in Groundwater in Maine for Assessment of Related Health Effects," in Natural Radiation Environment III, T.F. Gessell and W.M. Lowder, eds., vol. 1, pp. 529-546, U.S. Department of Energy CONF-780422.

Jackson, P.O., J.A. Glissmeyer, W.I. Enderlin, L.C. Schwendiman, N.A. Wogman, and R.W. Perkins, 1980. "An Investigation of Radon-222 Emissions from Underground Uranium Mines." Progress Report 2, NUREG/CR-1273, PNL-3262, Pacific Northwest Laboratory, Richland, Washington, February.

Killeen, P.G., 1972. "Gamma Ray Spectrometric Methods in Uranium Exploration --Application and Interpretation," in Geophysics and Geochemistry in the Search for Metallic Ores, Peter J. Hood, ed., pp. 163-230, Geol. Survey of Canada, Economic Geology Report 31.

Løvborg, L., P. Nyegaard, E.M. Christiansen, and B.L. Nielson, 1980. "Borehole Logging for Uranium by Gamma-Ray Spectrometry." Geophysics, 45, No. 6, June, pp. 1077-1090.

Nelson, P.H., B. Paulsson, R. Rachiele, L. Andersson, T. Schrauf, W. Hustrulid, O. Degerman, and K.A. Magnussen, 1979. Preliminary Report on Geophysical and Mechanical Borehole Measurements at Stripa. Lawrence Berkeley Laboratory report LBL-8280, SAC-16. Berkeley, California.

Olkiewicz, A., K. Hansson, K. Almen, and G. Gidlund, 1978. "Geologisk och hydrogeologisk grunddokumentation av Stripa Forsoksstation," KBS Teknisk Rapport 63, KarnBranslesakerhet, Stockholm, February, 1978.

Olkiewicz, A., J.E. Gale, R. Thorpe, B. Paulsson, 1979. Geology and Fracture System at Stripa. Lawrence Berkeley Laboratory Report LBL-7051, SAC-21, Berkeley, California., February.

Rhodes, D.F., R.A. Stallwood, and W.E. Mott, 1961. "Intensity of Unscattered Gamma-Rays Inside Cylindrical Self-Absorbing Sources." Nuclear Science and Engineering: 9, 41-46.

Schrauf, T., H. Pratt, E. Simonson, W. Hustrulid, P. Nelson, A. DuBois, E. Binnall, and R. Haught, 1979. Instrument Evaluation, Calibration and Installation for the Heater Experiments at Stripa. Lawrence Berkeley Laboratory report LBL-8313, SAC-25. Berkeley, California.

Smith, A.R. and H.A. Wollenberg, 1972. "High-Resolution Gamma Ray Spectrometry for Laboratory Analysis of the Uranium and Thorium Decay Series" in Natural Radiation Environment II, J.A.S. Adams, W.M. Lowder and T.F. Gesell, eds., vol. 1, pp. 181-232, U.S. Department of Commerce CONF-720805-P2.

Stoker, A.K. and P. Kruger, 1975. "Radon in Geothermal Reservoirs" in Proc. Second United Nations Symposium on the Development and Use of Geothermal Resources, pp. 1797 - 1803.

Tanner, A.B., 1964. "Radon Migration in the Ground: A Review," in The Natural Radiation Environment, edited by J.A.S. Adams and W.M. Lowder, University of Chicago Press, Chicago.

Tanner, Allen B, 1980. "Radon Migration in the Ground: A Supplementary Review." in Natural Radiation Environment III, Vol. 1, Technical Information Center, U.S. Department of Energy, edited by T.F. Gessell and W.M. Lowder.

Thorpe, R., 1979. Characterization of Discontinuities in the Stripa Granite --Time-Scale Heater Experiment. Lawrence Berkeley Laboratory report LBL-7083, SAC-20. Berkeley, California.

West, Francis G. and A.W. Laughlin, 1976. "Spectral Gamma Logging in Crystalline Basement Rocks." Geology, 4, p. 617-618.

Wilson, R.D., D.C. Stromswold, M.L. Evans, M. Jain and D.A. Close, 1979. "Spectral Gamma-ray Logging II: Borehole Correction Factors," in Transactions of the SPWLA 20th Annual Logging Symposium, pp. EE1-EE16, June.

Witherspoon, P.A., N.G.W. Cook, and J.E. Gale, 1980. Progress with Field Investigations at Stripa. Lawrence Berkeley Laboratory report LBL-10559, SAC-27. Berkeley, California. 1980.

Wollenberg, H.A., S. Flexser and L. Andersson, 1981 (forthcoming). Petrology and Radiology of the Stripa Pluton. Lawrence Berkeley Laboratory report LBL-11654, Berkeley, California.

APPENDIX A

RADIOELEMENT CONCENTRATION AND RADON-222 EMANATION FROM GAMMA SPECTROMETRY ON STRIPA SAMPLES

Measurement of uranium, thorium, and potassium concentrations were performed at the LBL Low Background Facility, using a high-sensitivity γ spectrometer to analyze samples of 800-1000 gram weight. In this system, events detected in an 8-in diameter by 4-in thick NaI(Tl) crystal are processed by a gain-stabilized multichannel pulse height analyzer to produce 400-channel spectra that span the γ energy range from 0.1 to 4.1 MeV.

Radioelement assays derived from these data are based on three spectral intervals that are commonly used for this purpose: the "potassium" interval, centered at 1.46 MeV; the "uranium" interval, centered at 1.76 MeV; and the "thorium" interval, centered at 2.62 MeV. Since the γ-rays used for U-assay originate from decay of Rn-222 daughter nuclides, two analyses of a single sample can also provide a measure of emanating Rn-222: the first, while Rn-222 is free to emanate; the second, at a suitable time after sealing against Rn-222 escape. The difference between the two apparent U-concentrations can be converted into a value for Rn-222 emanation.

All materials studied here were first processed in a jaw crusher to reduce the size of the largest fragments to about -1/2"; all finer sizes were retained in the samples. Although for very small particles, the emanation rate of Rn-222 is known to be sensitive to particle size, no significant fraction of these materials is believed to be in the size range for which such effects are important. The observed Rn-222 is more likely to be related either to the degree of chemical weathering, or to radiation damage that has

accrued over the formation's long life, due to decay of the unusually high concentration of uranium.

Values are listed for the absolute U, Th, and K concentrations, along with errors associated with counting statistics. The errors (enclosed in parentheses) are also in terms of concentrations, and represent single standard deviation values. For U and Th these errors, when smaller than 1% of the amount present, are useful only for relative purposes, since the U and Th content of calibration standards are known only to 1%. For K, absolute concentrations can be known to better than 1% precision, since the calibration standard is CP potassium chloride.

Values for Rn-222 emanation are given as that fraction of total sample Rn-222 that was observed to emanate. The errors (enclosed in parentheses) also represent a single standard deviation based on propagation of counting errors. Note that these errors are expressed in percent, and apply to all three quantities listed for emanating Rn-222.

Borehole DBH V-1

Thirteen of the 15 samples have high uranium concentrations, ranging from 39 to 47 ppm. Rn-222 emanation ranges from 0.6 to 2.2 pCi/gram of material. An average value is 1.4 $\pm$ 0.5 pCi/gram, and represent emanation of approximately 10% of the total Rn-222 in the materials.

Borehole SBH-1

Four of the 5 samples have high uranium concentration, ranging from 36 to 41 ppm. Rn-222 emanation ranges from 1.6 to 2.4 pCi/gram of material. An average value is 2.1 $\pm$ 0.3 pCi/gram, and represents emanation of approxi-

mately 16% of the total Rn-222 in the materials.

Boreholes N1 and SBH-2

The single sample from borehole N1 has high uranium concentration and Rn-222 emanation similar to the average value for DBH V-1 borehole samples. The single sample from borehole SBH-2 has approximately 1/2 the uranium concentration of the high-U samples, but shows about the same fraction of emanating Rn-222 as do the high-U materials.

Hand Specimens

The 6 hand specimens tested for Rn-222 emanation had uranium concentrations ranging from 15 to 41 ppm. Rn-222 emanation ranges from 0.8 to 2.3 pCi/gram of material, and represents emanation of 10 to 25% of the total Rn-222 in the materials. Some of these samples were taken from surface outcrops (see Wollenberg et al. (1980), for location), for which the effects of chemical weathering may enhance Rn-222 emanation rates compared to values obtained from fresher (borehole) materials.

DBH V-1 Borehole: Crushed Core Samples

Depth Meters	Concentration Values			Rn-222 Emanation		
4.55 - 4.92 granite	U ppm	39.5	(0.2)	fraction	0.044	(26%)
	Th ppm	31.1	(0.3)	pCi/g	0.57	
	K pct	3.75	(0.02)			
73.33 - 73.50 granite	U ppm	43.8	(0.2)	fraction	0.126	(9.8%)
	Th ppm	33.1	(0.3)	pCi/g	1.84	
	K pct	3.83	(0.03)			
125.23 - 125.38 granite	U ppm	38.9	(0.2)	fraction	0.094	(15%)
	Th ppm	26.4	(0.3)	pCi/g	1.22	
	K pct	3.49	(0.03)			
149.42 - 149.61 granite	U ppm	42.6	(0.2)	fraction	0.158	(7.6%)
	Th ppm	30.6	(0.4)	pCi/g	2.24	
	K pct	3.38	(0.03)			
168.50 - 168.68 granite	U ppm	41.5	(0.2)	fraction	0.132	(9.4%)
	Th ppm	30.6	(0.4)	pCi/g	1.83	
	K pct	3.10	(0.03)			
178.00 - 178.19 granite	U ppm	39.6	(0.2)	fraction	0.108	(12%)
	Th ppm	29.1	(0.4)	pCi/g	1.42	
	K pct	3.77	(0.04)			
234.60 - 234.79 granite	U ppm	46.1	(0.2)	fraction	0.044	(27%)
	Th ppm	35.8	(0.4)	pCi/g	0.67	
	K pct	3.89	(0.03)			
264.88 - 265.10 granite	U ppm	41.2	(0.2)	fraction	0.088	(11%)
	Th ppm	32.2	(0.3)	pCi/g	1.20	
	K pct	3.79	(0.02)			
289.68 - 289.90 granite	U ppm	46.6	(0.2)	fraction	0.132	(8.2%)
	Th ppm	34.1	(0.4)	pCi/g	2.05	
	K pct	3.92	(0.03)			
299.35 - 299.53 granite	U ppm	41.2	(0.2)	fraction	0.054	(24%)
	Th ppm	30.9	(0.2)	pCi/g	0.74	
	K pct	4.17	(0.02)			

DBH V-1 Borehole: Crushed Core Samples

Depth Meters	Concentration Values			Rn-222 Emanation		
325.12 -	U ppm	43.4	(0.2)	fraction	0.122	(8.6%)
325.36	Th ppm	32.4	(0.3)	pCi/g	1.76	
granite	K pct	3.78	(0.03)			
349.52 -	U ppm	12.8	(0.1)	fraction	0.098	(27%)
349.73	Th ppm	39.6	(0.3)	pCi/g	0.42	
granite	K pct	4.57	(0.02)			
404.70 -	U ppm	47.4	(0.2)	fraction	0.103	(12%)
404.84	Th ppm	38.3	(0.4)	pCi/g	1.63	
granite	K pct	3.90	(0.03)	pCi/sample		
414.43 -	U ppm	20.9	(0.2)	fraction	0.054	(48%)
414.61	Th ppm	33.5	(0.5)	pCi/g	0.38	
brecciated granite	K pct	4.74	(0.04)	pCi/sample		
464.54 -	U ppm	45.5	(0.2)	fraction	0.084	(16%)
464.70	Th ppm	35.4	(0.5)	pCi/g	1.27	
granite	K pct	4.10	(0.04)	pCi/sample		

N1 Borehole: Crushed Core Samples

3.10 -	U ppm	40.8	(0.2)	fraction	0.096	(14%)
3.49	Th ppm	38.8	(0.3)	pCi/g	1.30	
granite	K pct	3.92	(0.03)	pCi/sample		

SBH-1 Borehole: Crushed Core Samples

Depth Meters	Concentration Values			Rn-222 Emanation		
148.58 - 148.75 leptite	U ppm	4.14	(0.04)	fraction	0.051	(50%)
	Th ppm	11.3	(0.1)	pCi/g	0.07	
	K pct	2.42	(0.01)			
232.77 - 232.93 brecciated granite	U ppm	39.9	(0.2)	fraction	0.179	(6.8%)
	Th ppm	28.7	(0.4)	pCi/g	2.38	
	K pct	4.26	(0.03)			
255.12 - 255.29 granite	U ppm	38.8	(0.1)	fraction	0.166	(6.1%)
	Th ppm	30.3	(0.3)	pCi/g	2.14	
	K pct	3.89	(0.02			
320.27 - 320.45 granite	U ppm	35.7	(0.2)	fraction	0.193	(5.7%)
	Th ppm	29.4	(0.3)	pCi/g	2.30	
	K pct	3.87	(0.02)			
371.68 - 371.83 granite	U ppm	41.3	(0.2)	fraction	0.117	(9.4%)
	Th ppm	30.6	(0.3)	pCi/g	1.61	
	K pct	4.02	(0.02)			

SBH-2 Borehole: Crushed Core Samples

196.41 granite	U ppm	29.96		(no emanation data)		
	Th ppm	31.95				
	K pct	4.01				
206.74 granite	U ppm	7.76				
	Th ppm	31.06				
	K pct	3.97				
213.13 granite	U ppm	9.03				
	Th ppm	29.67				
	K pct	3.63				
340.24 - 340.35 granite; fractures with epidote and fluorite	U ppm	23.3	(0.1)	fraction	0.108	(20%)
	Th ppm	22.5	(0.2)	pCi/g	0.84	
	K pct	2.82	(0.02)			

Stripa Workings/Vicinity: Hand Specimens

Sample	Concentration Values			Rn-222 Emanation		
ST-3 granite	U ppm	24.4	(0.1)	fraction	0.223	(3.7%)
	Th ppm	31.2	(0.2)	pCi/g	1.81	
	K pct	3.98	(0.02)	pCi/sample		
ST-9 granite	U ppm	34.2	(0.2)	fraction	0.166	(5.6%)
	Th ppm	32.1	(0.5)	pCi/g	1.89	
	K pct	3.97	(0.04)	pCi/sample		
ST-12 granite	U ppm	40.9	(0.2)	fraction	0.098	(7.8%)
	Th ppm	31.4	(0.4)	pCi/g	1.33	
	K pct	3.84	(0.04)	pCi/sample		
ST-21 granite	U ppm	35.2	(0.2)	fraction	0.193	(3.8%)
	Th ppm	29.2	(0.4)	pCi/g	2.26	
	K pct	3.76	(0.03)	pCi/sample		
ST-47 granite, coarse to pegmatitic	U ppm	15.1	(0.1)	fraction	0.246	(6.4%)
	Th ppm	8.71	(0.23)	pCi/g	1.24	
	K pct	2.95	(0.02)	pCi/sample		
ST-48 granite	U ppm	15.4	(0.1)	fraction	0.162	(11%)
	Th ppm	30.5	(0.4)	pCi/g	0.83	
	K pct	3.99	(0.03)	pCi/sample		

APPENDIX B

DEFINITION OF WORKING LEVEL

[Note: the following definition and discussion of Working Level and Working Level Month is taken from Sect. 3 of Instrumentation for Environmental Monitoring--Radiation by Environmental Instrumentation Group, LBL (LBL-1, Vol. 3), October 1973. Refer to Fig. 2.3 in the main body of this report for decay series nomenclature.]

For the purposes of radiological protection of the lungs in the uranium mining industry, a specialized unit of exposure to radon-222 has been developed. This is the Working Level (WL), defined as "any combination of radon daughters in one liter of air that will result in the ultimate emission of 1.3×10^5 MeV of potential alpha energy" (Ref. 1). This value is derived from alpha energies released by the total decay of the short-lived daughters (RaA, RaB, RaC, RaC') at radioactive equilibrium with 100 pCi of ^{222}Rn/liter of air. Note that the WL considers only the alphas from radon-222 daughters and not from radon gas itself.

The reason for the specialized unit is mainly operational: the WL is a concept having validity in any mixed concentration of radon and its daughters, whether or not they are in equilibrium. Just as important, it lends itself to practical measurements in the mines.

An extension of the WL concept is the "Working Level Month" (WLM), which expresses a cumulative exposure. It is defined as follows: "Inhalation of air containing a radon daughter concentration of one WL, for 170 working hours results in an exposure of one WLM" (Ref. 1).

The Secretary of Labor, acting under provisions of the Walsh Healy Act, promulgated the following standard in late 1968 (Ref. 2):

> Occupational exposure to radon daughters in mines shall be controlled so that no individual will receive an exposure of more than 2 WLM in any consecutive 3-month period and no more than 4 WLM in any consecutive 12-month period. Actual exposures shall be kept as far below these values as practicable.

In early 1969, the Department of the Interior issued the following standard calling for action on the basis of individual concentrations (Ref. 3):

> If samples show an atmospheric concentration of radon daughters of more than 1 WL, but less than 2 WL, immediate corrective action shall be taken or the men shall be withdrawn. When concentrations higher than 2 WL are indicated, the men shall be withdrawn from the area until corrective action is taken and the radon-daughter atmospheric concentrations are reduced to 1 WL or less....Smoking shall be prohibited where uranium is mined.

The above two standards are now considered the operational guidelines for exposure of miners to radon daughters.

The absorbed dose (rad) and dose equivalent (rem) resulting from 1 WL of exposure depend upon the exact nature of the mine atmosphere. With modern ventilation procedures, the equilibrium condition is never reached for any but the first daughter, RaA. Consider as an example the "reference atmosphere" discussed by Altshuler (Ref. 4), which contains in one liter of air the following activities totaling 200 pCi: 94 pCi of ^{218}Po, 62 pCi of ^{214}Pb, 44 pCi of ^{214}Bi. This yields 7.4×10^4 MeV or 57% of a WL. We quote from the Federal Regulation Council (Ref. 5):

> Altshuler's reference atmosphere results in 60% of a 'WL dose' to the bronchi, and has a value between 10 and 30 rads per year. In view of the ambiguities of conversion, Altshuler's reference atmosphere will be considered, with important reservations, to produce 20 rads in a normal working year....Exposure for one year at...one WL would give 33 rads. The mean organ dose would be

lower. In the absence of an appropriate factor for the RBE, the calculated dose cannot be converted to rem.

It should be emphasized that the WL standards are based on epidemiological evidence, rather than on calculated dose equivalent to the lungs (Ref. 5).

Exposure to radiation other than the inhalation of radon daughters must be considered separately. The usual occupational limits apply: that is, 5 rem/year for whole body exposure, and so on. These limits have been discussed in detail in the introductory section of this volume (see "Radiation Guides"), [i.e., LBL-1, Vol. 3].

A limit for radon-222 gas itself is not considered separately by the Federal Radiation Council, because of the general recognition that the impact of the radon daughters is the more important consideration.

The International Commission on Radiological Protection (ICRP) explicitly considers the impact of RaA in its recommendation. We quote from ICRP Report No. 6, written in 1959 (Ref. 6):

> Recent studies have indicated that when radon and its daughters are present in ordinary air the free ions of RaA constitute only about 10 percent of the total member of RaA atoms that would be present at equilibrium and these unattached atoms deliver all but a small fraction of the dose to the bronchi. Based on these measured dose rates the $(MPC)_a$ for exposure to radon and daughter products is found to be
>
> $$(MPC)_a = \frac{3000}{(1 + 1000f)} \text{ pCi } ^{222}\text{Rn/liter of air}$$
>
> where f is the fraction of the equilibrium among of RaA ions which are unattached to nuclei.

If we set f = 10%, as the ICRP indicates might be typical, then the occupational $(MPC)_a$ is 30 pCi/liter.

There is no explicit guideline for exposure of the general public to radon and its daughters. However, both the ICRP (Ref. 7) and the NCRP (Ref. 8) have recommended in their general overviews that individuals in the general public be limited to exposures at levels one-tenth as high as those for occupational exposure. Also, for a suitably large sample of the general population, the general guideline is another factor of 3 smaller still.

REFERENCES FOR APPENDIX B

1. R.L. Rock, D.K. Walker, R.W. Dalzell and E.J. Harris, Controlling Employee Exposure to Alpha Radiation in Underground Uranium Mines, U.S. Bureau of Mines Handbook Volumes I and II (1970 and 1971).

2. Federal Register, Vol. 33, No. 252, December 28, 1968.

3. Federal Register, Vol. 34, No. 11, January 16, 1969.

4. B. Altshuler, N. Nelsen and M. Kuschner, "Estimation of the Lung Tissue Dose from Inhalation of Radon and Daughters," Health Physics 10, 1137 (1964).

5. Federal Radiation Council, Guidance for the Control of Radiation Hazards in Uranium Mining, Report FRC No. 8 (revised), Washington, D.C. (1967).

6. ICRP Pub. 6 (as amended 1959 and revised 1962). Pergamon Press, 1964.

7. ICRP Pub. 2: "Report of Committee II on Permissible Dose for Internal Radiation." Pergamon Press, 1959.

8. Maximum Permissible Body Burdens and Maximum Permissible Concentrations of Radionuclides in Air and in Water for Occupational Exposure, National Bureau of Standards Handbook 69. Washington, D.C. (1959).

*USGPO: 1982 — 559-099/5324